An investigation into the structural behaviour of a novel cellular beam structure in fire

by

Michael Kloos

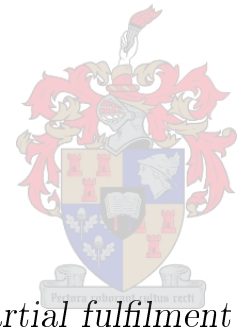

Thesis presented in partial fulfilment of the requirements for the degree of Master of Engineering in Structural Engineering in the Faculty of Engineering at Stellenbosch University

Supervisor: Dr. Richard Walls

December 2017

Declaration

By submitting this thesis electronically, I declare that the entirety of the work contained therein is my own, original work, that I am the sole author thereof (save to the extent explicitly otherwise stated), that reproduction and publication thereof by Stellenbosch University will not infringe any third party rights and that I have not previously in its entirety or in part submitted it for obtaining any qualification.

Date: ..... December 2017 .....

Abstract

An investigation into the structural behaviour of a novel cellular beam structure in fire

M. Kloos

Department of Civil Engineering,
University of Stellenbosch,
Private Bag X1, 7602 Matieland, South Africa.

Thesis: MEng Structural Engineering

December 2017

The Southern African Institute of Steel Construction (SAISC) has developed a novel cellular beam structure (CBS), which has been specifically designed for the construction of two to ten storey office blocks. The concept is based on the factory production of modules, which can be transported to site and quickly erected, thereby reducing construction time and cost. The modules consist of cellular steel beams and a ceiling board system, thus avoiding any wet trade, and remaining lightweight. The modularity allows for architectural freedom, as multiple configurations are possible. Furthermore, modules can later be added, or even re-used in another structure. However, the primary challenge hindering the commercialisation of this system is its unknown fire resistance.

In South Africa, and worldwide, all structures require a fire rating, and thus an investigation into the fire resistance of the CBS has been carried out in this thesis to assist in bringing the system to production. As part of a larger project, this thesis focuses on the structural behaviour of the CBS under fire conditions, with an emphasis on numerical modelling. With the unconventional layout of the structure, standard fire design methods do not necessarily apply, or conversely could result in an over-conservative and costly specification of passive fire protection. Thus, a rational/performance-based approach has been developed, in which non-linear finite element (FE) models developed in Abaqus are used to characterise the behaviour of the CBS.

Non-linear FE modelling procedures are required to model the CBS, as the material properties, geometry, structural loads and temperatures change over the course of a fire. The models developed have been validated based on three case studies in the literature. The CBS is then investigated using a total of 18 single element models consisting of isolated elements, and 9 global structure models. Three different time-temperature fire scenarios are considered: (a) a standard fire with the fire-rated ceiling remaining in place, (b) a standard fire with the ceiling failing, leading to significantly hotter beam temperatures, and (c) a parametric fire. This allowed the CBS to be tested under a variety of boundary conditions, thermal loads and possible fire scenarios.

Overall, the models indicate that the CBS performs well under fire conditions. The structure is able to deflect and expand as the steel heats up, which reduces the internal forces. An ultimate failure mode, which could cause a collapse, is only detected under conservative conditions that are unlikely to occur. The models developed are used to predict the maximum vertical and lateral deflections of the steel members. The vertical deflections were found to be relatively small in terms of typical fire deflections, with a maximum predicted value of 35 mm (span/229) under the standard fire with the ceiling in place (the primary design scenario). However, a maximum lateral deflection of 185 mm is anticipated, which will require careful detailing considerations. Under parametric fire conditions, negligible permanent deformation is predicted by the global structure models once the steel returns to ambient temperature.

Ultimately, design recommendations are made to increase the fire resistance. Firstly, steel end connections should be designed to provide negligible moment restraint, and to allow free thermal expansion using slotted bolt holes. Secondly, if the ceiling system is designed to accommodate the predicted deflections, the integrity of the entire system is protected and the chance of a structural failure is significantly reduced.

Uittreksel

'n Ondersoek van die stukturele gedrag van 'n sellulêre balkstruktuur tydens 'n vuur

M. Kloos

Departement Siviele Ingenieurswese,
Universiteit van Stellenbosch,
Privaatsak X1, 7602 Matieland, Suid Afrika.

Tesis: MEng Structural Engineering

Desember 2017

Die Suider-Afrikaanse Instituut vir Staalkonstruksie (SAISC) het 'n nuwe sellulêre balkstruktuur (SBS) ontwikkel, wat spesifiek ontwerp is vir die bou van kantoorgeboue met twee tot tien verdiepings. Die konsep is gebaseer op die fabrieksproduksie van modules, wat vinnig opgerig kan word op die perseel, waardeur konstruksietyd en -koste verminder kan word. Die modules bestaan uit sellulêre staalbalke en 'n plafonbordstelsel, waardeur enige beton vermy word, en die struktuur lig bly. Die modulariteit maak voorsiening vir argitekturele vryheid, aangesien verskeie konfigurasies moontlik is. Verder kan modules later bygevoeg word, of selfs weer in 'n ander struktuur gebruik word. Die primêre uitdaging wat die kommersialisering van hierdie stelsel belemmer, is egter die onbekende brandweerstand.

In Suid-Afrika en wêreldwyd vereis alle strukture 'n brandgradering, en daarom is 'n ondersoek van die brandbestandheid van die SBS in hierdie tesis gedoen, om hierdie stelsel tot produksie te bring. As deel van 'n groter projek, fokus hierdie tesis op die strukturele gedrag van die SBS onder brandtoestande, met die klem op numeriese modellering. Uitgesien die onkonvensionele uitleg van die struktuur, is standaard brandontwerpmetodes nie noodwendig van toepassing nie, aangesien dit 'n oor-konserwatiewe en duur spesifikasie van passiewe brandbeskerming kan veroorsaak. Dus, is 'n rasionele/prestasiegebaseerde benadering ontwikkel, waarin nie-lineêre eindige element modelle wat in Abaqus ontwikkel is, gebruik word om die gedrag van die SBS te karakteriseer.

Sulke modelleringsprosedures word benodig, aangesien die materiaal eienskappe, meetkunde, strukturele laste en temperature verander deur die loop van 'n brand. Die ontwikkelde modelle is bevestig op grond van drie gevallestudies in die literatuur. Die SBS word ondersoek deur gebruik te maak van 'n totaal van 18 enkel-element-modelle, wat bestaan uit geïsoleerde elemente, asook 9 globale-struktuurmodelle. Drie verskillende brandsituatsies word oorweeg: (a) 'n standaardvuur met die brand gegradeerde plafon in plek (b) 'n standaardvuur met die plafon wat misluk, wat lei tot aansienlik warmer temperature in die balke en (c) 'n parametriese vuur. Hierdeur is die SBS getoets onder 'n verskeidenheid van randvoorwaardes, termiese vragte en moontlike brandsituasies.

Oor die algemeen, wys die modelle dat die SBS goed vaar onder brandtoestande. Die struktuur is in staat om te buig en uit te sit soos die staal verhit, wat die interne kragte verminder. 'n Strukturele vaaling, wat 'n ineenstorting kan veroorsaak, word slegs onder konserwatiewe toestande waargeneem wat onwaarskynlik sal voorkom. Die ontwikkelde modelle word gebruik om die maksimum vertikale en laterale defleksie van die staallede te voorspel. Die vertikale defleksies is relatief klein ten opsigte van tipiese branddefleksies, met 'n maksimum waarde van 35 *mm* (span/229) onder die standaardvuur met die plafon in plek (die primêre ontwerp situasie). 'n Maksimum laterale defleksie van 185 *mm* word voorspel, wat egter sorgvuldige detailering sal benodig. Onder die parametriese vuur, word weglaatbare permanente vervorming voorspel deur die globale struktuurmodelle nadat die staal terugkeer na omgewings temperatuur.

Uiteindelik word ontwerpaanbevelings gemaak om die brandweerstand van die SBS te verhoog. Eerstens moet die staal-eindkonneksies ontwerp word om weglaatbare momentbeperking te bied, en om vrye termiese uitbreiding toe te laat deur middel van gleufboutgate. Tweedens, as die plafonstelsel ontwerp is om die voorspelde defleksies te akkommodeer, word die integriteit van die hele stelsel beskerm en die kans van 'n stukturele vaaling verminder.

Acknowledgements

I would like to thank the following people:

- Richard Walls, for being the best supervisor in the world.
- Amanuel Gebremeskel of the Southern African Institute of Steel Construction (SAISC), for always being available to answer questions, and giving insightful advice.
- Mohammad Pourbehi, for helping me uncover the mysteries of Abaqus.
- My parents, for whom I have unending gratitude and love.
- And finally, my classmates, for sharing the journey of a masters degree with me.

Contents

Declaration i

Abstract ii

Uittreksel iv

Acknowledgements vi

Contents vii

List of Figures x

List of Tables xvi

Nomenclature xvii

1 Introduction 1
- 1.1 Problem statement . . . 1
- 1.2 Research goal and objectives . . . 2
- 1.3 Scope . . . 3
- 1.4 Thesis layout . . . 4
- 1.5 Conclusion . . . 5

2 Literature review 6
- 2.1 Introduction . . . 6
- 2.2 Fire dynamics . . . 6
  - 2.2.1 Combustion . . . 6
  - 2.2.2 Heat transfer . . . 8
  - 2.2.3 Compartment fires . . . 8
- 2.3 Structural fire engineering . . . 9
  - 2.3.1 Fire safety . . . 10
  - 2.3.2 Introduction to structural fire engineering . . . 10
  - 2.3.3 Standard fire curve . . . 12
  - 2.3.4 Prescriptive fire design . . . 13
  - 2.3.5 Performance-based fire design . . . 13

2.4 Steel in fire . . . 14
2.4.1 Material properties . . . 14
2.4.2 Steel beams . . . 18
2.4.3 Cellular beams . . . 18
2.4.4 Connections . . . 22
2.4.5 Passive protection for steel . . . 22
2.5 Physical fire testing . . . 25
2.5.1 Standard fire testing . . . 25
2.5.2 Full-scale testing . . . 25
2.5.3 The Cardington tests . . . 26
2.6 Global modelling of structures in fire . . . 26
2.6.1 Motivation for global analysis . . . 26
2.6.2 Non-linear behaviour . . . 27
2.6.3 Uncoupled vs. coupled analyses . . . 28
2.6.4 Mechanical analysis types . . . 28
2.6.5 Case studies of finite element modelling of structures in fire . . . 30
2.6.6 Software considerations . . . 31

3 SAISC cellular beam structure 33
3.1 Introduction . . . 33
3.2 The motive . . . 33
3.3 The solution . . . 34
3.4 Site visit . . . 37
3.5 Structural layout and terminology . . . 38
3.6 Conclusion . . . 40

4 Finite element modelling validation 41
4.1 Introduction . . . 41
4.2 Gillie benchmark . . . 42
4.3 COST benchmarks . . . 46
4.3.1 Abaqus implementation of Eurocode material model for steel at elevated temperatures . . . 46
4.3.2 COST 1: Steel beam with varying boundary conditions . 48
4.3.3 COST 2: Buckling behaviour of Class 4 beam . . . 53
4.4 Conclusion . . . 55

5 Single element modelling 57
5.1 Introduction . . . 57
5.2 Thermal analysis . . . 57
5.2.1 Overview of thermal analysis . . . 58
5.2.2 Standard fire results . . . 61
5.2.3 Parametric fire results . . . 63
5.3 Structural loading . . . 65

5.4 J-beam modelling . . . 66
5.4.1 FEM input . . . 66
5.4.2 Standard fire analyses . . . 72
5.4.3 Parametric fire analyses . . . 77
5.5 P-beam modelling . . . 81
5.5.1 FEM input . . . 81
5.5.2 Standard fire analyses . . . 84
5.5.3 Parametric fire analyses . . . 88
5.6 Conclusion . . . 90

6 Global structural modelling 92
6.1 Introduction . . . 92
6.2 FEM input . . . 92
6.2.1 Geometry . . . 92
6.2.2 Elements and mesh . . . 93
6.2.3 Material models . . . 95
6.2.4 Interactions . . . 96
6.2.5 Loads and boundary conditions . . . 98
6.2.6 Fire cases . . . 100
6.2.7 Solution procedure . . . 100
6.3 Results and analysis . . . 101
6.3.1 Fire case 1 . . . 101
6.3.2 Fire case 2 . . . 105
6.3.3 Fire case 3 . . . 107
6.4 Conclusion . . . 112

7 Conclusions and recommendations 114
7.1 Overview . . . 114
7.2 Summary of findings . . . 115
7.3 Design considerations . . . 118
7.4 Future research . . . 119

List of References 120

Appendices 124

A Parametric fire 125

B Shop drawings 127

List of Figures

1.1 General arrangement drawing of SAISC cellular steel beam structure (Courtesy of SAISC) 2

2.1 The Fire Triangle (Powell, 2017) 7
2.2 Typical time-temperature behaviour of a real fire (Walls, 2016) . . . 9
2.3 Typical time-temperature curves for a standard, hydrocarbon and external fire 12
2.4 Examples of steel structures after a fire 14
(a) 'Squashed' steel column (courtesy of Ali Moradi) 14
(b) Beams from the Cardington tests showing severe midspan deflections, and web buckling close to supports (Lamont, 2001) 14
2.5 Stress-strain formulae for carbon steel (CEN, 2005) 15
2.6 Schematic stress-strain relationship for carbon steel at an elevated temperature (CEN, 2005) 16
2.7 Reduction factors for the stress-strain relationship of carbon steel at elevated temperatures (CEN, 2005) 16
2.8 Relative thermal elongation of carbon steel as a function of the temperature (CEN, 2005) 17
2.9 Two-stage cutting and welding process to create a cellular beam (Kuchta and Maślak, 2015) 19
2.10 Failure mechanisms of cellular beams 20
(a) A Vierendeel mechanism in a cellular beam (Kuchta and Maślak, 2015) 20
(b) Web post buckling due to shear (Kerdal and Nethercott, 1984) 20
2.11 Steel connections after being exposed to a fire (Wang *et al.*, 2013) . 23
(a) Fin plate 23
(b) Flush end plate 23
(c) Flexible end plate 23
(d) Extended end plate 23
(e) Web cleats - side view 23
(f) Web cleats - top view 23

2.12 Output of finite element model of Britomart building showing displacements (Hicks *et al.*, 2012) 31

3.1 General drawing of three connected modules, forming a single sub-structure (Courtesy of SAISC) 35
3.2 A larger structure made up of multiple sub-structures (Courtesy of SAISC) 35
3.3 Schematic cross-sections of cellular beam structure (CBS) floor system (Marx, 2018). Note: drawing not to scale. 36
(a) Elevation 36
(b) Side elevation 36
3.4 Hendrig Marx at the site of the prototype cellular beam structure (CBS) 37
3.5 Terminology used for the structural elements of the cellular beam structure (CBS) 38
3.6 Sketch of a 'J-beam'. Note: not to scale 39
3.7 Diagram illustrating the transfer of loading through the cellular beam structure (CBS) 40

4.1 Gillie benchmark - problem definition (Gillie, 2009) 42
4.2 Abaqus kinematic coupling constraint 43
(a) Interaction between reference point (RF) and beam edge. Note, a 5 mm offset was applied between the RF and beam edge for visual clarity. 43
(b) Abaqus constraint input 43
4.3 Gillie benchmark - axial force 45
4.4 Gillie benchmark - midspan deflection 45
4.5 Stress-strain relationship of steel at elevated temperatures (CEN, 2005) 47
4.6 Initial Young's modulus of steel at elevated temperatures (CEN, 2005) 48
4.7 Coefficient of thermal expansion of steel at elevated temperatures (CEN, 2005). The simplified constant value of 1.4×10^{-5} is also shown. 48
4.8 Non-uniform temperature distribution in beam based on standard fire 49
4.9 COST 1 - deflection (fully fixed) 51
4.10 COST 1 - axial force (fully fixed) 51
4.11 COST 1 - deflection (pin-pin) 52
4.12 COST 1 - axial force (pin-pin) 52
4.13 Elevation view of the beam used in the COST 2 benchmark, showing the geometry, position of point loads and the heated area. Adapted from COST (2014). 53

4.14 Abaqus model of COST 2 steel beam, from this work. The stiffeners are shown, as well as the mesh used. 54
4.15 COST 2 - load-deflection relationship 55

5.1 Example of an Abaqus thermal analysis of the sandwich floor system (Marx, 2018) 58
5.2 Parametric and standard fire temperatures used in the thermal analysis of the cellular beam structure (CBS) (Marx, 2018) 59
5.3 Cross-section of the cellular beam structure (CBS) floor system during a 'no ceiling' analysis (StF-NoC) 60
5.4 Homogenous temperature zones of a J-beam 60
5.5 J-beam - predicted steel temperatures during a 60 minute standard fire (Marx, 2018) 62
5.6 P-beam - predicted steel temperatures during a 60 minute standard fire (Marx, 2018) 62
5.7 Channel - predicted steel temperatures during a 60 minute standard fire (Marx, 2018) 63
5.8 J-beam - predicted steel temperatures during the parametric fire (Marx, 2018) 64
5.9 P-beam - predicted steel temperatures during the parametric fire (Marx, 2018) 64
5.10 Channel - predicted steel temperatures during the parametric fire (Marx, 2018) 65
5.11 J-beam dimensions 67
5.12 25 *mm* mesh used for the single J-beam model 67
5.13 Elevation view of single J-beam model showing loads and boundary conditions 68
5.14 Diagram illustrating the four end boundary condition cases used for the J-beam model 69
5.15 Reference point (RF) and kinematic constraint superimposed on a photo of a J- to P-beam connection 69
5.16 Abaqus artificial damping implementation 71
5.17 50 *mm* and 40 *mm* meshes used in the mesh sensitivity analysis . . 72
5.18 Mesh sensitivity analysis - axial force and midspan deflection of a pin-pin (PP) J-beam, during a standard fire analysis with no ceiling (StF-NoC). The time at which the top flange (TF) buckles is indicated. 73
5.19 J-beam - axial force (axial) and midspan deflection (def.) during a standard fire the ceiling remaining intact (StF-C), with varying end boundary conditions 73
5.20 J-beam - axial force (axial) and midspan deflection (def.) during a standard fire with no ceiling (StF-NoC), with varying end boundary conditions 74

5.21 Fixed-fixed (FF) J-beam experiencing lateral deflection of the bottom flange caused by restrained thermal expansion 76
5.22 Pin-pin (PP) J-beam after the top flange has buckled 76
5.23 Expected steel temperatures in the J-beams during a 120 minute parametric fire, including the enforced linear cooling stage after 80 minutes 78
5.24 J-beam - axial force and midspan deflection during a parametric fire, with varying end boundary conditions 78
5.25 Deflection behaviour of a pin-pin (PP) J-beam through the course of a parametric fire 80
5.26 P-beam dimensions 82
5.27 25 *mm* mesh used in the single P-beam model 82
5.28 Elevation view of single P-beam model showing loads and boundary conditions 82
5.29 Analytical stiffness of a fixed-fixed beam with a central point load . 83
5.30 Reference point (RF) and constrained surface used to model the P-beam to column connection 84
5.31 P-beam - axial force (axial) and midspan vertical deflection (def.) during a standard fire with a ceiling (StF-C) 85
5.32 P-beam - axial force (axial) and midspan vertical deflection (def.) during a standard fire with no ceiling (StF-NoC) 85
5.33 P-beam - midspan lateral deflection of bottom flange during a standard fire with and without a ceiling (StF-C and StF-NoC) . . . 86
5.34 Extract from shop drawing A - CB49, showing a plan view of the notch in the P-beam flanges 86
5.35 P-beam experiencing lateral deflection under ambient and standard fire conditions. 87
(a) Twisted P-beam under ambient loading conditions. Note: a large deformation scale factor of 10 was applied for visual clarity. 87
(b) Lateral deflections of a P-beam during a standard fire with a ceiling. Deformation scale factor = 1 87
5.36 Plasticity near the P-beam connections that causes a runaway deflection under standard fire 'no ceiling' conditions (StF-C). The equivalent plastic strain is shown. Deformation scale factor = 1. . . 88
5.37 P-beam - axial force and midspan vertical deflection during a parametric fire 89
5.38 P-beam - midspan lateral deflection of bottom flange during a parametric fire 89

6.1 Structural layout used for the cellular beam structure (CBS) illustrating the terminology used for structural elements and bays . . . 93
6.2 Plan view of the cellular beam structure (CBS) showing the main structural elements and dimensions (in m) 94

6.3 Dimensions (in mm) of channels used in the cellular beam structure (CBS) . . . 94
(a) C160×65 used to carry ceiling . . . 94
(b) C100×50 used as knee-brace . . . 94
6.4 30 *mm* mesh used for the C160x65 channel sections . . . 95
6.5 Reference points (RFs) and kinematic constraints used to model the J- to P-beam connections . . . 97
(a) Initial vs. final RF position and kinematic constraint superimposed on a photo of a J- to P-beam connection. This modification to connection specifications will be implemented in future CBS structures. . . . 97
(b) RFs and kinematic constraints seen in Abaqus viewer . . . 97
(c) Enlarged view of interaction between J- and P-beam RFs . 97
6.6 Double angle cleat connection after being exposed to a fire (Wang *et al.*, 2013) . . . 98
(a) Double angle cleats - side view . . . 98
(b) Double angle cleats - top view . . . 98
6.7 All loads and boundary conditions (BCs) in the global model . . . 99
6.8 Diagram showing the three fire cases (FCs), and the corresponding structural elements that experience elevated temperatures . . . 101
6.9 Fire case 1 (FC1) - midspan vertical deflection of J2 in the global model compared with single element J-beam models. The deflections are for the standard fire analysis whilst the ceiling remains intact (StF-C) . . . 102
6.10 Fire case 1 (FC1) - global structure at 60 minutes in a standard fire with the ceiling remaining intact (StF-C) analysis, in which only J2 has been heated. This figure focuses on the deflection of C1 and C2. . . . 103
6.11 Fire case 1 (FC1) - global structure at 60 minutes in a standard fire with the ceiling remaining intact (StF-C) analysis, in which only J2 has been heated. This figure focuses on the deflection of C1 and C2. . . . 104
6.12 Fire case 2 (FC2)- global model at 51 and 60 minutes in the standard fire with the ceiling remaining intact analysis (StF-C) . . . 106
(a) 51 minutes - both P-beams are still rotating and deflecting outwards, in opposite directions relative to one another. P2 buckles shortly after 51 minutes, causing both P-beams to deflect as shown in (b). . . . 106
(b) 60 minutes - P2 has buckled, causing both P-beams deflect laterally to the right. . . . 106
6.13 Fire case 3 (FC3) - lateral deflection under standard fire with a ceiling conditions (StF-C) . . . 108

6.14 Fire case 3 (FC3) - severe plasticity near the column connections after 31 minutes of a standard fire 'no ceiling' analysis (StF-NoC). Collapse occurred shortly after this time. 109
6.15 Fire case 3 (FC3) - midspan vertical deflection at bottom flange of P1, under standard fire 'no ceiling' conditions (StF-NoC) 109
6.16 Fire case 3 (FC3) - global model at 0, 38 and 120 minutes in a parametric fire analysis 111
(a) 0 minutes - ambient deflection state 111
(b) 38 minutes - maximum lateral deflections of P-beams . . . 111
(c) 120 minutes - near return to ambient deflection state . . . 111

List of Tables

5.1 Nominal loads used in the structural analysis of the cellular beam structure (CBS) 66
5.2 Maximum lateral deflection (in mm) of the bottom flange of the J-beam, under all fire and boundary condition scenarios 75

6.1 Fire case 1 (FC1) - maximum deflections (in mm) of J-beam J2 . . 103
6.2 Fire case 1 (FC1) - maximum midspan deflection (in mm) of channel C2 104
6.3 Fire case 2 (FC2) - maximum deflections (in mm) of critical elements 107
6.4 Fire case 3 (FC3) - maximum deflection (in mm) of critical elements 110

A.1 Assumptions made for parametric fire calculations (Marx, 2018) . . 126

Nomenclature

Abbreviations

BC	Boundary condition
BF	Bottom flange
CBS	Cellular beam structure
COST	European Cooperation in the field of Scientific and Technical Research
ECCS	European Convention for Constructional Steelwork
EN	European Standard (Eurocode)
FC	Fire case
FE	Finite element
FEM	Finite element method
FF	Fixed-fixed
FLS	Fire limit state
FR	Fixed-roller
J-beam	Secondary beam. Cross-section resembles the letter "J"
LW	Lower web
P-beam	Primary beam
PP	Pin-pin
PR	Pin-roller
RF	Reference point
SAISC	Southern African Institute of Steel Construction

SPM	Slab panel method
StF-C	Standard fire with fire-rated ceiling included
StF-NoC	Standard fire with fire-rated ceiling excluded
TF	Top flange
UW	Upper web
W	Web

Symbols

E	Young's modulus
I	Moment of inertia
k	Spring stiffness

Chapter 1

Introduction

1.1 Problem statement

All structures in South Africa require a fire rating which quantifies the fire resistance of the structure in relation to the ISO 834 standard fire curve (SABS, 2011*b*). This ensures that structures are protected from the all-too-common natural hazard of fire. Within this setting the Southern African Institute of Steel Construction (SAISC) has developed a novel lightweight structure that makes use of cellular steel beams and a 'sandwich' floor system made up of fibre-cement and fire-resistant boards. The system is designed to be modular, allowing the transportation of pre-fabricated modules to site. Figure 1.1 shows three connected modules supported by four columns. The problem is that the unconventional nature of this structure leaves its fire resistance mostly uncertain. There is no precedent for the new structure and thus standard design methods for fire resistance do not necessarily apply. Resorting to prescriptive fire protection without further analysis is not an attractive option, as it is often over-conservative and costly.

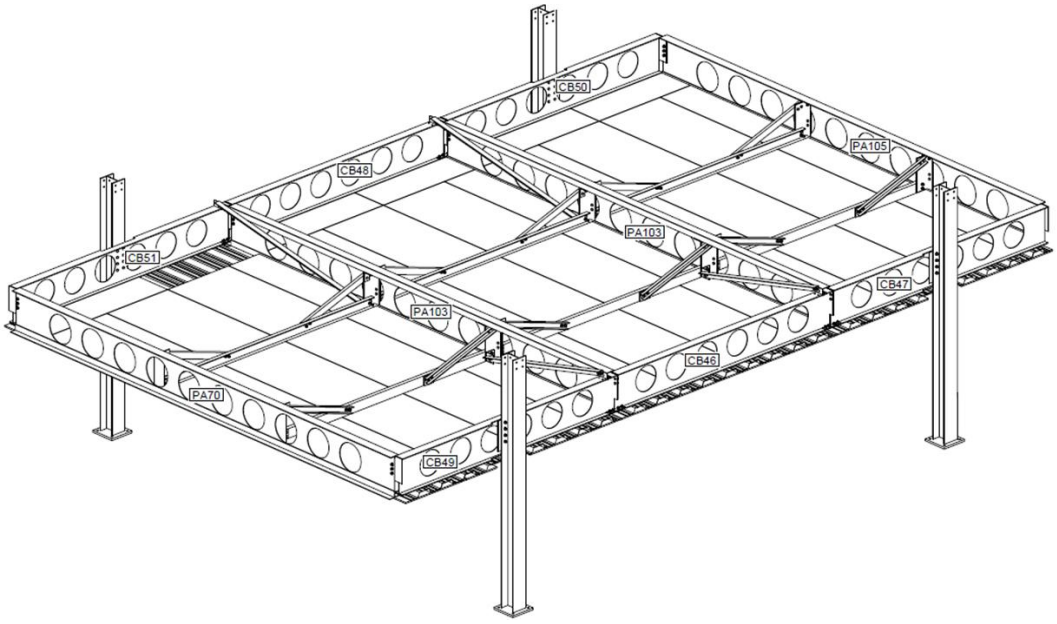

Figure 1.1: General arrangement drawing of SAISC cellular steel beam structure (Courtesy of SAISC)

1.2 Research goal and objectives

The goal of this research is to characterise the structural behaviour of the SAISC cellular beam structure (CBS) under fire conditions, in order to develop a structure that is safe in fire. The sub-objectives are as follows:

- Reproduce benchmark finite element (FE) models to develop a competence for modelling structures under fire conditions.
- Develop FE models of single structural members in isolation to determine failure modes and the effect of end boundary conditions.
- Create a FE model of the full sub-structure shown in Figure 1.1.
- Under a variety of fire conditions, predict the deflections of critical parts of the structure over the duration of a fire.
- Determine if the CBS is able to maintain sufficient structural strength during a fire to avoid sudden failure or collapse.
- Give performance-based recommendations for design considerations, which increase the fire resistance, whilst balancing safety and cost.

1.3 Scope

This thesis forms part of a larger project investigating the fire resistance of the CBS. Different students have focused on other aspects of the problem. This thesis is strictly investigating the *structural* behaviour at elevated temperatures, and does not include any direct thermal analyses i.e. heat transfer. The thesis of Hendrix Marx (Marx, 2018) fulfills this role, and predicts the temperature of the steel sections within the sandwich floor under a variety of fire loads. Thus, these predicted steel temperatures serve as a direct input into the structural FE models presented in this thesis. This process will be explained in greater detail in Chapter 5.

In this research, a series of FE models are used to describe the structural behaviour of the CBS in a fire. However, no physical fire testing of structural elements was performed. Ultimately, this will most likely be necessary if the fire resistance of the CBS must be proven. Whilst numerical modelling is a powerful tool, it cannot reproduce all the complexities of a real fire that can only be simulated in a physical fire test. Nevertheless, the numerical models presented in this work serve as a first-step in determining the fire resistance, and will be able to better inform the design of any future phyiscal tests.

The majority of fire scenarios that are presented in this thesis are based on the ISO 834 standard fire. A single parametric fire is also utilised (the difference between various design fires is discussed further in Section 2.3). It will be shown that a standard fire is not realistically representative of most typical real fires in structures. However, as a long-standing international benchmark, the standard fire forms the basis of any structural fire investigation. Furthermore, in the legislative environment, all fire protection measures must be specified according to the standard fire. Thus, despite being unrealistic, the standard fire is still useful and is used extensively in this project. Nevertheless, a parametric fire scenario is used as well, and arguably gives a better representation of the actual behaviour of the structure in a fire. In future research, when conducting a full-scale fire experiment, the CBS will be subjected to a real fire which will address this shortcoming.

1.4 Thesis layout

Chapter 1 - Introduction: Introduces the problem statement, research goal and scope of this thesis.

Chapter 2 - Literature review: Literature is reviewed to form the basis of knowledge that is required for an understanding of the work presented in this thesis. This includes the science of fire dynamics, the field of structural fire engineering, the behaviour of structural steel under elevated conditions, physical testing and numerical modelling of structures in fire.

Chapter 3 - SAISC cellular beam structure: The novel cellular beam structure (CBS) that this thesis is focused on is discussed in greater detail. The background and motivation for the new concept are discussed, after which the technical details are given. This includes an overview of the design methodology, which is used for an explanation of the structural system. Finally, the terminology used in this thesis for different structural members is introduced.

Chapter 4 - Finite element modelling validation: This chapter summarises the validation process that includes three separate finite element (FE) modelling benchmark studies. These studies were specifically chosen to incorporate important factors that affect structures in fires, such as material and geometrical non-linearity, time-dependent forces, complex boundary conditions and post-buckling behaviour. Modelling results are compared to the published data to validate the modelling techniques used in this research.

Chapter 5 - Single element modelling: Eighteen FE models of isolated single structural elements of the CBS, with various end boundary conditions, are presented in this chapter. An overview of the thermal analysis that provides the steel temperatures for this work is also given. The FE modelling input parameters are summarised for each model, followed by an analysis of results under three fire loads: (a) a standard fire with the fire-rated ceiling remaining intact, (b) a standard fire with the ceiling having failed, and (c) a parametric fire.

Chapter 6 - Global structural modelling: Nine FE models of a single sub-structure of the CBS, as shown in Figure 1.1 above, are presented in this chapter. The chapter begins by summarising the FE modelling input parameters, after which the results are analysed under three possible fire scenarios: (a) a single internal secondary beam is heated, (b) the central module of the CBS is heated, and (c) the entire sub-structure is heated. Each fire scenario is tested under the three fire loads from Chapter 5.

Chapter 7 - Conclusions and recommendations: The final chapter begins by providing an overview of the entire thesis, summarising important aspects covered. Thereafter, a summary of the findings deemed most significant is given. Based on the findings, design considerations to improve the fire resistance of the CBS are discussed. Finally, recommendations for future research are made.

1.5 Conclusion

The introduction chapter has briefly introduced the problem statement of this thesis, and listed the goal and objectives of this research, which will be addressed in the remaining chapters. Thereafter, the scope of the work was discussed, which was followed by an overview of the thesis, that guides the reader through the chapters that follow.

Chapter 2

Literature review

2.1 Introduction

This literature review aims to provide the specific knowledge and theory that is required to understand the remaining chapters. Firstly the fundamental principles of fire dynamics are covered. Thereafter, the field of structural fire engineering is introduced with important concepts being discussed. This is followed by a description of the behaviour of structural steel under fire conditions. Finally, physical fire tests, as well as global structure modelling using numerical methods, are discussed as ways of predicting fire behaviour.

2.2 Fire dynamics

Fire has been an integral part of humankind's development and is so ubiquitous that most people have a basic intuitive understanding of how a fire works. However, upon closer inspection it becomes clear that fire dynamics is a complex field with many facets and variables. A fire is the manifestation of a chemical reaction, but the nature of the fire is often more dependent on the physical and mechanical properties of the elements involved. The environment in which the fire takes place also plays an important role (Drysdale, 2011). A fair grasp and understanding of fire dynamics is of paramount importance for the fire engineer to be effective (Buchanan and Abu, 2017). For a comprehensive understanding of fire dynamics consult Drysdale (2011).

2.2.1 Combustion

Fire is the product of the chemical reaction known as *combustion*. Combustion involves a fuel reacting with oxygen to give off combustion products and release heat. The vast majority of fires, especially in structures, have carbon-based fuels. An important fact to recognise, especially so because it is not necessarily obvious, is that for any flame to occur all fuels, be they liquid or solid, must

first transform into gases before they can burn. With heat a liquid will simply evaporate thereby giving off a gas, but a solid must first undergo a chemical decomposition known as *pyrolysis* to burn. This is a complex process, but essentially it involves particles with a low molecular weight near the surface reaching a volatile state, which allows them to evaporate and combust. This requires substantially more energy than evaporation, and thus the surface of a solid must first attain a high temperature of approximately 400°C or more to pyrolise (Drysdale, 2011).

According to Drysdale (2011), the rate of heat release in a fire is a more important factor than the temperature itself. Furthermore, Buchanan and Abu (2017) state that this rate is entirely dependent on the nature of the fuel, the size and the heat of the fire, and the amount of oxygen available. The Fire Triangle in Figure 2.1 is a good schematic portrayal of this relationship. Without any one of these crucial components a fire is not able to sustain itself or grow. In some cases this is intuitively obvious, for instance the simple fact that one has to keep adding wood (fuel) if one wants to stay warm around the campfire. In other cases this may be counter-intuitive. Take for instance a fire in a farm shed with a light roof. As the fire gets larger and hotter it eventually burns through the roof, thereby allowing a much larger amount of air (containing oxygen) to enter the burning space. One might expect the increase in ventilation to allow the fire to burn even hotter. However, using fire dynamics it becomes clear that this is not necessarily true. The absence of a roof will indeed increase the ventilation, but it will also allow large amounts of heat to escape, which is one of the components of the Fire Triangle. Hence it is very likely that the heat of the fire will drastically reduce and the rate of heat release, previously identified as a decisive factor, will subsequently also decrease. This example serves to emphasise how critical it is that all the various components of any fire need to be thoroughly investigated for a clear understanding thereof.

Figure 2.1: The Fire Triangle (Powell, 2017)

2.2.2 Heat transfer

The three basic mechanisms with which heat is transferred are conduction, convection and radiation (Drysdale, 2011). These three mechanisms can all play important roles at a given stage or specific location in a fire.

2.2.2.1 Conduction

Conduction controls the manner in which heat is transferred through solids from hotter to colder areas. Conduction occurs as heat flows through the solid due to free electrons that interact with each other within the structural lattice (Drysdale, 2011). This is analogous to the flow of electricity and therefore, as a general rule, good electrical conductors are good heat conductors as well. Solids that lack free electrons make excellent thermal insulators, as the heat is transferred through mechanical vibrations of the molecules. This is a far less efficient process.

2.2.2.2 Convection

Convective heat transfer involves the movement of a fluid (liquid or gas), which transfers heat to or from a solid with which it is in contact. Heat convection is very complex with many facets, only a few of which are relevant to structural fires, and is usually not critical for structural fire engineering (Wang *et al.*, 2013).

2.2.2.3 Radiation

Radiation is the transfer of heat by electromagnetic radiation. No solid or fluid medium is required for these waves to travel (Drysdale, 2011). The heat energy emitted is dependent on the temperature to the 4th order. In other words, as a fire gets hotter and hotter, radiation quickly becomes increasingly active. Heat from the sun is emitted through radiative heat to warm the Earth (more than a million kilometres away) through the vacuum of space.

2.2.3 Compartment fires

Fires that occur inside enclosures often achieve much higher temperatures than fires in the open. This is due to radiative feedback which reflects large amounts of heat back at the fire. *Flashover* can occur, which is defined as "the transition from a localized fire to the general conflagration within a compartment when all fuel surfaces are burning" (Drysdale, 2011). This is associated with a very sudden and extreme increase in temperature. For this to happen the room temperature must be high enough that all combustible materials reach their pyrolysis temperature, thereby releasing a surplus of combustible gases into the room. The inferno that ensues fills the entire volume with flames. At this

stage the fire is no longer limited by the amount of fuel but by the amount of oxygen available. This is especially evident as flames emanate from doors and windows in search of oxygen. Afterwards, when most of the fuel has been consumed, the fire enters a decay phase with decreasing temperatures. A typical time-temperature relationship for a compartment fire is shown in Figure 2.2. Note the temperature spike during flashover.

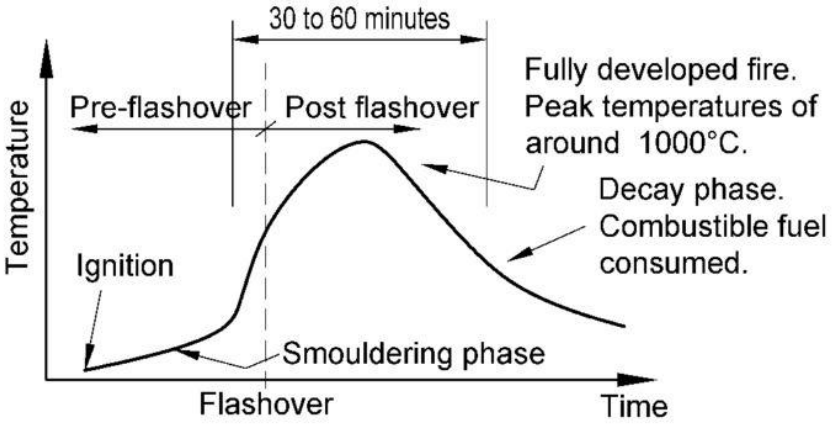

Figure 2.2: Typical time-temperature behaviour of a real fire (Walls, 2016)

Structures are inherently compartmentalised and the *post-flashover* phase is of main concern to the structural fire engineer (Buchanan and Abu, 2017). During this phase the temperatures are high enough to significantly alter the material properties of building materials, thereby directly threatening the stability of the structure. At this point human survival within the compartment is highly unlikely due to the extreme conditions (Drysdale, 2011). However, occupants within the rest of the building and the structure as a whole can still be saved. What remains is to ensure the structural strength to prevent disproportionate damage or total collapse, and to maintain integrity to prevent the spread of fire to adjacent compartments.

2.3 Structural fire engineering

This section aims to provide a better understanding of structural fire engineering by reviewing key concepts. The significance and meaning of fire safety in general is introduced, after which the basis of design of structural fire engineering is discussed. Thereafter the *standard fire*, an essential building block of fire engineering, is explained. Finally, the current competing design methodologies of prescriptive and performance-based design are analysed and contrasted with one another.

2.3.1 Fire safety

Although the probablity of fires breaking out in structures may be very low, the potential for harm is high enough that neglecting to consider fire safety can result in disastrous consequences. Fire safety design attempts to mitigate this risk through multiple layers of protection. Buchanan and Abu (2017) state that "the primary goal of fire protection is to limit, to acceptable levels, the probability of death, injury, property loss and environmental damage in an unwanted fire".

Fire protection is usually designed as a combination of active and passive fire protection measures (Buchanan and Abu, 2017). Both systems are designed to limit the growth of fires and prevent harm to people, the structure and possibly the environment. *Active protection* requires some kind of activation in the event of a fire by a person or automatic system. Examples include fire brigades, sprinkler systems and smoke extraction fans. *Passive protection* is permanently built into the structure and thus requires no activation. This is generally achieved through the choice of fire-resistant building materials and structural assemblies that resist fire growth and structural collapse. Structural fire engineering is intrinsically focused on the structure itself, and thus deals almost exclusively with passive protection measures (discussed further in Section 2.4.5).

2.3.2 Introduction to structural fire engineering

Fire safety is a large field combining many different disciplines and professions such as fire chiefs, fire safety officers and mechanical fire engineers, amongst others. Structural fire engineering is a relatively new development that combines the two older disciplines of structural engineering and fire engineering to better understand and enhance the performance of structures under fire conditions (Lennon, 2011). Thus, structural fire engineering focuses on the strength and integrity of structures in fire conditions. The ultimate goal in designing a structure for fires is the following deceptively simple design equation:

$$\text{fire resistance} > \text{fire severity} \tag{2.3.1}$$

Fire resistance measures the ability of a structure to withstand a fire. Fire resistance has three failure criteria: stability, integrity and insulation (Buchanan and Abu, 2017; Lennon, 2011). If any of these criteria are not met the fire resistance is insufficient and the structure is compromised. *Stability* refers to structural elements remaining strong enough to bear loads and prevent collapse. To determine this, general structural design methodology is used, with adaptations made to account for the effects of elevated temperatures. The US National Institute of Standards and Technology (NIST, 2010) identify the following key differences between fire- and ambient design:

- "The applied loads are less.
- Internal forces may be induced by thermal expansion.
- Strengths of materials may be reduced by elevated temperatures.
- Cross section areas may be reduced by charring or spalling.
- Smaller safety factors can be used because of the low likelihood of the event.
- Deflections may be important as they may affect strength and global stability.
- Different failure mechanisms need to be considered."

The *integrity* and *insulation* of barriers in the building prevent the spread of fire. *Integrity* refers to cracks or gaps forming which allow flames and hot gases to move between compartments. Sufficient *insulation* must be provided by compartment barriers to avoid the surface temperature of the cool side exceeding that which can initiate a fire. This is usually conservatively limited to an average increase of the initial temperature by 140°C, or 180°C at a single point (ECCS, 2001).

The *fire severity* is a measure of the intensity of a fire i.e. what temperatures will be reached, and for how long the structure will be exposed to these conditions. This is difficult to quantify due to the complexity of fire dynamics. Various approaches of greatly differing intricacy are possible and are largely governed by the legislative environment (Buchanan and Abu, 2017). Commonly the standard fire, also called the ISO 834 standard fire curve (ISO, 1999), is used which is a highly simplified approach (discussed in Section 2.3.3). However, structural building codes such as EN 1991-1-2 (CEN, 2002) are increasingly allowing for more advanced methods such as parametric and 'real' fires (discussed in Section 2.3.5)

Structural engineering commonly uses various limit state criteria for the design of structures e.g. ultimate and serviceability. Similarly, the fire limit state (FLS) is used in structural fire engineering, and generally entails much lower partial load factors. Significantly, imposed loads are usually factored *down*, as the chance of a characteristic design imposed load occurring during the rare event of a fire is low. South African design codes have not yet incorporated the FLS. However, Walls *et al.* (2014) and Walls and Botha (2016) have recommended a partial load factor of 1.0 for permanent loads, and 0.5 for imposed loads, for use in South Africa, based upon the Canadian code, CSA-S16 (CSA, 2009).

2.3.3 Standard fire curve

The standard fire is arguably the most commonly used model to estimate temperatures in burning buildings. It has a long history originating in tests undertaken during the early 20th century (Wang *et al.*, 2013) It is based on the following logarithmic relationship:

$$T = 20 + 345log(8 \times t + 1) \tag{2.3.2}$$

Where:

$$T = \text{gas temperature } (^{\circ}\text{C})$$
$$t = \text{time in minutes}$$

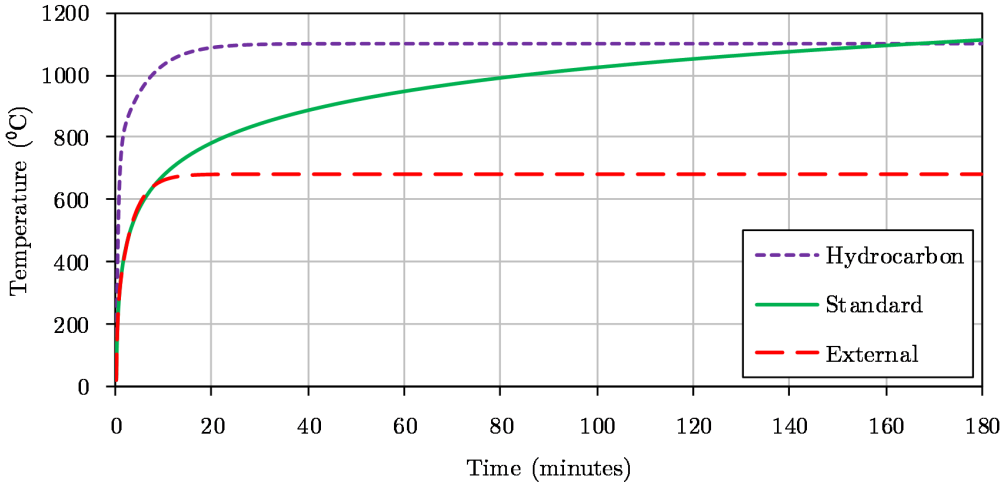

Figure 2.3: Typical time-temperature curves for a standard, hydrocarbon and external fire

Variations of the standard fire curve exist for hydrocarbon fires, where higher fuel loads are expected, and external fires, for fires in the open. These are all shown in Figure 2.3. However, the validity of all three curves is questionable as they assume indefinitely increasing temperatures and do not take into account any of the physical parameters that affect a fire, such as ventilation or fuel load. As such the standard fire is heavily criticised for being unscientific and archaic. Bisby *et al.* (2013) state that "the standard temperature-time curve is not representative of a real fire in a real building - indeed it is physically unrealistic and contradicts available knowledge of fire dynamics". Despite these serious shortcomings, the standard fire is still ubiquitous in fire design methodologies and remains a useful benchmark. In a complex field with a multitude of variables, the standard fire is easy for all parties to understand and fosters collaboration, even if it is technically incorrect.

2.3.4 Prescriptive fire design

Prescriptive design methods are a set of simple rules that are applied in a 'deemed-to-satisfy' manner. These are based on a long history of development, mostly based on experience, and have been refined over the years to the current state. Using these methods it is possible to quickly determine the necessary fire protection for any given material for any given fire severity. The data is often tabulated in building codes and requires little understanding of actual fire behaviour to implement in a quick and easy fashion. However, critical factors such as global structure interaction are entirely neglected, and so prescriptive design has come under criticism for being over-conservative, unscientific and inflexible (University of Edinburgh, 2000). Gillie (2009) even states that these methods can be *unconservative* and thus possibly unsafe. Nevertheless, the reality is that prescriptive design has been widely used and has been shown to perform satisfactorily under fire conditions in the vast majority of cases, most likely due to their conservative nature (Wang *et al.*, 2013). Ultimately, prescriptive methods remain a highly useful tool but should be used with their considerable drawbacks in mind.

2.3.5 Performance-based fire design

Performance-based fire design evolved more recently as fire engineers sought to find a holistic approach to fire design based on a sound scientific understanding, rather than simple prescriptive rules. In this approach the standard fire curve, already discussed as being wholly unrealistic, is replaced by more specialised fire curves that are based on an analysis of the likely fire environment. A good example is the 'parametric' fire from EN 1991-1-2 (CEN, 2002) that gives a more realistic time-temperature curve for any combination of fuel load, ventilation and wall lining materials (this requires detailed calculations that are not further discussed, as it does not fall within the scope of this literature review, for more information see Annex E of 1991-1-2 (CEN, 2002)). Thereafter, scientific and engineering principles must be applied, sometimes in a creative and unguided way, to attempt to understand the structure's behaviour under the fire conditions. The open-ended approach can take into account important factors such as global structural stability, the interaction between building elements and varying end-boundary conditions under a variety of fire conditions. This can lead to a more flexible design that is safer and/or more economical. However, the inevitable complexity that arises requires considerably more computational effort and technical know-how than a simple prescriptive design, and so the use of performance-based design should be carefully considered and justified (Wang *et al.*, 2013).

2.4 Steel in fire

This section provides an overview of how structural steel behaves under fire conditions. Firstly, the relevant material properties are discussed and how they change with elevated temperatures. Thereafter, the behaviour of steel beams is explored with a detailed focus on cellular beams. Next, the importance of steel connections and the applicability of various connection types for fire are examined. Finally, various passive protection options and their primary advantages/disadvantages are discussed.

2.4.1 Material properties

The material properties of steel are highly dependent on temperature, with the structural strength, stiffness and, in the case of fire engineering, the coefficient of thermal expansion being of interest to the structural engineer. These relationships are not linear, but generally an increase in temperature will cause a reduction in strength and stiffness, whereas the coefficient of thermal expansion remains relatively constant. See Figure 2.4 for examples of steel structures after a fire event. Significant research has been done to understand these complex phenomena and is incorporated into design standards such as *Eurocode 3* (CEN, 2005) and the *AISC Specification for Structural Steel Buildings* (AISC, 2010). These documents provide the engineer with the necessary tools to accurately define the stress-strain-temperature properties of structural building materials at elevated temperatures. The Eurocode suite of standards is a leading authority and is widely used in literature (e.g. University of Edinburgh (2000), Hicks *et al.* (2012) and Najafi and Wang (2016)). This research also adopts the Eurocode (EN) guidelines, as discussed below.

(a) 'Squashed' steel column (courtesy of Ali Moradi)

(b) Beams from the Cardington tests showing severe midspan deflections, and web buckling close to supports (Lamont, 2001)

Figure 2.4: Examples of steel structures after a fire

2.4.1.1 Stress-strain-temperature relationship

The effects of creep in steel are accelerated at higher temperatures and should not be ignored. However, these effects are implicitly incorporated in the Eurocode stress-strain relationships (Wang *et al.*, 2013). The stress-strain formulae shown in Figure 2.5 retain the initial linear-elastic range equivalent to ambient temperature. Thereafter plastic behaviour begins and this relationship becomes increasing non-linear as the temperature increases. Whereas at ambient temperature the curve can be approximated as bi-linear, at high temperatures this is no longer possible and the concept of a *proportional limit*, which defines the onset of plasticity, becomes important. This phenomenon can be seen in Figure 2.6 and is represented by the curve between linear-elastic and perfectly plastic behaviour.

Strain range	Stress σ	Tangent modulus
$\varepsilon \le \varepsilon_{p,\theta}$	$\varepsilon E_{a,\theta}$	$E_{a,\theta}$
$\varepsilon_{p,\theta} < \varepsilon < \varepsilon_{y,\theta}$	$f_{p,\theta} - c + (b/a)\left[a^2 - (\varepsilon_{y,\theta} - \varepsilon)^2\right]^{0,5}$	$\frac{b(\varepsilon_{y,\theta} - \varepsilon)}{a\left[a^2 - (\varepsilon_{y,\theta} - \varepsilon)^2\right]^{0,5}}$
$\varepsilon_{y,\theta} \le \varepsilon \le \varepsilon_{t,\theta}$	$f_{y,\theta}$	0
$\varepsilon_{t,\theta} < \varepsilon < \varepsilon_{u,\theta}$	$f_{y,\theta}\left[1 - (\varepsilon - \varepsilon_{t,\theta})/(\varepsilon_{u,\theta} - \varepsilon_{t,\theta})\right]$	-
$\varepsilon = \varepsilon_{u,\theta}$	0,00	-
Parameters	$\varepsilon_{p,\theta} = f_{p,\theta}/E_{a,\theta}$ $\varepsilon_{y,\theta} = 0,02$	$\varepsilon_{t,\theta} = 0,15$ $\varepsilon_{u,\theta} = 0,20$
Functions	$a^2 = (\varepsilon_{y,\theta} - \varepsilon_{p,\theta})(\varepsilon_{y,\theta} - \varepsilon_{p,\theta} + c/E_{a,\theta})$ $b^2 = c(\varepsilon_{y,\theta} - \varepsilon_{p,\theta})E_{a,\theta} + c^2$ $c = \frac{(f_{y,\theta} - f_{p,\theta})^2}{(\varepsilon_{y,\theta} - \varepsilon_{p,\theta})E_{a,\theta} - 2(f_{y,\theta} - f_{p,\theta})}$	

Figure 2.5: Stress-strain formulae for carbon steel (CEN, 2005)

To construct a stress-strain curve with the equations presented, the elastic modulus, limit of proportionality and yield strength are needed. For this the Eurocode supplies reduction factors relative to the ambient properties, as shown in Figure 2.7. This graph makes it clear how drastically the properties of structural steel change at higher temperatures. Melting only occurs at about 1500°C, but steel structures will likely fail at much lower temperatures. For instance, the yield strength drops from 100% ambient-temperature strength at 400°C to 23% at 700°C. At 900 °C only 6% remains. Finally, at 1200 °C, steel has negligible strength.

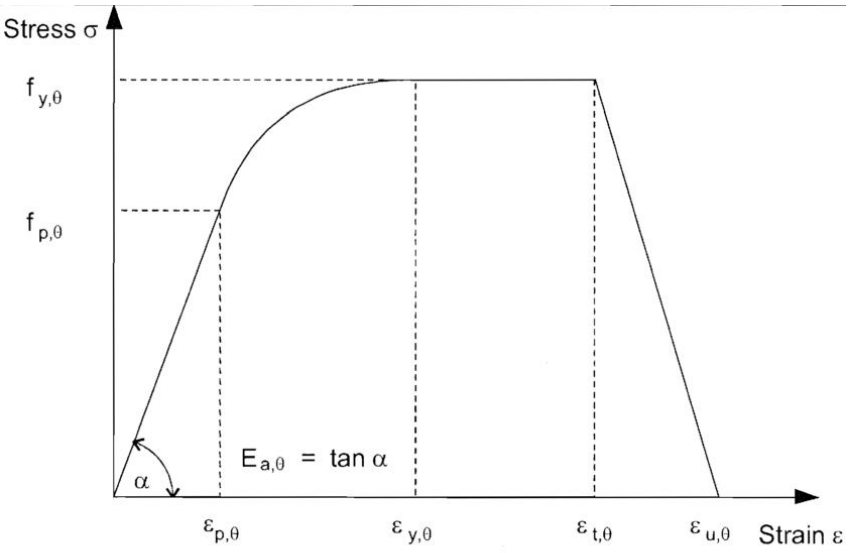

Key:

$f_{y,\theta}$	effective yield strength;
$f_{p,\theta}$	proportional limit;
$E_{a,\theta}$	slope of the linear elastic range;
$\varepsilon_{p,\theta}$	strain at the proportional limit;
$\varepsilon_{y,\theta}$	yield strain;
$\varepsilon_{t,\theta}$	limiting strain for yield strength;
$\varepsilon_{u,\theta}$	ultimate strain.

Figure 2.6: Schematic stress-strain relationship for carbon steel at an elevated temperature (CEN, 2005)

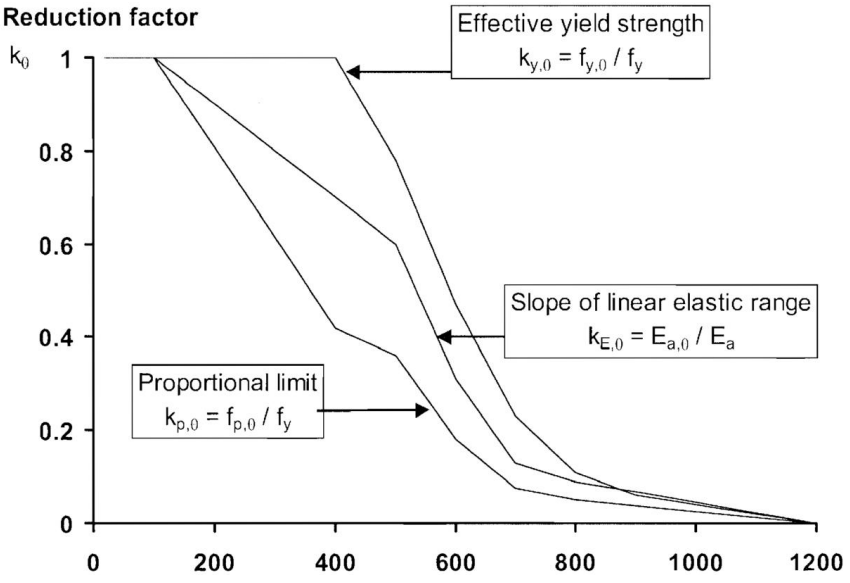

Figure 2.7: Reduction factors for the stress-strain relationship of carbon steel at elevated temperatures (CEN, 2005)

2.4.1.2 Coefficient of thermal expansion

The thermal elongation of steel shown in Figure 2.8 is given in the Eurocode by the following formulae:

$$20°C \leq T < 750°C : \delta L/L = 1.2 \times 10^{-5} \times T + 0.4 \times 10^{-8} \times T^2 - 2.416 \times 10^{-4} \tag{2.4.1}$$

$$750°C \leq T \leq 860°C : \delta L/L = 1.1 \times 10^{-2} \tag{2.4.2}$$

$$860°C < T \leq 1200°C : \delta L/L = 2 \times 10^{-5} \times T - 6.2 \times 10^{-3} \tag{2.4.3}$$

Where:

L = length at 20°C
δL = elongation due to change in temperature
T = temperature (°C)

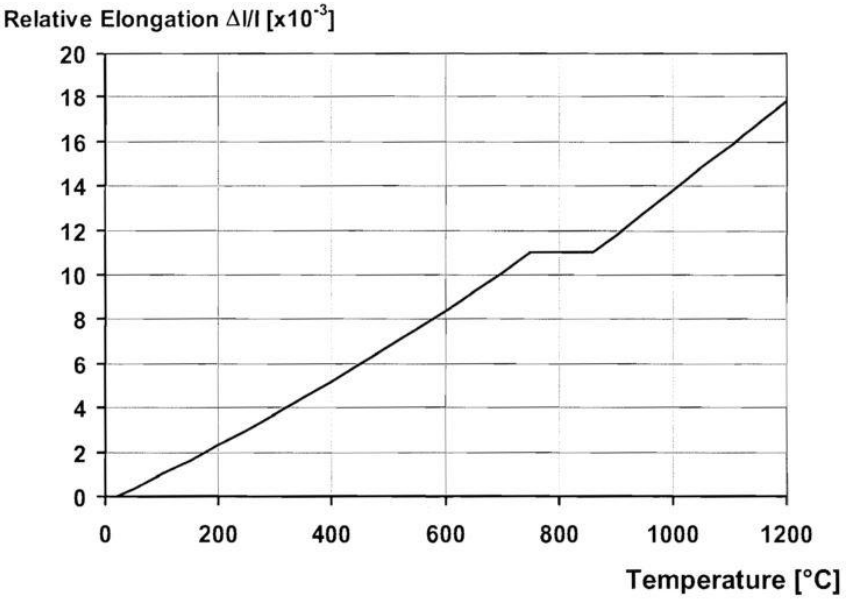

Figure 2.8: Relative thermal elongation of carbon steel as a function of the temperature (CEN, 2005)

From the slope of the elongation-temperature curve, one obtains the coefficient of thermal expansion. Alternatively, a constant value of 1.4×10^{-5} can be used as recommended by the European Convention for Constructional Steelwork (ECCS) (ECCS, 2001).

2.4.2 Steel beams

The behaviour of steel beams in fire conditions has received considerable attention across the world. Initially the research focused on simply supported beams with no axial restraint. However, this is not a good representation of reality, as the surrounding structure will almost certainly resist thermal strain and the connections will provide some level of support. Researchers began to investigate this gap in knowledge and concluded that neglecting these important factors resulted in conservative results. In fact, continuous steel beams can be very robust and resist far higher temperatures than an individual element analysis would suggest, mainly due to a greater amount of redundancy. This is true provided that connections provide axial restraint and are flexible enough to allow large deflections (Liu *et al.*, 2002; Yin and Wang, 2004; Li and Guo, 2008).

A common pattern has been observed in research experiments when axial restraint is provided. Initially the beam goes into compression as it heats up and thermal expansion is prevented by the surrounding structure. This 'squashing', together with the steadily decreasing bending strength, eventually causes the beam to yield and buckle. This results in a rapid drop in axial force as large vertical deflections develop. At certain points the effect of vertical deflection can exceed that of the thermal expansion and the beam enters catenary action i.e. tension. For this reason it is critical that connections are as flexible as possible and able to resist tension. In fact, Yin and Wang (2004) state that "if a realistic amount of axial restraint stiffness is available at the beam ends and fire engineering design is not concerned with the amount of large deflection in a beam, it is possible that the beam can have virtually unlimited survival temperature".

2.4.3 Cellular beams

The use of cellular[1] beams in the construction industry is becoming increasingly widespread due to the advantages of built-in servicing ducts and the ability to achieve long spans, as well as the aesthetic appearance (Najafi and Wang, 2016). Figure 2.9 illustrates how a cellular beam with circular cells is created from a regular I-beam.

2.4.3.1 Cellular beam failure modes

An important consideration when using cellular beams is the presence of additional failure modes due to the influence of the cell size and spacing. Kerdal

[1]Historically the term 'castellated beam' was commonly used. This refers to a beam with a one-stage cutting process that results in a beam with hexagonal holes in the flange. 'Cellular beam' is a more modern term and can refer to any shape of hole or 'cell', with the circular cell becoming increasingly popular.

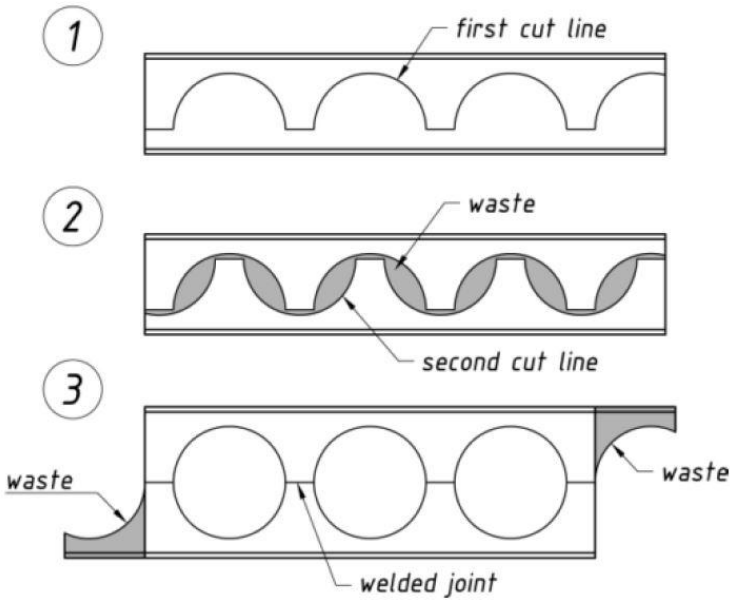

Figure 2.9: Two-stage cutting and welding process to create a cellular beam (Kuchta and Maślak, 2015)

and Nethercott (1984) reviewed and summarised previous studies investigating the structural failure modes of castellated beams. When compared with the more recent work of Kuchta and Maślak (2015) it can be be seen that these are the same as for cellular beams, with minor differences in stress distributions. A brief description of the separate failure modes is given below, but without detailed design procedures for the sake of conciseness. These modes do not act in isolation and combinations are possible (Kerdal and Nethercott, 1984).

Formation of a flexure mechanism: In the case of a high bending moment the T-sections above and below a cell can can yield in normal compression and tension and form a plastic hinge. This is very similar to the plastic yielding of a regular steel beam. According to Kerdal and Nethercott (1984), the resistance of a castellated beam can be simply calculated using the plastic moment of a section passing through the centre of the cell i.e. the weakest section. They comment that this is unlikely to happen in discretely braced beams with lateral-torsional buckling likely occurring before the full plastic moment is reached.

Lateral-torsional buckling: The compression flange of a cellular beam can exhibit lateral torsional buckling similarly to regular beams. Both Kerdal and Nethercott (1984) and Kuchta and Maślak (2015) agree that the standard beam formulae found in design codes can accurately be used if the section properties used are calculated for a section passing through the centre of a cell i.e. the area of material at circular openings must be excluded from cross-sectional properties.

Formation of Vierendeel mechanism: It has been experimentally shown that the area around a cell can act like a Vierendeel truss (Kuchta and Maślak, 2015). A Vierendeel truss is an unbraced rectangular truss where the nodes must resist moments. A mechanism can form due to a combination of moment and shear, especially if there are high shear forces present. The nodes yield, forming a four-hinge failure mechanism as shown in Figure 2.10a. The resistance to this type of failure is quite complex as the stress distribution and subsequent location of the plastic hinges are dependent on the interaction between the moment and the shear. Kerdal and Nethercott (1984) state that this type of failure is more likely to develop in beams with a short span, a long weld and a shallow T-section.

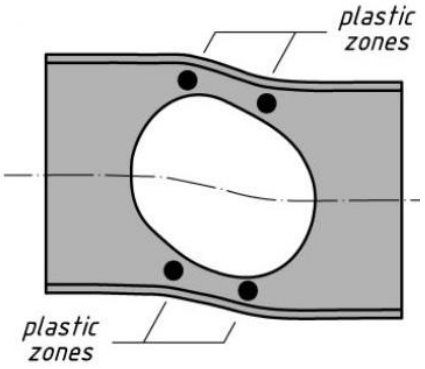

(a) A Vierendeel mechanism in a cellular beam (Kuchta and Maślak, 2015)

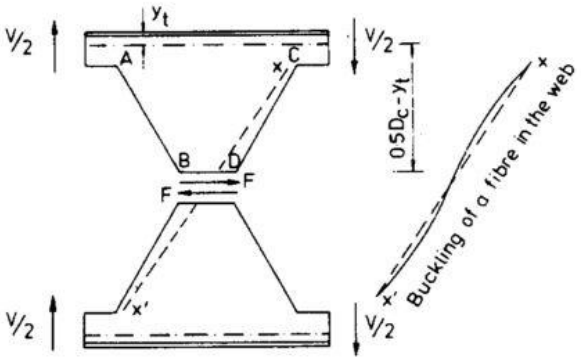

(b) Web post buckling due to shear (Kerdal and Nethercott, 1984)

Figure 2.10: Failure mechanisms of cellular beams

Rupture of a welded joint: If the distance between the cells is small enough the welded joint may not be able to withstand the internal shear force acting parallel to the weld (force 'F' Figure 2.10b). This is simply checked using the calculated stress and standard weld resistance codes (Kuchta and Maślak, 2015).

Web-post buckling due due to shear: The shear force that can cause the weld to rupture can also cause additional in-plane bending in the web-post. Figure 2.10b shows how edge A-B is in tension whilst edge CD is in compression and how the web-post can thus buckle along the diagonal line XX'. This failure mode is again dependent on a number of factors, with the geometry playing a crucial role in the determination of the shear resistance.

Web-post buckling due to compression: Under a concentrated load or high compressive forces a web-post can become unstable and buckle laterally. This can be likened to the web crippling of a regular beam. The resistance can be determined by considering the web-post as a column, but choosing an accurate effective length factor is difficult as the degree of fixity is a complex function of the highly variable geometry (Kerdal and Nethercott, 1984). There seems to be no consensus on the matter, with design codes such as the one by Lawson and Hicks (2011) specifying simple formulae and Kuchta and Maślak (2015) referring to two separate methods (both quite complex).

Top-tee buckling: This failure mechanism is specific to cellular beams in fire and is discussed in section 2.4.3.2 (immediately below).

2.4.3.2 Cellular beams in fire

Cellular beams are still relatively new to the industry and there are comparatively few studies of axially restrained cellular beams at elevated temperatures, especially for beams where composite behaviour is not considered. Najafi and Wang (2016) performed one such study which examined the effects of key parameters such as opening shape, size and position, load ratio, axial restraint and temperature distributions. An additional failure mechanism was identified whereby the top tee-section buckling plays a critical role. If the openings are large and placed at points with a high bending moment, the axial load in the top tee-section (assuming positive bending moment) will cause a local vertical buckling in the tee. Essentially the top-tee acts as a small column to support the moment couple and has a capacity dependent on its slenderness. However, the study found that beams with circular or small rectangular openings do not tend towards this failure mechanism as a plastic hinge or Vierendeel mechanism will form before top-tee buckling.

Nadjai *et al.* (2007) performed a study on composite cellular floor beams at elevated temperatures. A full shear connection was used and the test was specifically designed to induce web-post buckling. It was found that again the approaches in codes struggled to accurately predict this behaviour. Finite element (FE) modelling proved very successful in describing the behaviour with a good correlation between models and four full-scale test specimens. This study fell within the FICEB+ project funded by the Research Fund for Coal and Steel which supported a swathe of research attempting to understand cellular beams in fire. Their final publication, by Vassart *et al.* (2010), provides guidance for testing, modelling and design and is intended to be incorporated into the Eurocode. Nevertheless, it still seems that simplified design methods for cellular beams under fire conditions are in their infancy and FE modelling should be strongly considered for cellular beams, especially in unprecedented design situations.

2.4.4 Connections

Connections are a crucial part of any structure and their integrity must be protected. Unlike beams that often have some level of redundancy, the consequences of connection failure are potentially catastrophic. This was made clear with the World Trade Centre disaster, where it has been suggested that the failure of connections played a significant role in the progressive collapse (NIST, 2005). At that time there was limited scientific understanding of the behaviour of steel connections in a frame structure under fire conditions, although some investigation had already been carried out by the likes of Burgess *et al.* (1991) and Al-Jabiri (1999).

Since then there has been an increased focus in research into steel connections under fire conditions. One such study was by Wang *et al.* (2013), who conducted an experimental investigation to better understand the fire resistance of steel connections in a frame structure. A "rugby goalpost" test setup was used, whereby a beam was connected to two columns on either side. This allowed the connection type as well as the level of axial restraint to be investigated. Fin plate, web cleat, flush end plate, flexible end plate and extended end plate connections were tested as well as two different sets of columns. Importantly, it was found that all the connections only failed when the beam was experiencing catenary action, which implies that adequate tensile capacity is key. When connections did fail, it was due to weld failure or stripping of bolt threads due to the high tensile force developed by a combination of catenary action and hogging moment at the connection. It was found that the web cleat connection was the most robust connection due its flexibility which prevents a build-up of tension. The flush end plate and extended end plate were overly rigid, which attracted large tensile forces in the bolts causing them to strip. Finally, the flexible end plate and fin plate connections behaved poorly due to web shear failure and weld rupture respectively. Figure 2.11 provides photos of these connections after the test had taken place. Ultimately the research indicated that when designing connections for fire, the robustness, i.e. ability to safely undergo large displacements as well as resist tension, is more important than the bending moment resistance.

2.4.5 Passive protection for steel

Buchanan and Abu (2017) provide a comprehensive list of passive protection options for structural steel including:

Board Systems Steel members can be encased with boards made of fire-resistant materials such as calcium silicate or gypsum plaster. The advantage is that these systems are easy to install and can be made to look aesthetically pleasing, but they are more expensive than spray-on products.

(a) Fin plate

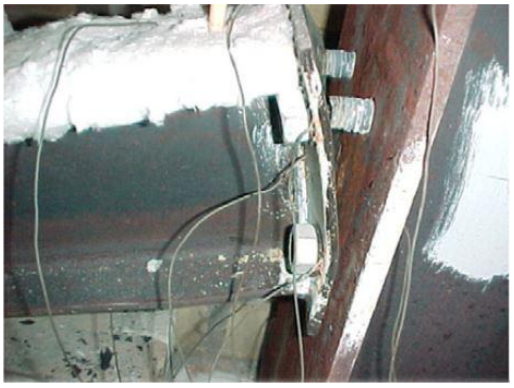

(b) Flush end plate

(c) Flexible end plate

(d) Extended end plate

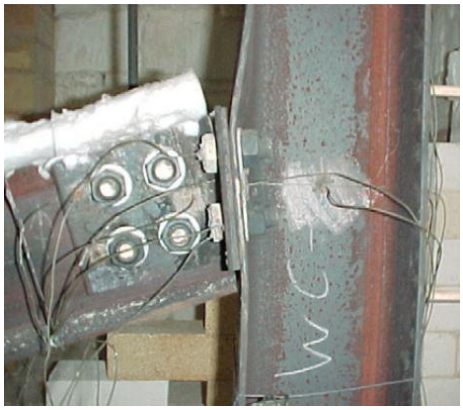

(e) Web cleats - side view

(f) Web cleats - top view

Figure 2.11: Steel connections after being exposed to a fire (Wang *et al.*, 2013)

Spray-on Systems These are propriety products (often vermiculite-based) that are sprayed onto steel members to provide a fire-resistant layer. The process is quick and relatively cheap, but it is also wet and messy and gives a finish that is generally not aesthetically pleasing. Spray-on systems are often used for steel sections that will not be visible after construction. The robustness and durability of these systems is critical for effectiveness.

Intumescent Paint This is a special type of paint that experiences a large increase in volume under an applied heat. In a fire, this results in a thick char layer with good insulation properties forming on the steel surface. The major advantages are that the application process is quick, the paint takes up minimal space and the visual impact is low i.e. steel members do not have to be hidden. Conversely, intumescent paints are very expensive and have questionable durability for external application.

Alternatives Other systems that have been shown to be effective, but are less widely used, are only briefly discussed here. Concrete can be used to completely encase steelwork, or to fill hollow sections. This is usually a very costly solution. Timber can be used similarly to regular fire-resistant boards. An innovative system is filling hollow sections with water, but this requires a plumbing system and intricate connection details. Finally, Buchanan and Abu (2017) add that flame shields can be used to protect steelwork from radiation.

A few practical considerations regarding fire protection can be taken from the Cardington Main Report (University of Edinburgh, 2000). These are informed by structural fire engineering, but are aimed at designers and builders as a practical design guidance for steel structures. These include: (a) pay attention to detailing, (b) fire protect all columns and edge beams and (c) ensure flexible beam-column connections.

Unprotected steel structures are generally less fire-resistant than reinforced concrete or timber structures (Buchanan and Abu, 2017). However, if steel structures are well-designed for fire, and passive protection is specified using performance-based design (possibly even leaving some members completely unprotected), research has shown that steel is robust and can have an inherent resistance to fire (Liu *et al.*, 2002; University of Edinburgh, 2000). However, in a prescriptive design environment all steelwork is often provided with passive protection. This is a blanket solution that is costly and possibly over-conservative. Through selective protection of critical members identified through rational design, significant savings can be made on passive fire protection (Hicks *et al.*, 2012). Performance-based design for structural steel is supported in contemporary design codes such as the Eurocode discussed in Section 2.3.5.

2.5 Physical fire testing

2.5.1 Standard fire testing

Standard fire tests are used very commonly to determine the fire resistance of structural elements, materials and passive fire protection methods. These are relatively simple tests specified by international standards such as ISO 834 (ISO, 1999). They take place within a furnace which can simulate the temperature-time history of a standard fire curve (discussed in Section 2.3.3). During the test, the applied load, temperature and deformation are monitored, thereby giving an indication of the fire resistance. Standard tests usually have size limitations due to the difficulty in attaining, and maintaining, such high temperatures, and so are limited to testing single structural elements or perhaps smaller assemblies. The end boundary conditions are often approximated as fully-fixed or pinned (Buchanan and Abu, 2017).

There is a growing consensus that standard fire tests can be misleading and insufficient to describe actual fire performance, as discussed in Section 2.3.3. In a contemporary review of structural fire testing, Bisby *et al.* (2013) agree that standard fire testing has advantages which allow it to be easily reproduced, controlled and used as a comparative test for benchmarking. However, they question its accuracy in determining the real performance of an element in an actual fire. They argue that this is due to the "many inherent problems associated with using simplified single element tests, on isolated structural members subjected to unrealistic temperature-time curves, to demonstrate adequate structural performance in real fires". In other words, there is a successive stacking of oversimplification and inaccuracy which results in final conclusions with suspect meaning. As a case in point, they note that in recent history the structures that have failed in fires did so due to failure mechanisms that could not have been predicted in standard fire tests.

2.5.2 Full-scale testing

The standard fire test has been the status-quo for over a century, but increasingly both the research and regulatory communities are taking note of its inherent inadequacy (Bisby *et al.*, 2013). This has been driven largely as a result of high-profile cases such as the World Trade Centre collapse (Wang *et al.*, 2013). In response there is a shift towards full-scale testing, which is better able to capture the interaction between structural members, identify alternative load carrying mechanisms under fire conditions and analyse the critical role of connections during, and directly after, a fire (Lennon, 2011).

Full-scale tests are, as their name implies, generally much larger than standard fire tests. Entire structural assemblies or sub-assemblies are constructed, and then subjected to a 'real' fire, meaning that an equivalent fuel load is supplied.

Thus these tests try, as much as possible, to replicate the actual conditions that the structure will have to survive in a fire. As in standard fire tests, important parameters such as temperature and deflection are measured at critical points. Over the past few decades, mainly starting in the 80s, there has been an increase in such testing which has resulted in major breakthroughs in scientific understanding. For a comprehensive review of large-scale tests that have taken place, the reader is referred to Bisby *et al.* (2013).

2.5.3 The Cardington tests

The Cardington fire tests that took place from 1994 - 2003 in the U.K. are considered some of the most influential full-scale fire tests to date. An ambitious testing regime on a large scale, it consisted of an eight-storey steel frame structure, a seven-storey reinforced concrete structure and a six-storey timber-framed structure constructed within an unused airship hanger. The findings led to several significant advances by enriching the understanding of whole structure behaviour in a real fire (Wang *et al.*, 2013). A notable finding was that, even under extreme temperatures of 1200°C, no structural collapse was observed in the steel building, even though contemporary design codes predicted collapse at about 680°C (Bailey *et al.*, 1999). Thus the inherent robustness of steel was highlighted and the over-conservative nature of prescriptive design exposed. This is a fine showcase of the potential for full-scale testing to provide insights that standard fire testing would not have been able to provide. The Cardington Main Report can be consulted for an in-depth discussion of the tests (University of Edinburgh, 2000).

2.6 Global modelling of structures in fire

This section firstly aims to motivate the need for global modelling of structures in fire, and thereafter to provide the theoretical background that is necessary to perform such an analysis. The complexity of global modelling is discussed as well as the various approaches that are possible. Two case studies, in which global modelling was implemented successfully, are showcased. Finally, the software options that are available are briefly discussed.

2.6.1 Motivation for global analysis

Through the recent growth in research activity in structural fire engineering there has been a growing recognition of the importance of global modelling (Wang *et al.*, 2013). A contemporary standard design approach is generally based on calculating a design temperature (e.g. with the standard fire curve), determining the reduced material properties and subsequently designing each element in isolation and as simply supported. However, experience from a

number of investigations like those by Usmani *et al.* (2001) and Wang *et al.* (2013) have shown how these approaches inadequately describe the behaviour of a structure in a fire, as discussed in Sections 2.3.3 an 2.3.4. They found that the inherent complexity of the interaction between members requires the whole structure - or at least large parts with applicable boundary conditions - to be modelled for accurate results. Hand calculations often cannot realistically incorporate all these factors, and thus numerical analyses are recommended to produce an accurate prediction of a structure in a fire. In particular, the Finite Element Method (FEM) is widely used as it is currently considered the most advanced tool to describe global structural behaviour (Buchanan and Abu, 2017).

2.6.2 Non-linear behaviour

At ambient temperatures many significant simplifications can often be safely made when modelling a structure (Gillie, 2009). Most structural elements are very stiff which means that small deflections are expected. This negates the need to incorporate geometric non-linearity. Furthermore, a simple material model such as linear-elastic or rigid-plastic is usually chosen which prevents the complications of material non-linearity. This allows for a relatively simple static analysis that nevertheless yields accurate results.

The behaviour of a structure at elevated temperatures does not allow the above simplifications to be made for several reasons. A material's mechanical properties change with high temperatures resulting in a loss of linearity, strength, modulus of elasticity and a clear yield point, as discussed in section 2.4.1. This often results in much larger displacements than at ambient temperatures due to the loss of stiffness and earlier onset of plastic behaviour. Furthermore, thermal expansion can cause large stresses if restrained. In fact, according to Usmani *et al.* (2001), this is the most critical factor in determining a real structure's response to a fire, with the level of restraint influencing the magnitude of stresses. Whereas at ambient temperature a structure under a constant mechanical load can be considered to have resultant constant stresses, the changing thermal load during a fire induces ever-changing stresses. Determining a critical design state is difficult because it is entirely possible that the peak thermal load or material temperature will not equate to the peak stress (Wang *et al.*, 2013). To further complicate matters, some areas may be heating up whilst others cool down, resulting in material properties and stresses changing in different ways within the structure. From the above it is clear that the highly inter-dependent factors involved in a structural fire analysis necessitate the use of material non-linearity, geometric non-linearity and time- and temperature-varying strength if the model is to produce accurate results (Wang *et al.*, 2013; Gillie, 2009).

2.6.3 Uncoupled vs. coupled analyses

The thermal and mechanical analyses of a structure in fire can be either *uncoupled* or *coupled*. This important choice which the analyst must make is dependent on the nature of the problem itself, the required accuracy and available input data (Wang *et al.*, 2013).

In an *uncoupled* analysis, separate models are created for the thermal and mechanical analyses and solved sequentially. First the relevant temperatures are calculated using an applicable thermal model. These temperatures serve as direct input for the mechanical model as predefined temperature states. Thereafter a mechanical load is applied and the stresses and strains within the structure are calculated. This approach has the distinct advantage of computational efficiency as optimal modelling approaches and software are often different for the two types of analyses (Wang *et al.*, 2013). Furthermore, breaking up a complex problem into smaller segments can make a project more manageable and thus easier to work on in a team, with separate groups working on different models.

Alternatively, the analyst can opt for a *coupled* analysis, where a single model is created which incorporates both the thermal and structural behaviour of the structure. This can be required where changing temperatures affect the geometry so significantly that the thermal boundary conditions change. The drawback is that the choice of finite elements becomes complicated with elements requiring both thermal and mechanical degrees of freedom and a mesh that is suitable for both. However, in most cases it has been found that this two-way coupling is not required (Wang *et al.*, 2013).

2.6.4 Mechanical analysis types

In reality a fire takes place over a certain amount of time with thermal loads changing as the fire progresses. However, the nature in which time is modelled varies significantly depending on the mechanical analysis type performed. Three broad categories exist: static, quasi-static and dynamic.

2.6.4.1 Static

A static analysis is both the simplest and most common analysis performed (Wang *et al.*, 2013). The actual physical time over which loads are applied is effectively ignored through the use of sequential load steps. In this way time becomes a non-physical parameter with only the order of steps affecting the output. This simplification is allowable if at every step the change in load is small enough that any inertial forces are negligible, which allows equilibrium to be maintained .

A drawback is that time-dependent effects like inertial forces (due to velocity and acceleration) cannot be modelled as in the case of rapid structural movement. Thus a static analysis is unsuitable if any collapse or loss of equilibrium occurs. Nevertheless, static analyses can still be very valuable to understand structural behaviour in a fire, as they are computationally efficient and able to produce useful results very quickly (Wang *et al.*, 2013).

2.6.4.2 Quasi-Static

In some cases certain time-dependent effects such as creep or local instabilities may arise. A dynamic analysis can however be avoided with a quasi-static analysis. For instance, the local buckling of members, which causes a temporary loss of equilibrium, can be modelled statically through the use of artificial damping. This allows the model to move through a temporary instability with damping that is sufficient to prevent sudden collapse, but small enough to have a negligible effect when the model is stable. This approach is supported in Abaqus, with the *Abaqus Analysis User's Guide* (Abaqus, 2014) stating that this is valid if localised buckling is expected where there is a local transfer of strain energy rather than a global buckling situation. This method has been successfully used by Yin and Wang (2004) and Najafi and Wang (2016). In both cases a viscous damping factor of 1×10^{-10} was chosen through trial and error. The Abaqus user manual recommends that a manual check be performed, in which the total strain energy is compared with the viscous damping energy. Thus, if it is found that a negligible amount of load is carried by the damping, it implies that the effect thereof on the structural behaviour is minimal.

2.6.4.3 Dynamic

In a dynamic analysis, actual time is used which allows inertial forces to be incorporated in the model. This is unavoidable if any type of impact or collapse is to be modelled. Thus, advanced numerical integration schemes are required which satisfy equilibrium incrementally through real time. Of interest here is the benchmark model set up by Gillie (2009), in which both a quasi-static and an explicit dynamic analysis were used to model a structural example. The results were practically identical. This agrees with Wang *et al.* (2013), who state that dynamic analyses have been successfully used to model structures in fire, but should only be used if absolutely necessary as they add significant complexity and computational expense to a model.

2.6.5 Case studies of finite element modelling of structures in fire

The FEM has been successfully implemented in a multitude of cases, including research studies such as the Cardington fire tests (section 2.6.5.1), as well as commercial projects, such as the Britomart analysis (section 2.6.5.2).

2.6.5.1 Cardington fire tests

The prime objective of the Cardington fire tests, as discussed in Section 2.5.3, was to develop rational design guidelines for composite structures based on an understanding of structural behaviour in a fire. A crucial component in this process was the development of rigorous finite element (FE) models that were continuously validated and calibrated using the physical large-scale fire test data. This was done effectively and supports the viability of FE models to accurately describe structural fire behaviour. Based on these models further parametric studies could be conducted to set up a comprehensive set of guidelines. These findings were presented with considerable confidence based on the large research effort involved (University of Edinburgh, 2000).

When modelling a structure, simplifying assumptions need to be made to allow for a model that is computationally feasible. However, it is vital that the structure is not over-simplified as this can lead to an unrealistic model if key phenomena are missed. To help an analyst to find this balance, the following selected simplifications (amongst others) were deemed allowable:

- Geometrically non-linear beam elements may be used.
- The material behaviour at high temperature can be based on any "reasonable" model (such as the Eurocode).
- Elastic-plastic behaviour without softening is sufficient.
- Connections between beams and columns can be modelled as fully pinned provided a sufficiently flexible connections is specified (they recommend partial depth end-plate).
- A lateral restraint boundary condition can be used if there are stiff points within the surrounding (cooler) structure.

With the last two points in mind, it is emphasised that the correct boundary conditions be applied to the model, as the effect of thermal expansion is often dominant. It is further recommended that results from models be continuously checked with simple hand calculations.

2.6.5.2 Britomart

Hicks *et al.* (2012) used a full-scale FE model to analyse the fire performance of a twelve-storey office building with long-span cellular beams and concrete slabs. These findings were used in conjunction with the fire model known as the slab panel method (SPM) to determine the efficacy of passive fire protection. For information on the SPM, the reader is referred to Walls *et al.* (2017). It was found that the long-span secondary beams could be left completely unprotected with only key elements requiring protection. An 80% cost saving on passive fire protection was realised, which equated to NZD 300 000 (EUR 189 000) at the time. This is a testament to the massive potential that a rational fire design with the aid of the FEM has for the design of passive fire protection.

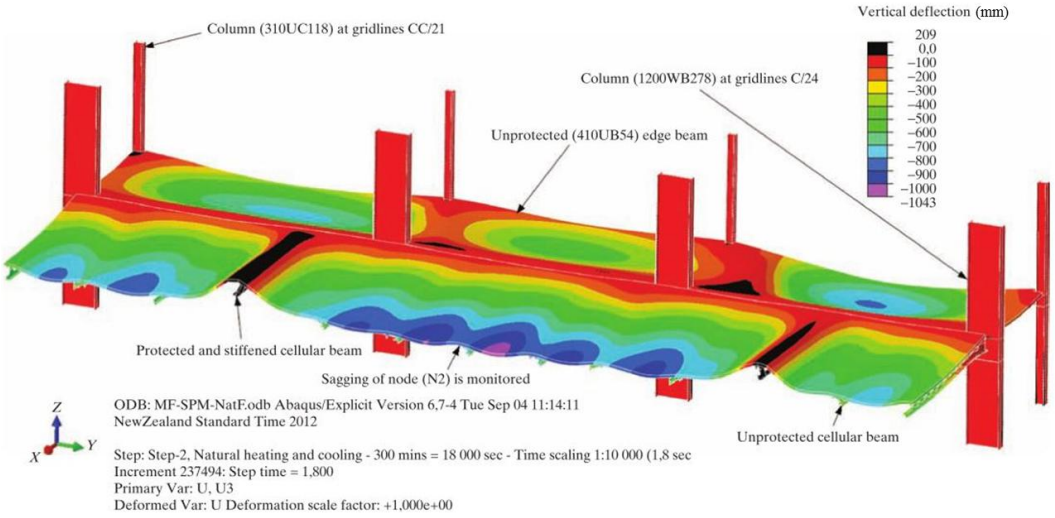

Figure 2.12: Output of finite element model of Britomart building showing displacements (Hicks *et al.*, 2012)

2.6.6 Software considerations

Software can almost be considered a prerequisite tool due to the complexity and number of equations to be solved in numerical analyses. As stated by (Wang *et al.*, 2013) the FEM is used almost universally and will likely continue to be the most sensible choice in the near future. There is a wide array of FEM software available and includes commercial general-purpose packages such as Abaqus and ANSYS, as well as research-based programs such as Vulcan, ADAPTIC and Safir.

In this arena the analyst is free to choose which software to use following careful consideration. A useful guideline of important criteria when choosing software

is given in the main technical report from the Cardington tests (University of Edinburgh, 2000). These include:

- The functionality must allow non-linear material properties and geometry.
- The software has been thoroughly scrutinised and verified through an extensive history of benchmarking. This ensures the algorithms are indeed accurate and produce realistic results.
- The software is well-known and used widely within the industry and academia. Together with a solid user and support network this will ensure that major bugs are corrected.
- The software is updated regularly so that new developments in computational mechanics are easily transferred to the user.

Whilst not explicity recommending Abaqus, they go on to state that "after careful reflection and consultation" Abaqus was chosen to model the Cardington tests. This directly implies the compliance with the above criteria. More recently Abaqus has proven to be very popular amongst researchers in the field of structural fire engineering, and has been used successfully in a wide array of cases (Yin and Wang, 2004; Gillie, 2009; Najafi and Wang, 2016; Hicks *et al.*, 2012). Based on this reputation, the availability of the software at Stellenbosch University and the prior experience of the researcher in using the software, Abaqus was used in this research.

Regardless of software used or complexity of the model, the Cardington research team recommend that the single most important consideration is the knowledge and expertise of the analyst (University of Edinburgh, 2000). Without a solid understanding of structural fire engineering based on first principles, the reliability of any model is compromised.

Chapter 3

SAISC cellular beam structure

3.1 Introduction

The SAISC has developed a novel cellular steel beam structure that aims to meet the performance based criteria of the construction industry. The structure is discussed in a concept paper which the SAISC released in 2013 at the *Steel Future* conference (Gebremeskel, 2013). This chapter summarises the concept paper, and begins by explaining the background and motive for this innovation, after which the technical details of the structure are introduced. Thereafter, a site visit to view the structure's prototype is briefly discussed. Finally, the structural layout and the terminology used in this thesis for the various structural members are explained.

3.2 The motive

The motivation for the cellular beam structure is based on two assumptions. Firstly, a growing service sector in South African economy is causing a large migration of workers into office buildings. Consequently, there is a greater demand on the construction industry for such structures. This industry is mostly based on tried-and-tested techniques that have proven to be safe and reliable. However, the SAISC has recognised that the status quo is struggling to meet the performance requirements of the public, developers and tenants. Thus, the second assumption is that innovative construction techniques have the ability to meet specific performance requirements. After market research, the SAISC has identified the following four requirements for office buildings in their case study:

- "Architecturally expressive and economical
- Flexible to reconfiguration and space optimisation

- Consumers of significantly reduced energy and materials
- Fast and safe to build and fit for occupancy"

These criteria were further investigated, and a solution was developed that aimed to satisfy all of the above. The emergence of the new structural system is further discussed below, in Section 3.3.

3.3 The solution

In response to the demand discussed above, the SAISC has proposed a new type of structure built up almost entirely of cellular steel beams and a variety of floor panels. The novel structure, which will hereafter be referred to as the cellular beam structure (CBS), specifically aims to meet the performance criteria listed above. Importantly, there is an absence of any wet trade (e.g. concrete, mortar, plaster). This allows the factory construction of modules that can be transported and quickly erected on site. Figure 3.1 shows three modules that form a single sub-structure. An example of a number of sub-structures forming a larger structure is shown in Figure 3.2. The modularity has several clear advantages. Firstly, architectural freedom is allowed as the modules can be configured in multiple ways. Secondly, buildings can easily be enlarged later with the addition of more sub-structures. Furthermore, the construction time is significantly decreased allowing an earlier occupancy, thus reducing cost and leading to increased rental incomes. Finally, the lack of wet trade means that the entire building system can eventually be disassembled and re-used.

Generally office buildings have concrete or composite slabs, upon which an access floor is placed that allows for the placement of mechanical, electrical and plumbing services. A unique feature of the CBS is the use of cellular beams and a sandwich decking system, which allows for any servicing to be placed within the floor itself. Thus, the need for an additional access floor is negated and the overall floor to floor spacing is reduced. The sandwich system (shown in Figure 3.3) is made up of fire-resistant and fibre-cement boards that encase the cellular beams to form the ceiling and floor. The fire-resistant board specification is not clear yet, but it is likely that a gypsum or calcium silicate board will be used. The resulting floor system has an average mass of 100 kg/m^2 (including access floor). A typical composite floor without an access floor, with bay sizes comparable to the CBS i.e. 7.5 - 8.5 m, is considerably heavier at 400 kg/m^2. The outer walls will utilise a modular cladding system consisting of light steel frames with insulating material sandwiched between boards. The lightweight nature of the structure, the ability to be re-used and the planned use of energy-efficient cladding systems all serve to minimise the required energy and materials.

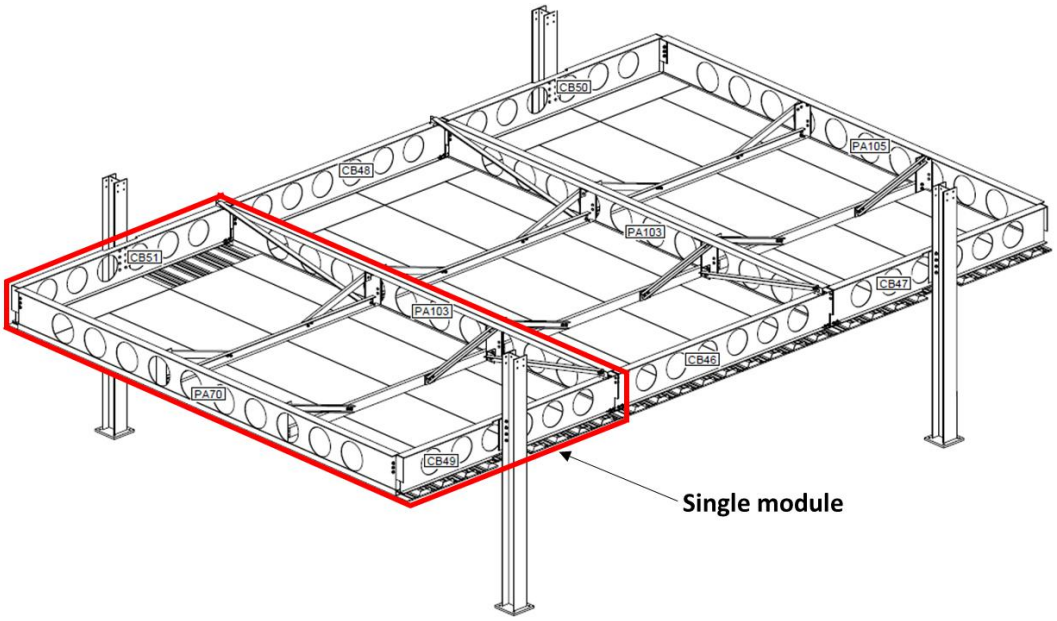

Figure 3.1: General drawing of three connected modules, forming a single sub-structure (Courtesy of SAISC)

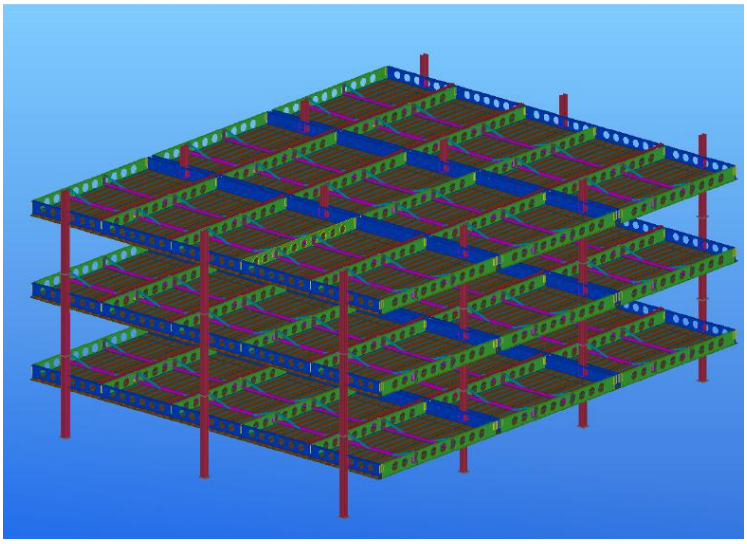

Figure 3.2: A larger structure made up of multiple sub-structures (Courtesy of SAISC)

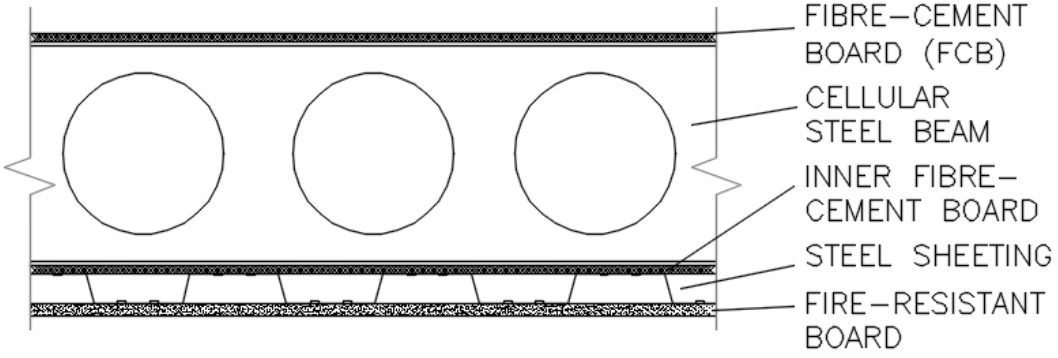

(a) Elevation

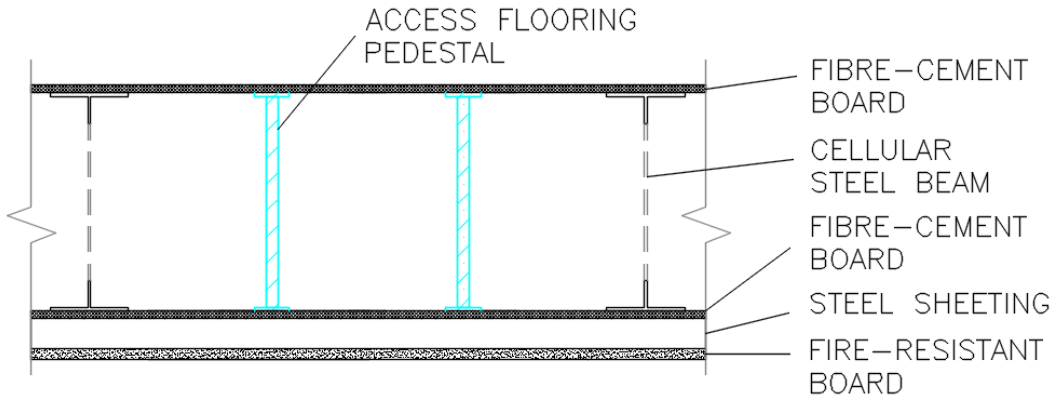

(b) Side elevation

Figure 3.3: Schematic cross-sections of cellular beam structure (CBS) floor system (Marx, 2018). Note: drawing not to scale.

However, the SAISC recognises that the CBS faces a number of challenges that remain to be solved. The lightweight nature of the structure, combined with relatively long spans (8m), means that the structure is possibly susceptible to vibrations. This could cause the structure to fail under the serviceability limit state, as vibrations can cause discomfort to occupants. Furthermore, acoustic insulation possibilities must still be investigated. Non-impact generated noise is not expected to be a problem, but it is possible that impact generated noise might easily be transmitted between floors.

Together with the above serviceability concerns, the CBS faces challenges that could affect the ultimate structural capacity. Firstly, the structure lacks any additional lateral cross-bracing. However, it has been assumed that the sandwich decking system will act as a membrane to provide the necessary stiffness. Physical tests conducted by the SAISC have shown this to be true, provided there are sufficiently robust connections between the beams and decking. Secondly, the seismic resistance of the CBS is still uncertain, and needs to be verified. Such an investigation does not fall within the scope of this work. Finally, the unconventional nature of the structure has made it diffi-

cult to quantify the fire resistance of the structure. Specifically, the lack of a cast in-situ concrete slab (which is a good insulator) that would normally be present in a conventional composite slab is a cause for concern. Currently, the only thermal barriers are the fire-resistant and fibre-cement boards, and to a certain extent the steel sheeting. If it is shown that these can provide the necessary thermal insulation, it must also be ensured that the steel beams do not fail due to the heightened temperatures. Failure can be defined here as serious structural damage leading to collapse, or a deflection significant enough to threaten the integrity of the floor system. As previously discussed, characterising the structural behaviour of the CBS at heightened temperatures is the ultimate goal of this research.

3.4 Site visit

On 14 September 2017 Michael Kloos and Hendrig Marx travelled to Johannesburg to inspect a prototype of the CBS. The prototype was constructed in 2014 and is located at the Tass Engineering headquarters in Kempton Park. All previous knowledge was based on shop drawings and photos, and thus the visit was invaluable in attaining a comprehensive understanding of the structure. Specifically, the research team was able to: (a) validate structural drawings, (b) identify possible failure mechanisms, (c) inspect connections and (d) look at fixing details. Figure 3.4 shows Hedrig Marx during the site visit.

Figure 3.4: Hendrig Marx at the site of the prototype cellular beam structure (CBS)

Furthermore, the visit included a meeting with Amanuel Gebremeskel of the SAISC, who is currently the driving force behind the CBS concept. This

research was conducted in collaboration with the SAISC, and thus it was vital to discuss the expectations of the SAISC. These expectations are to determine: (a) the temperature of the steel sections after a 1 hour standard fire, (b) the level of insulation the sandwich floor provides and (c) the structural behaviour of the CBS under fire conditions.

3.5 Structural layout and terminology

Initially, the CBS has a strange 'upside-down' look with steel sheeting *below* the beams and upward-slanting knee-braces. However, these unconventional characteristics perform definite roles, and form part of an innovative structural system. Before this structural system is explained further, it is necessary to introduce the terminology that will be used in this thesis to refer to specific parts of the CBS. Figure 3.5 shows a sub-structure labelled with this terminology.

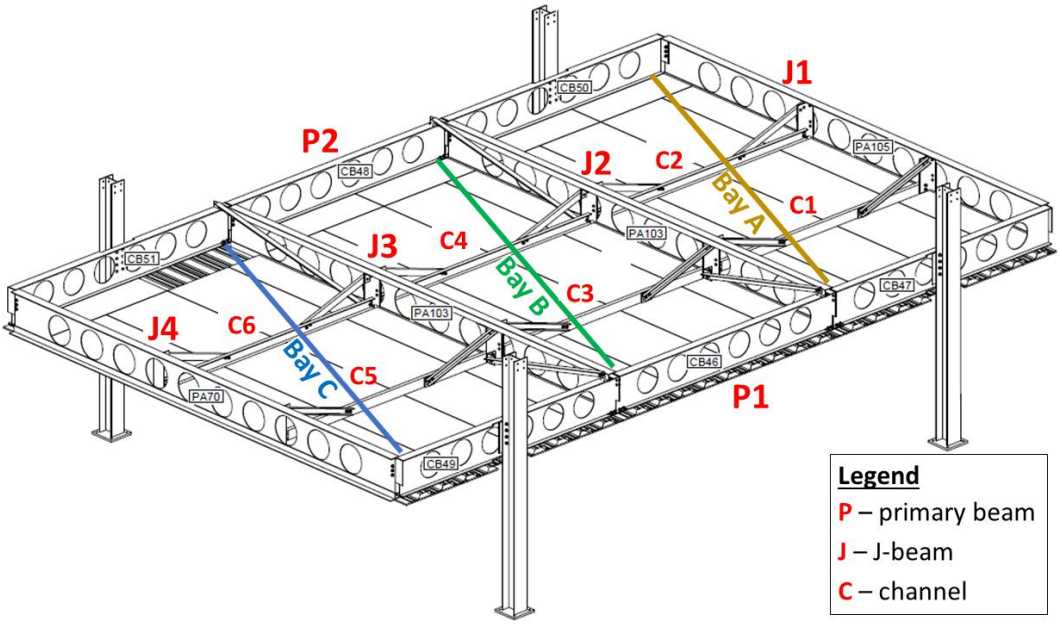

Figure 3.5: Terminology used for the structural elements of the cellular beam structure (CBS)

The three modules are individually referred to as 'bays' and are labelled A, B and C. Each bay is 4.2 m wide and 8 m long, giving the full sub-structure a dimension of 12.6 $m \times 8$ m (these dimensions are shown in Figure 3.7 below). There are two types of beams used, both of which are cellular. Firstly, the two primary beams that are connected to the columns will hereafter be referred to as 'P-beams' (P1 and P2). Although each P-beam is made up of three sub-beams (one per bay), it has been assumed they are fully continuous based on

the connection between sub-beams. The connection provides moment continuity through web plates and lower flange plates. Secondly, the four secondary beams that support the channels will hereafter be referred to as 'J-beams' (J1, J2, J3 and J4). This is due to a one-sided bottom flange which makes the beam resemble the letter 'J', as shown in Figure 3.6. This has been done to provide sufficient stiffness during transportation, and to make module assembly on site as easy as possible whilst maintaining the same level between modules. There are two channels per bay that support the steel sheeting. These are labelled C1 - C6.

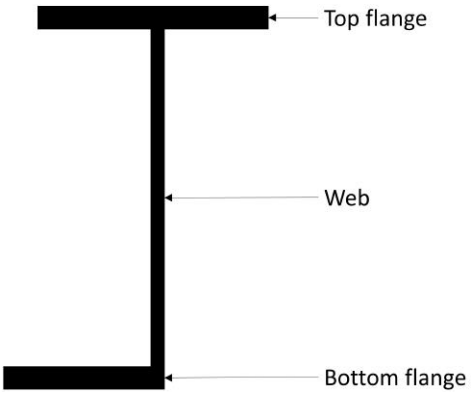

Figure 3.6: Sketch of a 'J-beam'. Note: not to scale

Visualising the transfer of loads through the structure is vital to an understanding of the design philosophy behind the CBS. The flow of loading is illustrated in Figure 3.7, and explained below: (1) The lack of a slab means that the access flooring pedestals rest on the fibre-cement boards, as previously shown in Figure 3.3. The fibre-cement boards are supported by the steel sheeting, which has been specified to span across the P-beams. Thus, the central area loading is transferred from the sheeting to the channels (green arrows), whilst the outer area loading is transferred directly to the P-beams (brown arrows). (2) The channels then transfer their loading to the J-beams (blue arrows), where they act as point loads. (3) The J-beams in turn transfer their loading to the P-beams (golden arrows), where they also act as point loads. Thus, the P-beams carry four point loads (one for each J-beam) as well as a line load from the adjacent sheeting (grey arrows). (4) The P-beams transfer their load to two columns (purple arrows). (5) The knee-braces do not carry any loading directly, but serve two important roles. Firstly, they supply lateral bracing to the top of the J-beam at two points along its span (in a conventional composite structure, the concrete slab usually provides continuous lateral restraint to the top flange). Secondly, they increase the vertical stiffness of the channels, which are carrying the load of the ceiling.

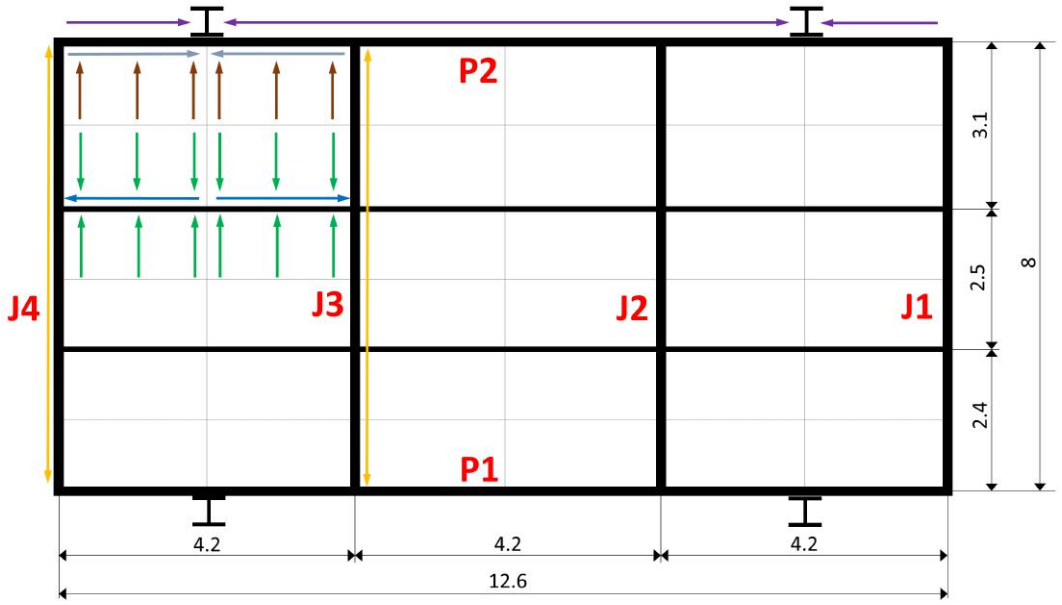

Figure 3.7: Diagram illustrating the transfer of loading through the cellular beam structure (CBS)

In this research, a number of finite element models have produced for various parts of the CBS, under different fire conditions. Chapter 5 focuses on a single J-beam in isolation, with various end boundary conditions. A model of an isolated P-beam has also been created. These single element models are used to identify failure modes of the beams, and test the sensitivity to end boundary conditions. However, modelling only single elements cannot capture the interaction between different structural members. Chapter 6 contains the global model which incorporates all the P-beams, J-beams, channels and knee-braces for the three bay sub-structure shown in Figure 3.5. Thus, this model is able to give more accurate predictions of structural behaviour by taking into account the inter-dependence of structural members.

3.6 Conclusion

This chapter has introduced the CBS to the reader as the subject of this research. This places the research within context and motivates the ultimate goal of determining the fire resistance. The novel nature of the structure is unfamiliar, and thus the structural system is examined in detail. Finally, the terminology used throughout this thesis is introduced. All the above combines to give the reader a good understanding of the CBS, and equips them with the knowledge to correctly interpret the findings of this thesis.

Chapter 4

Finite element modelling validation

4.1 Introduction

At the core of the research presented in this thesis are a range of finite element (FE) analyses which model the cellular beam structure (CBS) under fire conditions. As stated in the literature review, the FEM is widely regarded as a highly advanced tool to model structural behaviour in a fire. However, it is by no means the simplest approach, and caution must be exercised if there is to be any amount of confidence in the results. Ultimately any FEM results remain, at best, a numerical *approximation* of reality, rather than reality itself. In the worst case, badly chosen user input or a weak modelling approach can yield results that may look convincing, but are completely false. This emphasises that a competent analyst who is comfortable with the theory and application of the FEM is essential.

In order to overcome this uncertainty, rigorous validation is necessary to build confidence in the modelling skills of the analyst. A useful validation tool is a benchmark study, which consists of a strictly defined problem together with a proven set of results. However, a benchmark purposefully lacks the finer details of the user input (Cook *et al.*, 2002). It is left to the analyst to formulate a FE model based on theory and their experience. Thus, if the analyst is able to replicate the results, they are assured that their approach is sound, or at least to the extent that the benchmark is correct.

The minimum number of benchmarks required to complete a validation study is subjective. In this work, three benchmarks were specifically chosen as they address factors that were initially deemed to be important for further models of the CBS: (1) The Gille benchmark (Gillie, 2009) is purposefully kept structurally simple, yet was formulated to include several non-linearities that are vital for structural fire analyses. (2) The COST 1 (COST, 2014) benchmark

tests the sensitivity of a typical steel beam to varying end boundary conditions. (3) The COST 2 (COST, 2014) benchmark investigates the buckling behaviour of steel beams in fire. Abaqus was used, as motivated in Section 2.6.6, throughout the validation process. This chapter discusses these three benchmarks, as well as the material model developed in this work, in greater detail.

4.2 Gillie benchmark

Gillie (2009) has developed a benchmark that incorporates non-linearity (geometric and material), complex boundary conditions and time-dependent forces. In most structural analyses under ambient temperatures these phenomena are usually not modelled as they are either not applicable, or their effects are negligible. However, under fire conditions Gillie asserts that they are crucial to accurately predict the behaviour of a structure. In order to avoid any possible misinterpretation that could affect results, the benchmark consists of a beam which is conceptually simple but incorporates all the key phenomena in a closely-defined manner. The problem definition is well-summarised in Figure 4.1. The Young's modulus and coefficient of thermal expansion have constant values of 207 GPa and 1.2×10^{-5} respectively. To investigate the correlation between different FEM software packages, Gillie used Abaqus, Ansys and Vulcan to run quasi-static analyses. Furthermore, he also compared the quasi-static and the explicit dynamic results of Abaqus. This benchmark only includes numerical analyses i.e. there is no experimental result from a physical test.

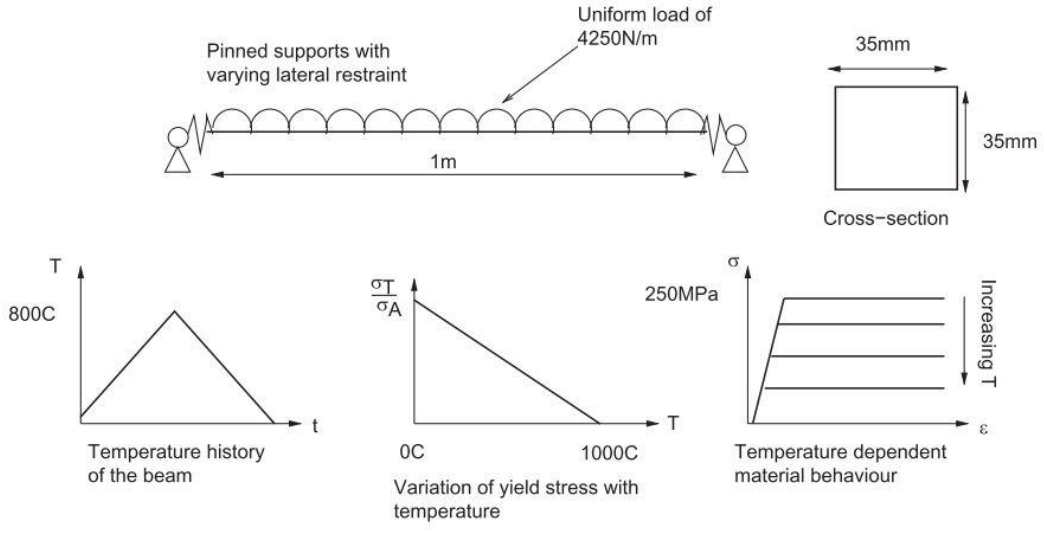

Figure 4.1: Gillie benchmark - problem definition (Gillie, 2009)

In this work, shell elements with four nodes (S4) were used to model the beam. Four elements were used across the height and fifty along the length of the beam, yielding an element size of 8.75 $mm \times 20$ mm. The line load was applied as a shell edge load. The boundary conditions were defined at a single reference point (RF), which was fully linked to the beam using a kinematic coupling constraint as shown in Figure 4.2. A pin support was used on one end, and a roller support on the other. A spring element was added on the roller side to resist thermal expansion. The stiffness was equivalent to 75% of the axial stiffness of the beam ($k = 0.75 \times \frac{AE}{L} = 0.75 \times \frac{0.035^2 \times 207 \times 10^6}{1} = 190.2\ kN/mm$), as specified in the original work. The analysis was split into two steps, both using a "General, static" solution algorithm which uses the Newton-Rhapson method to solve non-linear equations (Abaqus, 2014). Thus, a computationally efficient static analysis was used in favour of a dynamic analysis. In the first step the mechanical load was applied in a single time step. Thereafter a thermal step changed the temperature of the beam over a normalised time period. The temperature was defined using a predefined field based on the given time-temperature history.

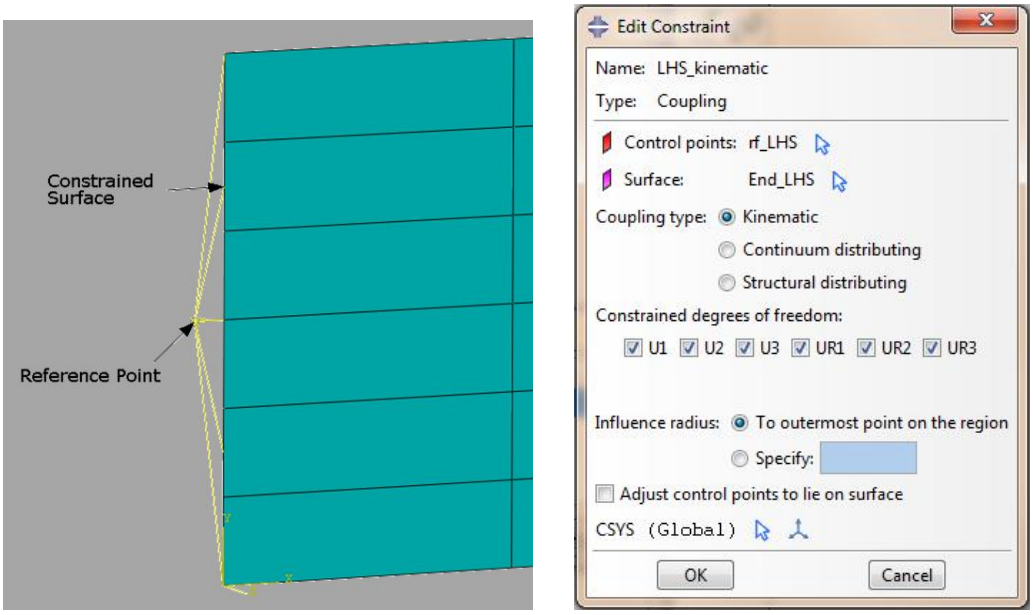

(a) Interaction between reference point (RF) and beam edge. Note, a 5 mm offset was applied between the RF and beam edge for visual clarity.

(b) Abaqus constraint input

Figure 4.2: Abaqus kinematic coupling constraint

As the beam was heated according to the time-temperature graph of Figure 4.1, the axial force and midspan vertical deflection were extracted from the Abaqus model. These results are compared to the benchmark predictions in Figures 4.3

and 4.4. As there are multiple Abaqus results shown on the graph, the results of this work are labelled "Abaqus (Stellenbosch)" for clarity. A clear sequence of events can be inferred from the graphs. Initially the beam undergoes a linear increase in axial force due to the restrained thermal expansion. This continues until a plastic hinge forms at the centre of the beam. The resulting reduction in stiffness causes a rapid increase in the midspan deflection, which in turn relaxes the axial force. Thereafter the beam enters a phase in which the rate of thermal elongation is less than the effect of the sagging (increasing midspan deflection) on the beam-end deflection. This can be seen by the decreasing axial force. The sagging continues until the maximum temperature of 800°C is reached. Subsequently the cooling phase begins, during which catenary action occurs, as explained in Section 2.4.2. This is characterised by an increasing *tension* force due to thermal contraction. This has a 'straightening' effect on the beam, shown by the decreasing midspan deflection.

A good correlation was achieved with similar results between all five sets of modelling results. However, there is a significant difference in the temperature at which the plastic hinge forms, which ranges from 93 °C (Vulcan) to 154 °C (Ansys). This can be attributed to the fact that the linear increase rate in axial compression is not equivalent for all results. Therefore, the critical load is reached at different temperatures. The reason for this is unclear, as the rate of thermal expansion is a constant. However, it seems likely that minor differences in the way in which boundary conditions are applied, or the software itself, can result in a differing expansion-axial force relationship. Regardless, it is clear that, even in a validated benchmark, results can differ. This indicates that no single result should be taken as conclusive.

From the above it is clear that a seemingly simple problem can yield a complex pattern of events with significantly changing behaviour. Gillie draws attention to the fact that without a non-linear analysis, the above results would not be achievable. The catenary phase, which begins upon cooling, is perhaps the most significant result, as it shows the importance of providing connections with a robust tensile capacity. A good correlation has been achieved between the results of this work and those of the benchmark, indicating that accurate modelling procedures have been developed.

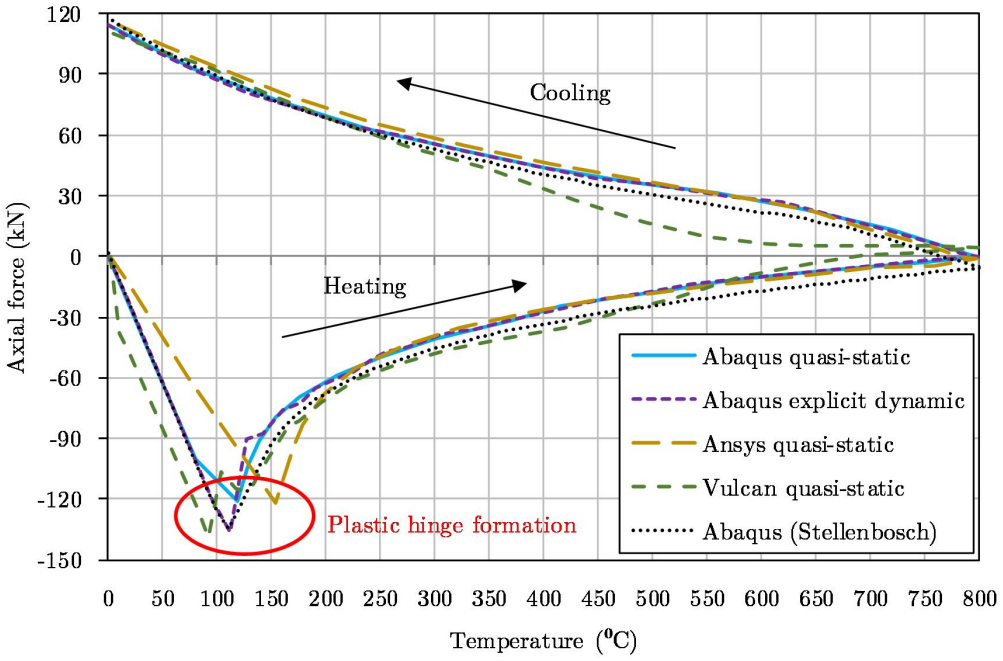

Figure 4.3: Gillie benchmark - axial force (compression is negative)

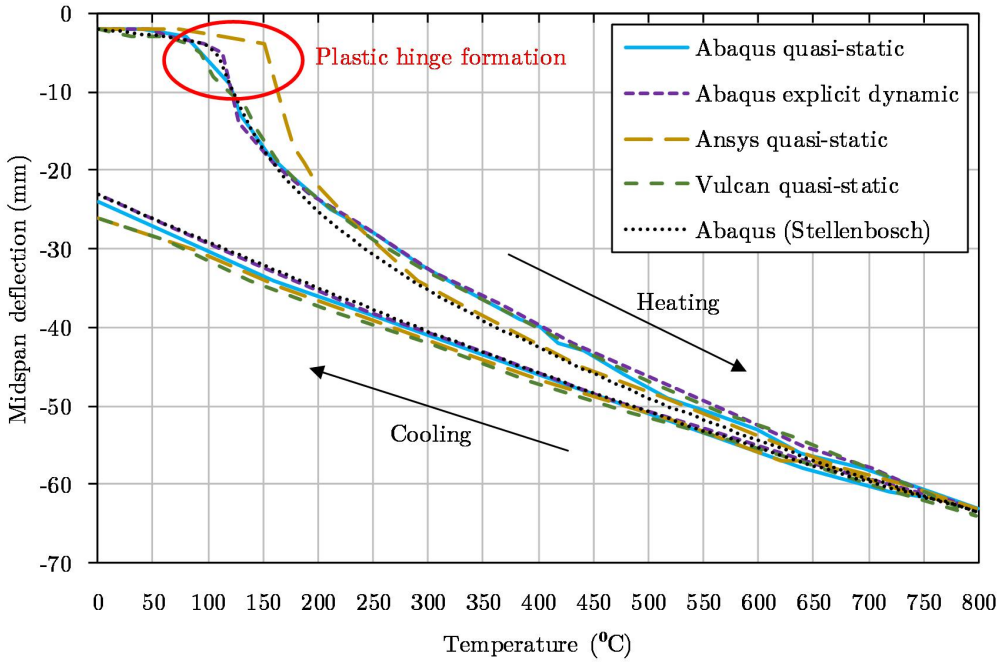

Figure 4.4: Gillie benchmark - midspan deflection

4.3 COST benchmarks

COST (European Cooperation in the field of Scientific and Technical Research) has released a publication that contains a number of benchmark studies focused on the field of structural fire engineering (COST, 2014). Two studies of steel beams were chosen. The first one showcases the effect that varying end boundary conditions can have. This is useful, as single elements within the cellular beam structure (CBS) were later modelled with different boundary conditions. Cellular beams can consist of thin sections, which could result in a Class 4 section i.e. vulnerable to local buckling. Therefore, the second benchmark considered in this work investigates the buckling behaviour of a Class 4 steel beam under fire conditions. Furthermore, the COST benchmarks provided an opportunity to validate the successful Abaqus implementation of the Eurocode material model for steel at elevated temperatures. Both COST benchmarks do not include physical tests, and thus form purely theoretical benchmarks that test numerical modelling procedures.

4.3.1 Abaqus implementation of Eurocode material model for steel at elevated temperatures

Unlike the simple material model used by Gillie, both COST benchmarks make use of the EN 1993-1-2 material model for steel at elevated temperatures (CEN, 2005). The Eurocode model has been discussed in detail in Section 2.4.1.1. This model includes formulae for the Young's modulus, stress-strain relationship and coefficient of thermal expansion as functions of temperature. This section explains how, in this research, the material model was implemented in Abaqus.

The stress-strain relationship was entered into Abaqus using a tabular format, for which 12 stress-strain curves consisting of 43 data points each were created at 100°C increments, as shown in Figure 4.5. For each of these, 40 of the points were evenly spaced along the non-linear curve between perfect elastic and plastic behaviour at 0.005 strain increments. The remaining 3 points were sufficient to describe the perfectly linear behaviour before and after the non-linear phase. To illustrate this, the data points have been marked on the 500°C curve. Using the above input, Abaqus can determine the stress-strain state for any temperature using linear interpolation between known data points (Abaqus, 2014).

Similarly, the initial Young's modulus and coefficient of thermal expansion were inputted as a tabular set of data points. The Young's modulus is based on the reduction factors shown in Figure 2.7 with 14 data points at 100°C increments, as shown in Figure 4.6. This initial Young's modulus is only used whilst the stress is still linear i.e. fully elastic. Once yielding begins the stress-strain relationship discussed above is used by Abaqus. The coefficient

of thermal expansion is based on Formulae 2.4.1, 2.4.2 and 2.4.3, which yield the relationship shown in Figure 4.7. The constant value of 1.4×10^{-5} recommended by ECCS is also shown on the graph (ECCS, 2001). However, the COST benchmarks do not specify whether the complete formulation or an approximation was used. Thus, in the replication of these benchmarks, it was assumed that the complete formulation was used.

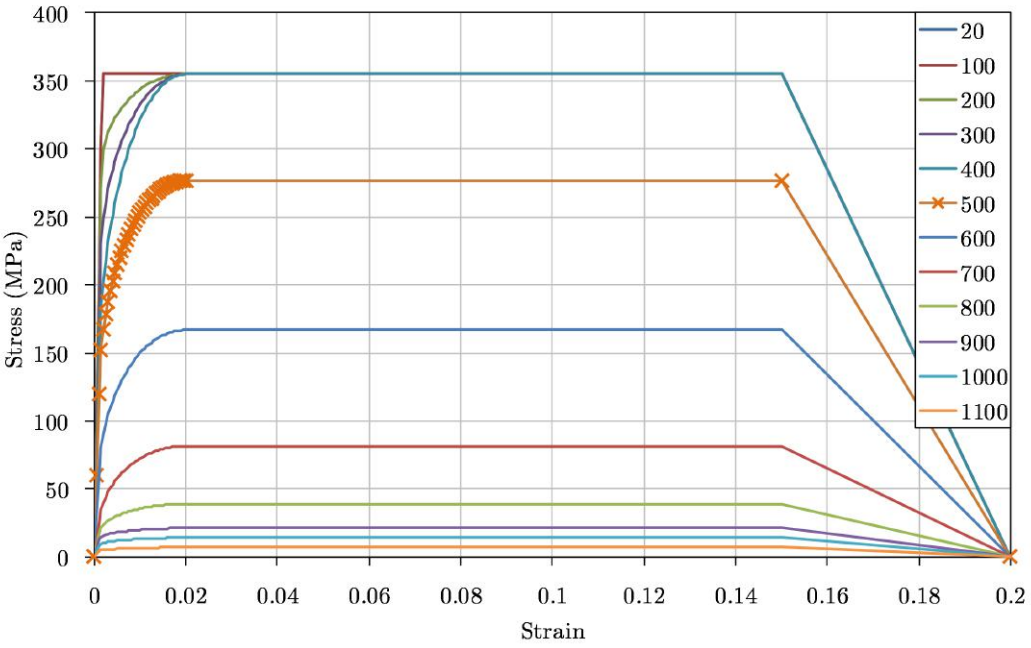

Figure 4.5: Stress-strain relationship of steel at elevated temperatures (CEN, 2005)

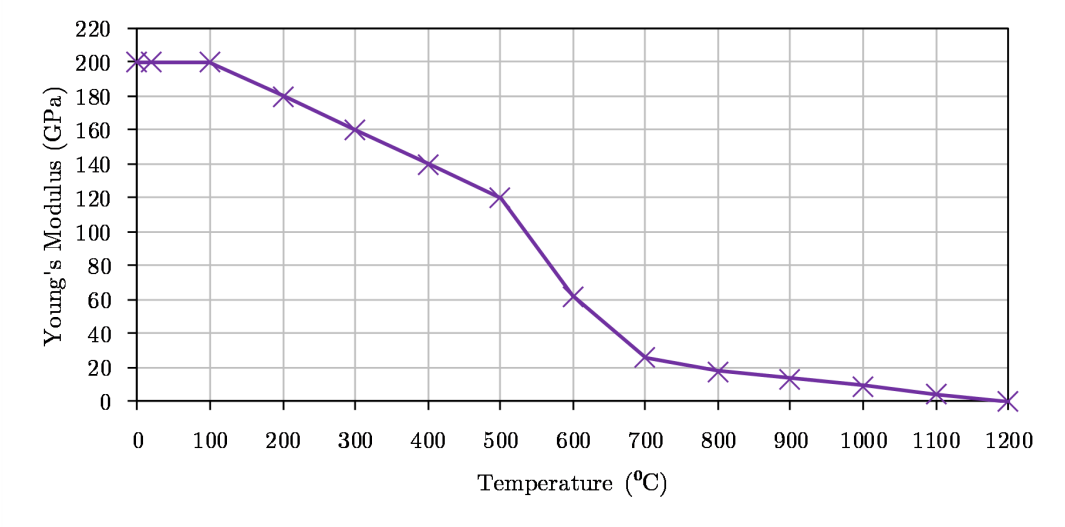

Figure 4.6: Initial Young's modulus of steel at elevated temperatures (CEN, 2005)

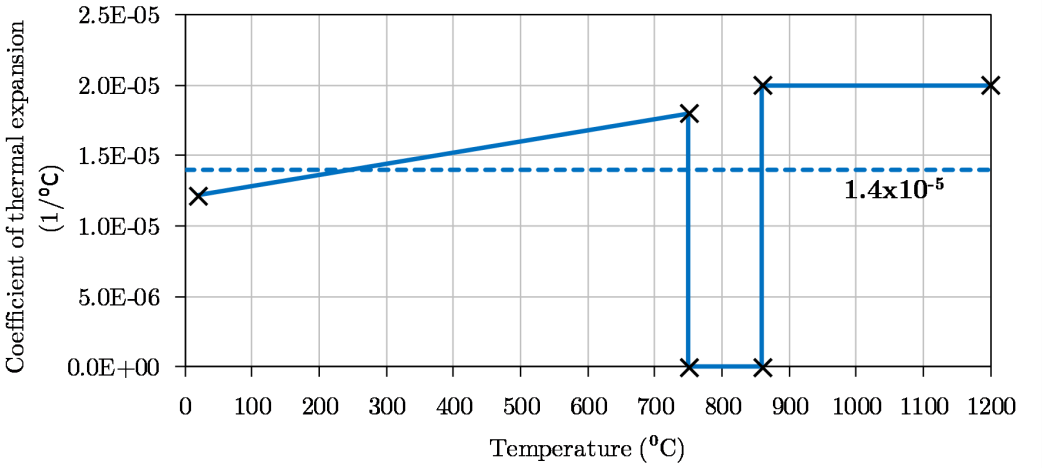

Figure 4.7: Coefficient of thermal expansion of steel at elevated temperatures (CEN, 2005). The simplified constant value of 1.4×10^{-5} is also shown.

4.3.2 COST 1: Steel beam with varying boundary conditions

This benchmark consists of a Grade S355 UB 457x191x98 of length 8 m subjected to a constant distributed load of 20 kN/m. The beam is subjected to a 90 minute standard fire. The temperature pattern is non-uniform, with the temperature of the top flange scaled at 60% of the ISO834 standard fire temperature, whilst the bottom flange and web are 70% (see Figure 4.8). There

are two cases with differing end boundary conditions: fixed-fixed (FF) and pin-pin (PP). COST used the Vulcan software for this benchmark in all of their analyses.

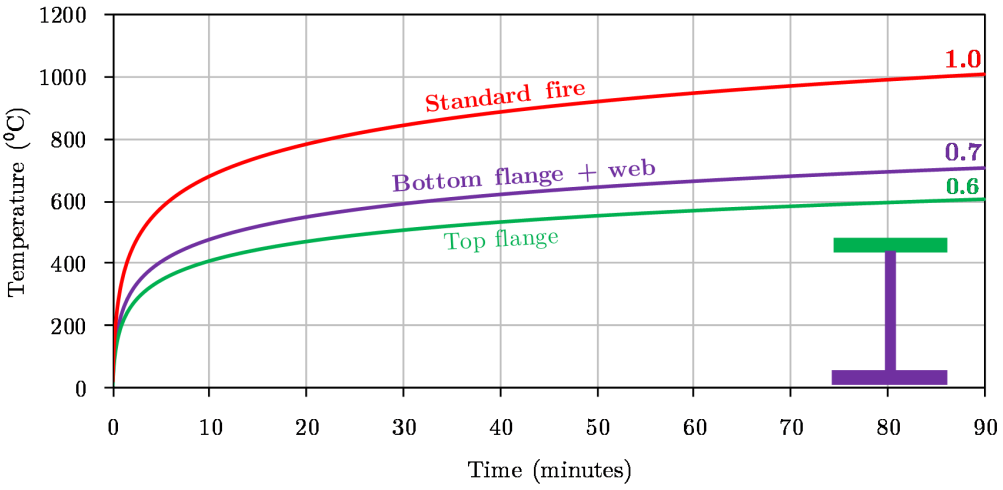

Figure 4.8: Non-uniform temperature distribution in beam based on standard fire

In this work, three separate shell parts were created for the two flanges and web, which were assembled to create the I-beam. S4 shell elements were used throughout with a mesh size of 50 $mm \times 50$ mm. The beam ends were constrained to a single point as in the Gillie benchmark. The solution procedure consisted of a mechanical load step followed by a thermal load step. The time-temperature curves given in Figure 4.8 were applied as predefined fields to the relevant shell parts (i.e. bottom flange and web, and top flange). The loading required special attention, as Abaqus does not allow a line load to be placed on a shell unless it is acting normal to a free edge (termed a 'shell edge load'). To overcome this, the total line load was applied as a series of 41 point loads with a spacing of 200 mm.

The deflection and axial force were extracted from the Abaqus models developed in this research, and are compared to the benchmark data in Figures 4.9 to 4.12. The deflection was always extracted at both the midspan (L/2) and quarter-point (L/4). The standard fire exhibits a rapid initial rise in temperature (for example: 108 °C at 6s, 261 °C at 30s, 349 °C at 60s) so that that within seconds the thermal expansion is considerable enough to cause significant axial forces if restrained. For both the FF and PP cases all thermal expansion is entirely restrained, and this explains why there is an almost immediate buckling event followed by decreasing axial force and increasing deflections.

For the FF case, the Abaqus and COST deflection curves (Figure 4.9) show a good correlation. However, after 65 minutes, the COST results show severe non-linearities which are not reflected by the Abaqus results. It is unclear why such perturbations are produced in the Vulcan model as there is no sudden buckling at this point in the analysis. However, it can be observed that overall there is good agreement between the models. The axial force curves (Figure 4.10) are similar in trend, but with a distinct offset that varies between 500 and 1000 kN throughout the analysis. An analytical calculation, based on the pre-buckling i.e. perfect geometry axial force of a longitudinally compressed beam, yields an axial force of 3550 kN after 13 seconds. This is within 310 kN (8%) of the maximum axial force of 3860 kN predicted in this work. Conversely, the COST results show a maximum axial force of 2907 kN at the same point in time. The difference in results between the analytical calculation and the COST analysis is $3550 - 2907 = 643$ kN, which is approximately the offset between the results of this work and the COST analysis, as explained above. This suggests that either COST or the Vulcan software applied an offset.

For the PP case, the deflection curves (Figure 4.11) are initially identical, but begin to diverge after approximately 5 minutes. This divergence eventually stabilises with a constant offset of approximately 40 mm (8%) between the midspan deflections, and 30 mm (10%) between the quarter-point deflections. The axial force curves (Figure 4.12) are almost identical in form, but with an offset of approximately 100 kN.

To conclude, there are some noticeable differences between the COST 1 benchmark and the Abaqus results. However, the trends and general behaviour of both sets of results agree with each other. It is worth keeping in mind that, as shown by the Gillie benchmark, the use of different software can possibly cause differing results. It is also possible that different data has been extracted from the COST analyses and plotted against the Abaqus results, as it is unlikely that such similar deflections could be coupled with such different axial forces.

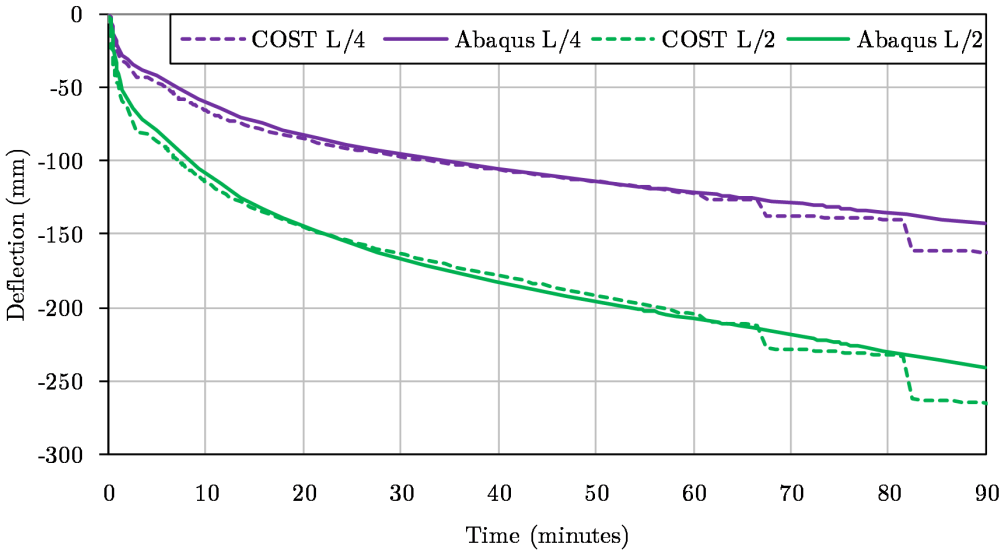

Figure 4.9: COST 1 - deflection (fully fixed)

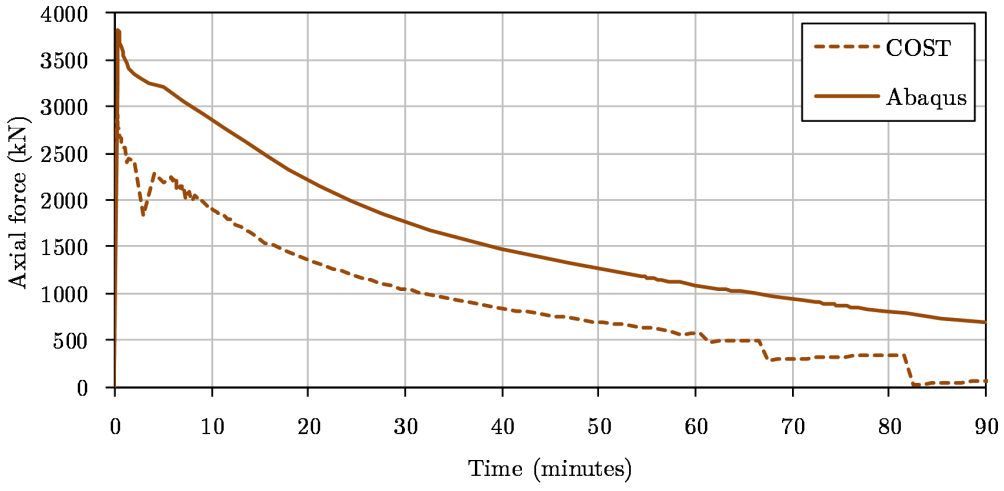

Figure 4.10: COST 1 - axial force (fully fixed)

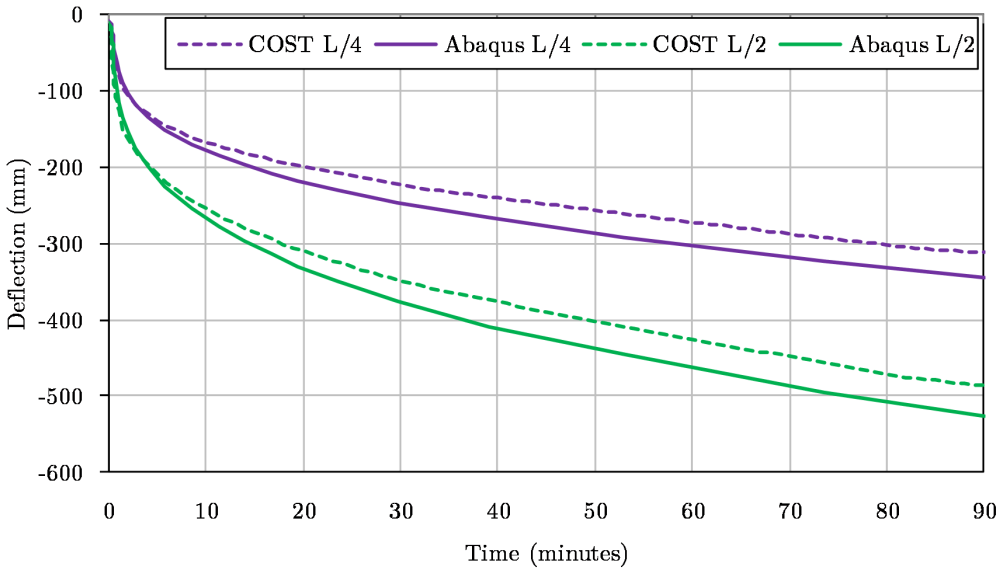

Figure 4.11: COST 1 - deflection (pin-pin)

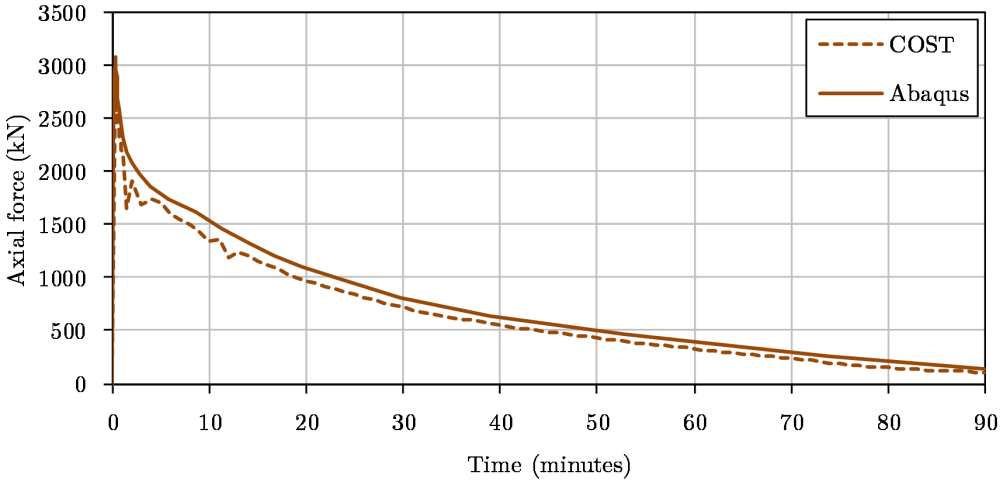

Figure 4.12: COST 1 - axial force (pin-pin)

4.3.3 COST 2: Buckling behaviour of Class 4 beam

This benchmark considers a simply supported steel beam that is considered Class 4 according to Eurocode 3 (CEN, 2009*a*). The classification of steel beams is used to characterise how they fail, with a Class 4 section generally being susceptible to local buckling due to thin cross-sections. The beam is subjected to two equivalent point loads equally spaced from the ends, thereby inducing a constant bending moment in the central part of the beam. The central part is uniformly heated to 450°C, whereas the outer parts remain at ambient temperature i.e. 20°C. The above input and the beam geometry is summarised in Figure 4.13. The beam can be also seen in Figure 4.14, which presents a screenshot from the Abaqus model created in this work. The width of the flanges is 150 *mm*. The beam is fully pinned on one end, but a roller support on the other end allows axial deformation. The beam is laterally restrained at the position of the point loads. Thermal expansion was not considered in the analysis. Both Abaqus and SAFIR were used by COST to model this benchmark.

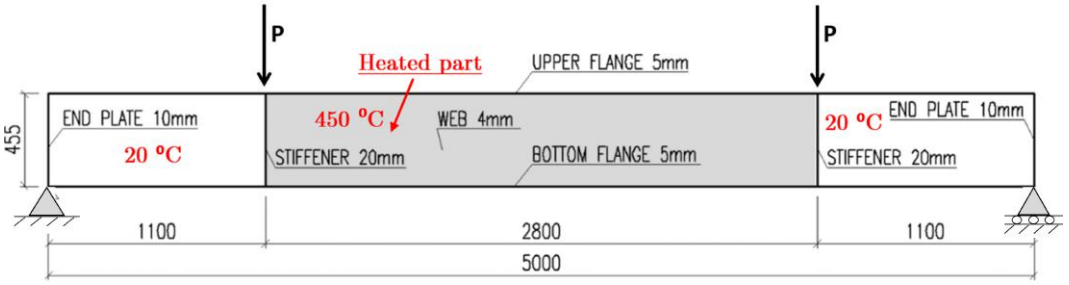

Figure 4.13: Elevation view of the beam used in the COST 2 benchmark, showing the geometry, position of point loads and the heated area. Adapted from COST (2014).

The benchmark focuses on the buckling analysis, in which the specification of initial imperfections is critical. These are based on the eigenmodes that are determined through an elastic buckling analysis. COST selected the first local buckling mode (plate buckling) and the first global buckling mode (lateral torsional buckling) and applied initial imperfections based on 80% of the manufacturer's tolerance (as suggested by CEN (2009*b*)). This equates to $0.8 \times \frac{L}{750} = 0.8 \times \frac{2800}{750} = 3\ mm$ for lateral torsional buckling (where L is the distance between lateral supports), and $0.8 \times \frac{H}{100} = 0.8 \times \frac{455}{100} = 3.64\ mm$ for local buckling (where H is the web height). Furthermore, these imperfections were used in combination according to CEN (2009*b*), which specifies that the amplitude of the leading buckling mode remains unchanged whereas the other mode is reduced to 70% of the original value.

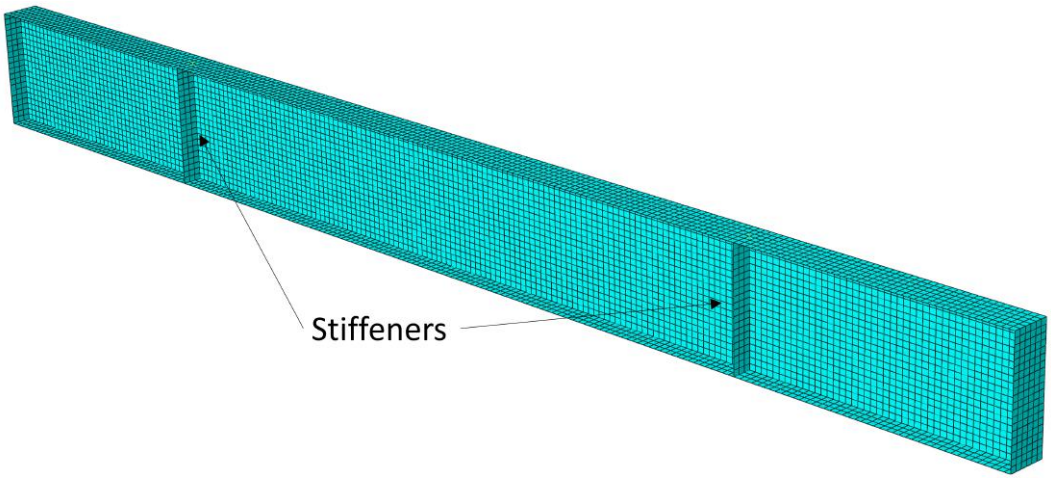

Figure 4.14: Abaqus model of COST 2 steel beam, from this work. The stiffeners are shown, as well as the mesh used.

In this work, S4 elements were used, similarly to previous benchmarks. The mesh size was 20 $mm \times 20$ mm, as shown in Figure 4.14. The end boundary conditions were defined at a single point at the centre of the bottom flange. Lateral support was provided to the flanges at the position of the web stiffeners. The point loads were applied at a single point which was kinematically constrained to the breadth of the flange at the location of the stiffeners. The solution procedure consisted of a linear elastic buckling step followed by a load step using the Riks solution technique. Lateral torsional buckling was found to be dominant, and thus the web imperfection was reduced to 70% of the original value i.e. $0.7 \times 3.64 = 2.55$ mm. No thermal load step was required as the temperature of the beam parts remained constant.

Figure 4.15 compares the deflection results of the COST analyses with the Abaqus model. The graph plots the relationship of the midspan deflection to the total force being applied i.e. the sum of both point loads. The point at which lateral torsional buckling occurs is shown on the graph, with all three models showing the onset of non-linear behaviour at 10 mm of midspan deflection and a load peak of approximately 100 kN. Thereafter, the Abaqus and COST Abaqus results show a very strong correlation. However, there is a gradual divergence in total force as the deflection increases, resulting in a maximum variation of 5.4 kN at 70 mm of deflection (a 8% difference). Conversely, the SAFIR model diverges significantly from both Abaqus models during the post-buckling phase. At 70 mm there is a difference of 22 kN in the total force (a considerable difference of 37%). Nevertheless, the buckling loads for all three analyses are within 2 kN (2%) of of each other. Whilst the deflections predicted in this work differ from those of the SAFIR model, the good correlation with the COST Abaqus results indicate that the modelling procedures developed in this work are sound. Thus, it is likely that the dif-

ference in results is due to the software used, and not a fundamental error in modelling procedures.

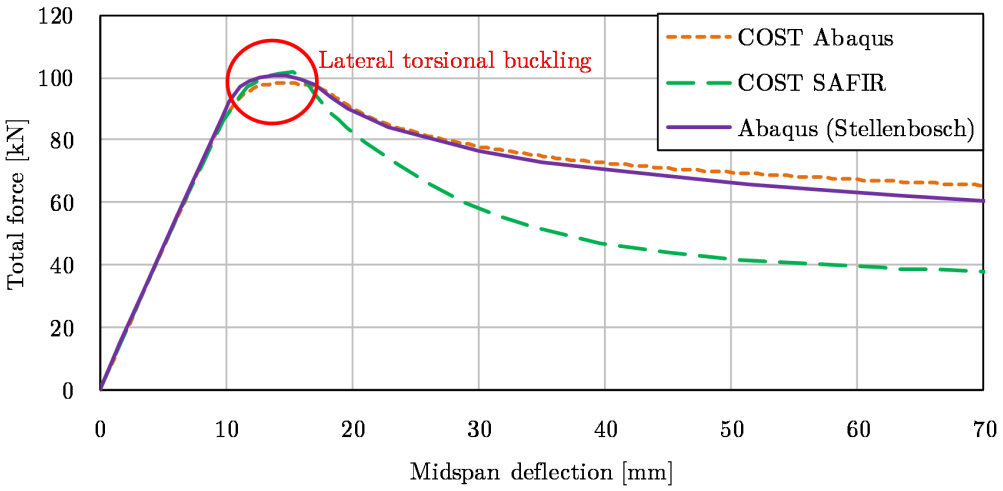

Figure 4.15: COST 2 - load-deflection relationship

4.4 Conclusion

Through the modelling of three benchmark tests using Abaqus, it has been shown that a solid understanding of simulating steel under fire conditions has been achieved. Specifically, a number of key parameters were validated, which are all required to model the cellular beam structure (CBS) under fire conditions:

- A material model based on the EN model for structural steel was accurately implemented in Abaqus. This model has been utilised throughout the COST benchmarks.
- An ability to model material and geometric non-linearity was proven. The CBS is made up mostly of steel beams, and thus both types of non-linearity are expected.
- Correctly inputting time-temperature histories into Abaqus to simulate a fire. This allows different thermal loads i.e. fires to be applied to the CBS.
- The successful specification of a variety of boundary conditions. Different boundary conditions have been used to model single elements of the CBS.

- The effect of initial imperfections and post-buckling analyses on steel beams. It was initially expected that a buckling analysis followed with specified initial imperfections would be necessary for the CBS.

However, the validation process also made it clear that results can be dependent on the software used, or how different users possibly apply the software. Nevertheless, the differences in the results are small enough that a reasonable level of confidence can be placed on Abaqus results alone. Ultimately, physical fire testing must validate any computer model.

Chapter 5

Single element modelling

5.1 Introduction

This chapter presents the results and analysis of finite element (FE) models that focus on single structural elements of the cellular beam structure (CBS). These models yield valuable results without resorting to the complexity of a global structural model. However, the limitations thereof must be kept in mind, as the behavior of the surrounding structural elements is inextricably interlinked to that of single structural elements. Nevertheless, the single element results are useful, as they serve to characterise the behaviour of the secondary beams (J-beams) and primary beams (P-beams) under a variety of fire and boundary conditions.

The chapter begins with an overview of the thermal analysis that was performed by Marx (2018), which provided the steel temperature results used throughout this thesis. Thereafter, a summary of all structural loads acting on the CBS is given. Subsequently, a detailed analysis of the single J-beam model is presented, which is followed by the single P-beam model analysis. Finally, the chapter concludes with a summary of all major findings.

5.2 Thermal analysis

As discussed in the scope in Chapter 1, this thesis presents a structural analysis of the CBS during a fire, whilst the thesis of Marx (2018) focuses on the thermal analysis. Thus, a fully *decoupled* analysis procedure was performed. Such an analysis is computationally efficient, as optimal modelling approaches can be used for the two different types of analyses (Wang *et al.*, 2013). Moreover, in a team project environment, a decoupled analysis is more manageable as different members have clearly defined roles. Besides, Wang *et al.* add that the alternative, a fully *coupled* analysis, is not required in most cases.

In this section, the findings of the thermal analysis are presented, as they serve as essential input for the structural analysis. Furthermore, an overview of the modelling approach used will be given. However, for a more detailed discussion on the thermal analysis that was performed, the reader is referred to the thesis of Marx (2018).

5.2.1 Overview of thermal analysis

In order to investigate the structural behaviour of the CBS in fire, the steel temperatures first needed to be determined. The level of insulation that the novel sandwich floor system would provide was unclear, and the complexity of the system necessitated a FE heat transfer analysis. Abaqus was used by Marx (2018) to create a series of FE models of the floor system to estimate the steel temperatures in a fire. Figure 5.1 is example of such an analysis, illustrating the temperature distribution through a J-beam. In the figure, the J-beam resembles a regular I-beam due to an additional angle. This angle is only partly bolted onto the J-beam for construction and transportation purposes, but was ignored in all further structural models, as specified by the SAISC. However, it was included in the thermal analyses as it affects the heat transfer through the ceiling system.

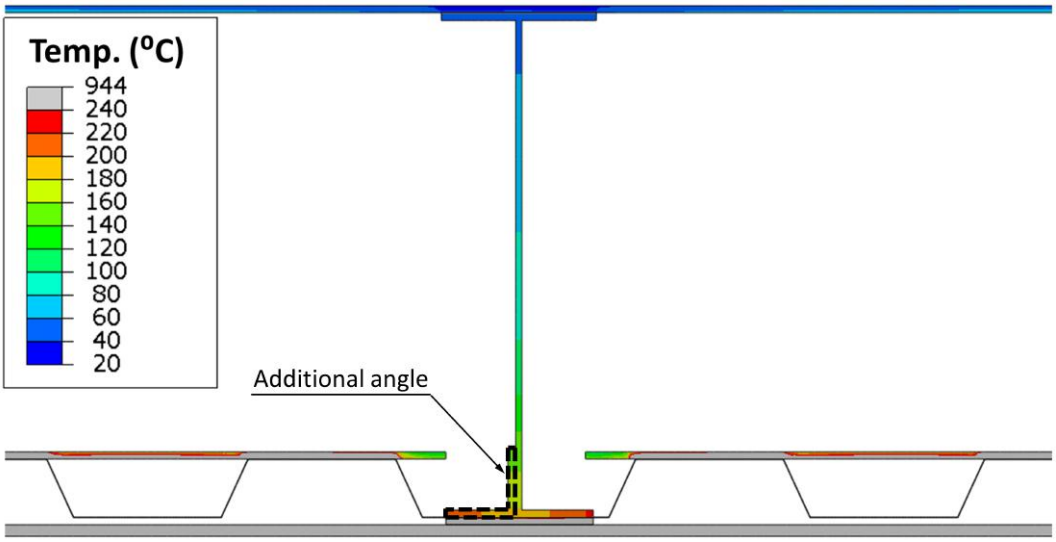

Figure 5.1: Example of an Abaqus thermal analysis of the sandwich floor system (Marx, 2018)

Two different thermal loads were used in the thermal analysis: (1) A 60 minute standard fire was utilised. This is the legislative requirement for office buildings between three and ten storeys in height, as per the *South African National Building Regulation Part T: Fire Protection* (SABS, 2011*b*). (2) A parametric fire was calculated using the Eurocode design equations (CEN, 2002), based

on the assumptions given in Table A.1 in Appendix A. The resultant time-temperature curve is based on the CBS layout, including fuel load, ventilation and lining materials. In this way the parametric fire is different to the standard fire, as it better simulates a real fire and is case-specific to the CBS, whilst the standard fire is a universal benchmark. The parametric fire models were run for 120 minutes to give the steel time to cool down. The two fire curves are shown in Figure 5.2. Notably, the parametric fire achieves a higher maximum gas temperature of 1188°C after 20 minutes, whilst the standard fire continuously rises until a maximum of 945 °C after the full 60 minutes. However, the most significant difference is the cooling stage of the parametric fire, which begins after 20 minutes and continues until 40 minutes, at which point the gas temperature is 20°C i.e. the fire has completely decayed.

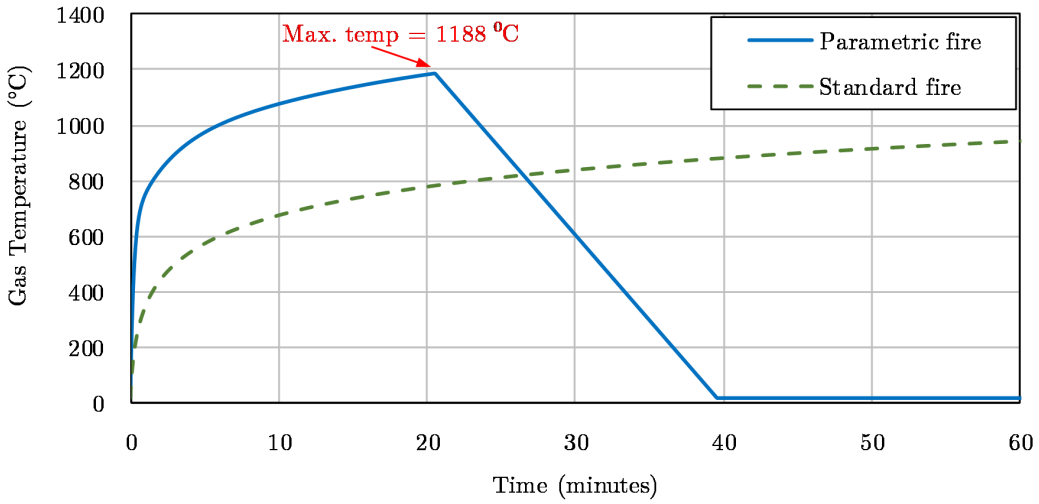

Figure 5.2: Parametric and standard fire temperatures used in the thermal analysis of the cellular beam structure (CBS) (Marx, 2018)

Furthermore, a worst-case scenario was considered, in which the fire-resistant board was ignored under standard fire conditions, as shown in Figure 5.3. This is very conservative, as only a severe loss of structural integrity could cause this. Nevertheless, such a scenario was included to determine what would happen if the primary thermal insulation were to fail entirely, and what structural behaviour may be observed in such a situation. Henceforth, this will be referred to as a 'no ceiling' (StF-NoC) analysis. Conversely, the standard fire analysis with the ceiling remaining intact will be referred to as a 'ceiling' (StF-C) analysis.

In the thermal analysis, it was generally found that the lowest areas of steel were the hottest, whilst the highest zones were the coolest at any one point. This is to be expected, as the fire occurs beneath the ceiling, placing the lower steel areas closer to the heat source. Thus, the thermal analysis yielded a

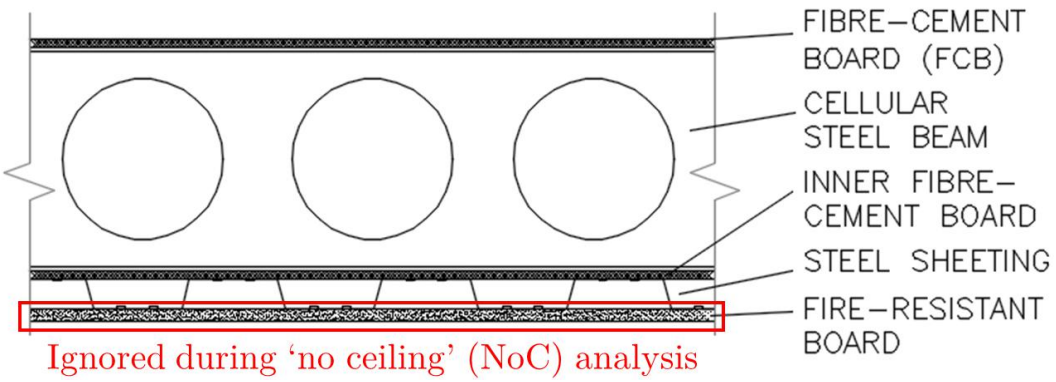

Figure 5.3: Cross-section of the cellular beam structure (CBS) floor system during a 'no ceiling' analysis (StF-NoC)

highly non-uniform temperature distribution over the entire section. However, when extracting the input temperatures for the structural analysis, a simplified temperature distribution was applied. The steel beams were separated into four segments: bottom flange (BF), lower half of the web (LW), upper half of the web (UW) and the top flange (TF). It is common in the literature that only a single temperature is defined for the web of a beam (Najafi and Wang, 2016; COST, 2014; Burgess *et al.*, 1991). However, due to the large depth of beams and corresponding large temperature differentials, a second zone was included. Conversely, the much smaller channels were not deemed to require this, and only a single temperature was specified for the entire web (W). Figure 5.4 shows a J-beam compartmentalised in this way. For each segment, the average of the nodal temperatures was applied over the entire segment in the structural analysis. This assumption significantly decreased the structural modelling complexity, yet was still able to capture the non-uniform temperature distributions within the sections.

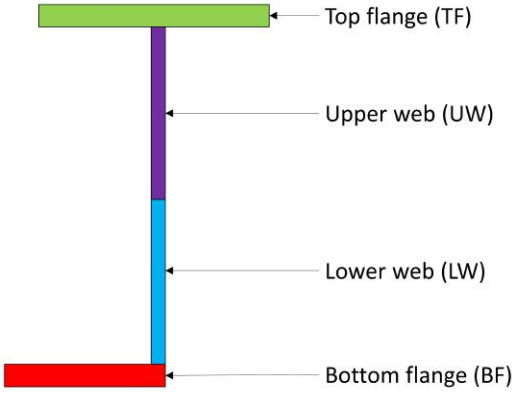

Figure 5.4: Homogenous temperature zones of a J-beam

As discussed in Section 2.3.2, the fire resistance of a structure has three criteria: stability, integrity and insulation (Buchanan and Abu, 2017; Lennon, 2011). As part of the insulation criteria, the lower ceiling is required to limit the conduction of heat into the plenum i.e. ceiling void. This serves to prevent any services from catching fire. In the thermal analysis, it was found that a 15 *mm* gypsum board was able to provide this insulation (Marx, 2018), and the predicted temperatures for this arrangement have been adopted in this work. Considering this, it follows that the resultant steel temperatures will be lower than would commonly be expected due to the significant insulation.

5.2.2 Standard fire results

Figures 5.5 to 5.7 present the steel temperature results of the standard fire thermal analyses. Figure 5.5, Figure 5.6 and Figure 5.7 are for the J-beam, P-beam and channel respectively. The figures show the temperature for each segment, during the StF-C analysis as well as the StF-NoC analysis. The acronyms and colour association illustrated in Figure 5.4 are used for the graph legends. Furthermore, the 'no ceiling' temperature curves are dashed. Two important observations can be made: (1) With no ceiling the steel temperatures were found to be between approximately 300°C and 500°C higher than the analysis with the ceiling included. (2) There is a 'lag effect' in the StF-C temperatures, whereby it takes approximately 20 minutes for the steel to begin heating up. However, with no ceiling present the steel temperatures begin rising much sooner. Both of these observations emphasise the importance of maintaining the integrity of the fire-resistant board.

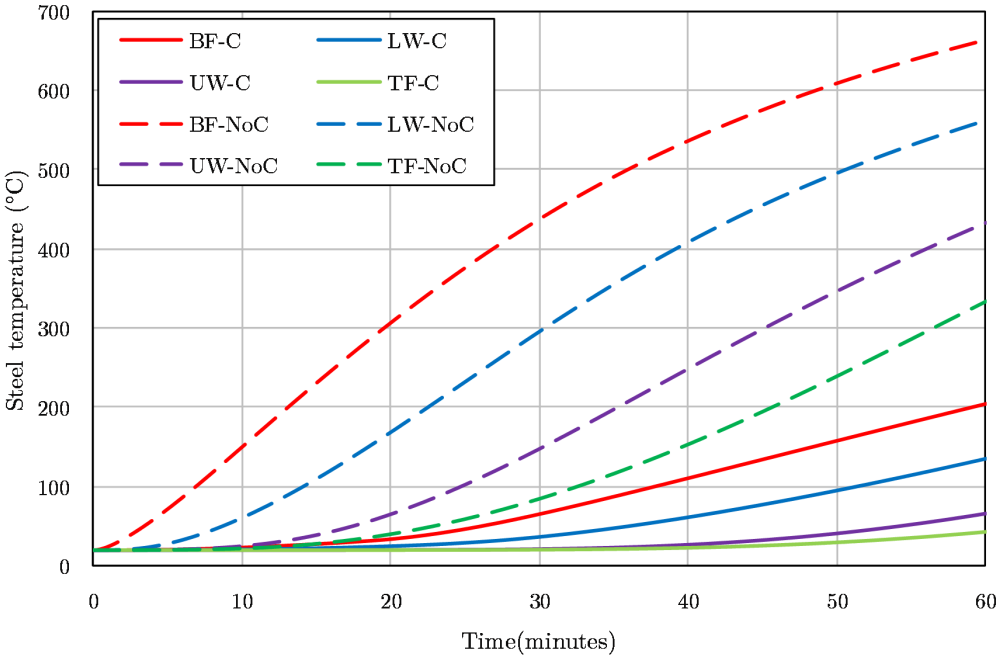

Figure 5.5: J-beam - predicted steel temperatures during a 60 minute standard fire (Marx, 2018)

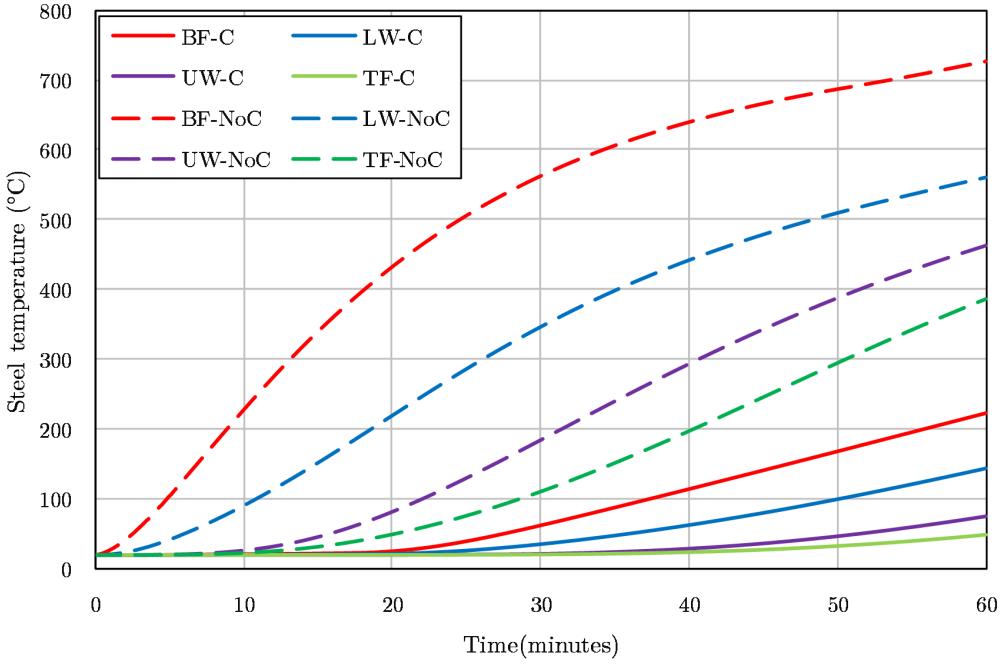

Figure 5.6: P-beam - predicted steel temperatures during a 60 minute standard fire (Marx, 2018)

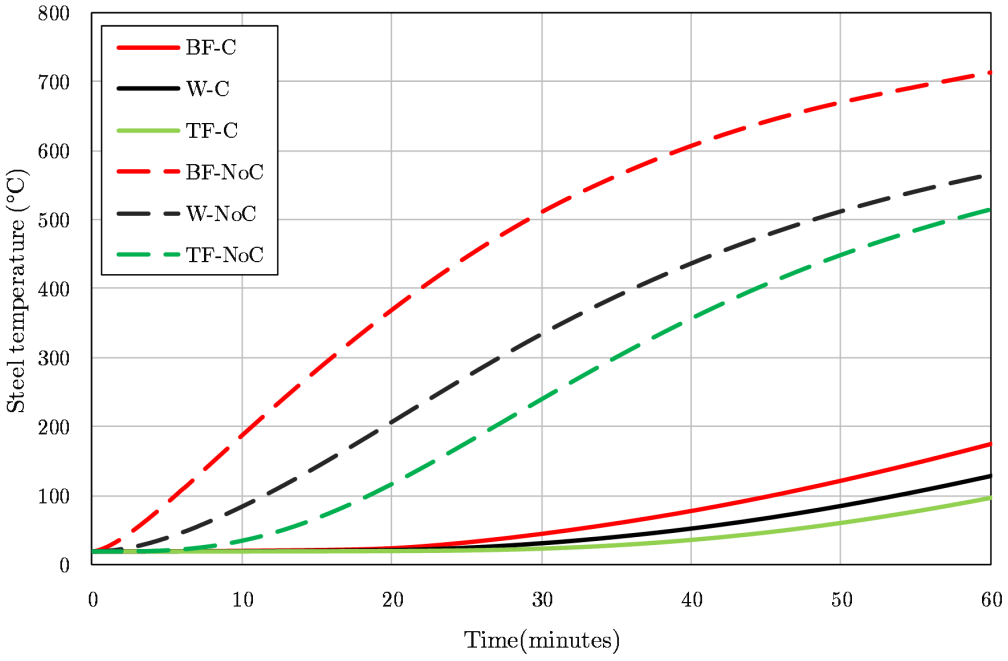

Figure 5.7: Channel - predicted steel temperatures during a 60 minute standard fire (Marx, 2018)

5.2.3 Parametric fire results

Figures 5.8 to 5.10 present the steel temperature results of the parametric fire thermal analysis. Figure 5.8, Figure 5.9 and Figure 5.10 are for the J-beam, P-beam and channel respectively. Again, two observations can be made: (1) An approximately 10 minute 'lag effect' can be seen, which is half the time of the StF-C analysis. This is likely due to the higher initial temperatures of the parametric fire. (2) The cooling phase of the parametric fire, which begins at 20 minutes, causes a decrease in steel temperatures. However, the time at which the steel temperatures begin to drop is not uniform throughout the steel sections. The curves show that the lower segments start cooling sooner than the upper segments. This can be attributed to the conduction of heat through the segments i.e. heat flowing from lower segments to upper segments, and the retention of heat in the ceiling void.

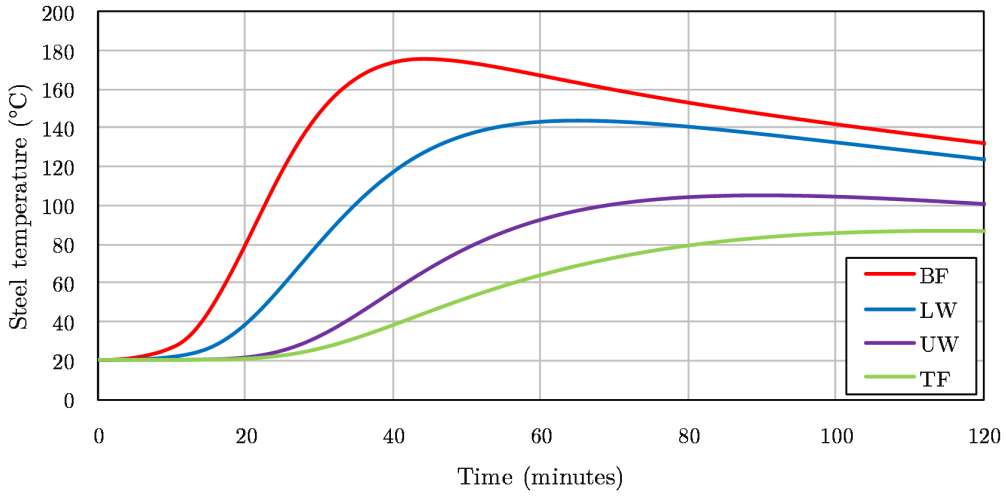

Figure 5.8: J-beam - predicted steel temperatures during the parametric fire (Marx, 2018)

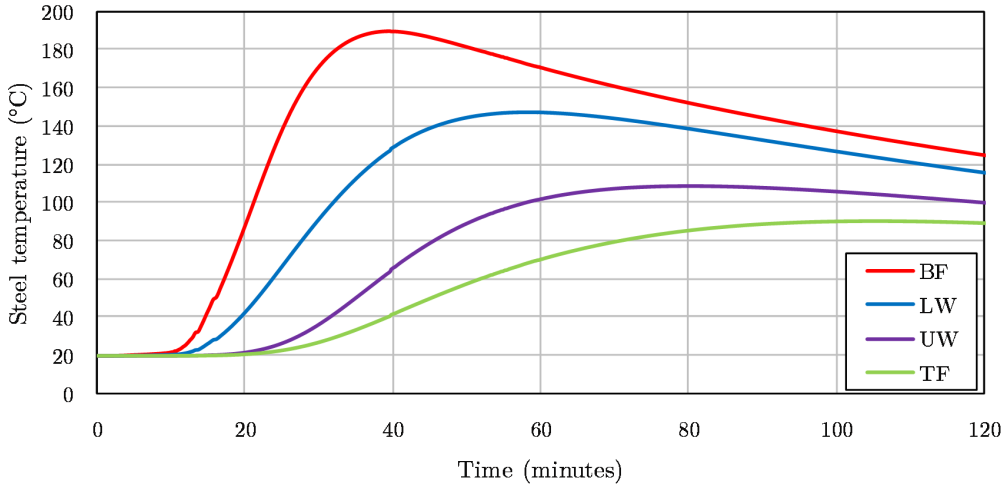

Figure 5.9: P-beam - predicted steel temperatures during the parametric fire (Marx, 2018)

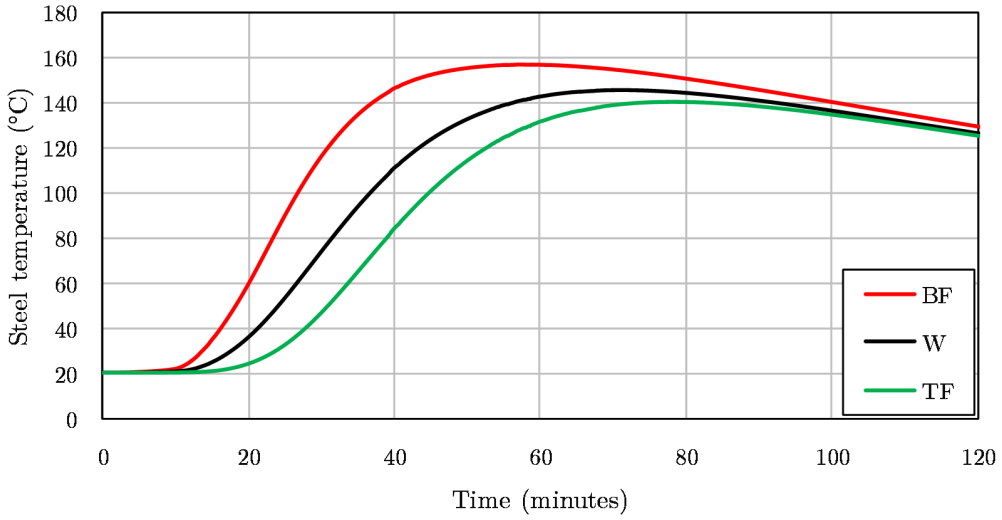

Figure 5.10: Channel - predicted steel temperatures during the parametric fire (Marx, 2018)

5.3 Structural loading

The CBS concept is still in a developmental stage, and the current design does not necessarily represent the final version. Presently, only the prototype CBS exists, upon which the structural loads were based. However, in some cases assumptions had to be made with regards to expected loading. Table 5.1 lists all the nominal loads that were identified. The fire limit state (FLS) recommended by Walls *et al.* (2014) was used to factor the nominal loads. Consequently, all permanent loads were multiplied by 1.0 and all imposed loads by 0.5.

The self-weight of the J-beam, P-beam and channel were calculated based on the shop drawings (Appendix B). The decks include all fibre-cement and fire-resistant boards, and were calculated assuming a total combined thickness of 25 mm and a density of 2360 kg/m^3. The steel sheeting corresponds to the weight of 0.8 mm Bondek®[1] sheeting. The access floor weight was obtained based on considering commonly available products on the market. The services, partitions and office floor loading are taken from the SANS 10160-2 loading code (SABS, 2011*a*).

[1]Bondek® is a proprietary sheeting product used in composite construction

Table 5.1: Nominal loads used in the structural analysis of the cellular beam structure (CBS)

Permanent Loads		
J-Beam	0.46	kN/m
P-beam	0.42	kN/m
Channel	0.191	kN/m
Decks	0.59	kPa
Steel sheeting	0.078	kPa
Access floor	0.5	kPa
Services	0.2	kPa
Imposed Loads		
Partitions	0.8	kPa
Office occupancy	2.5	kPa

5.4 J-beam modelling

5.4.1 FEM input

In Chapter 4, it was emphasised that a FE model can be highly sensitive to user-defined input values. The input used in this thesis to model a single J-beam is summarised below. This serves to detail the methodology of this thesis, and to allow a future validation of results if required.

5.4.1.1 Geometry

The geometry of the J-beam was based on the shop drawings (Appendix B) of the CBS supplied by the SAISC. Figure 5.11 illustrates the dimensions of the J-beam. Shell elements were chosen over solid elements as they contain significantly fewer nodes and elements, thereby increasing the modelling efficiency. The thickness of the flange and web were thus assigned to the appropriate shell segments. The web was extended to the midpoint of the top and bottom flanges, as shown in Figure 5.11. This was done to best describe the moment of inertia around the strong axis, as the flange shell segments thus act at the centroid of the actual flanges. Thus, there is a slight overlap in steel areas. However, van Jaarsveldt (2016) has shown that this overlap has a negligible effect on results, as the weld radii that are neglected by models are approximately replaced by this overlap.

5.4.1.2 Elements and mesh

Quadrilateral shell finite elements with four nodes (S4) were utilised. The use of shells and S4 elements has been validated in Chapter 4, and is widespread

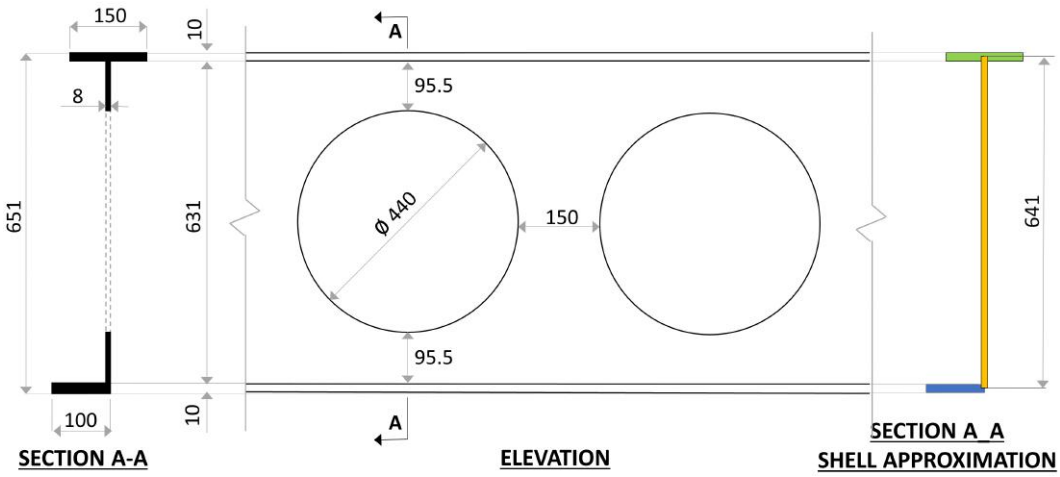

Figure 5.11: J-beam dimensions. The far right shows the shell approximation used. All dimensions in mm. Note: drawing not to scale

in previous studies of steel beams in fire (Wang *et al.*, 2014; Najafi and Wang, 2016; Yin and Wang, 2004). Whilst these studies opted for a reduced integration scheme with only one integration point, this research employed a more detailed linear integration scheme between all four points. An approximate seed size of 25 *mm* yielded a mesh with 6 elements across the width of the top flange, 16 along the height of the web, and 4 across the width of the bottom flange, as shown in Figure 5.12 below. The chosen mesh size was validated in a mesh sensitivity analysis presented in Section 5.4.1.6 below.

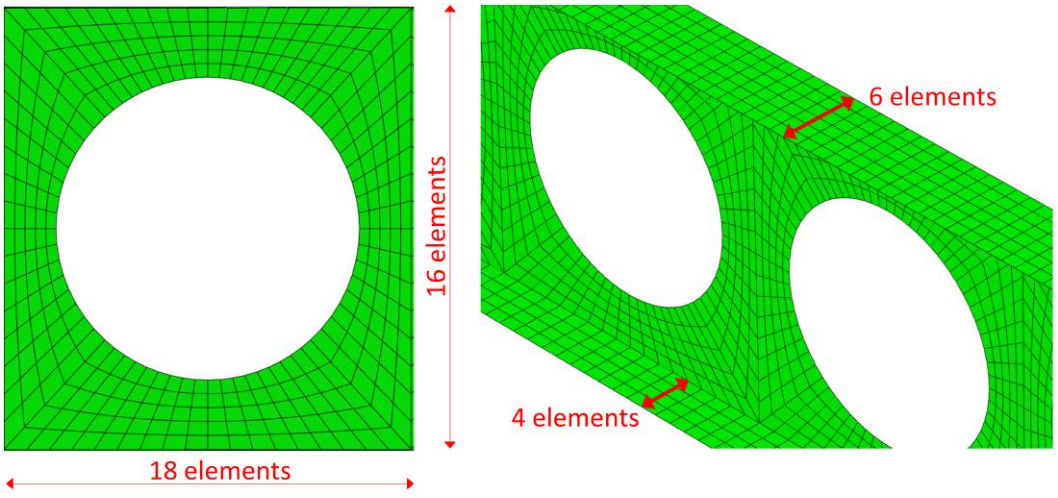

Figure 5.12: 25 *mm* mesh used for the single J-beam model

5.4.1.3 Material properties

The EN material model that was developed for the validation studies was applied (refer to Section 4.3.1). However, whereas the Eurocode uses 210 GPa as the ambient Young's modulus for steel, this research used 200 GPa as per South African norms (SAISC, 2013). Furthermore, a constant value of 1.4×10^{-5} was used for the coefficient of thermal expansion. This value is recommended by the European Convention for Constructional Steelwork (ECCS), and has been successfully implemented by Najafi and Wang (2016) in a study on axially restrained cellular beams at elevated temperatures.

5.4.1.4 Loads and boundary conditions

Figure 5.13 illustrates the loading and boundary conditions (BCs) applied to the J-beam. An internal J-beam was modelled (J2 or J3 in Figure 3.5), as these carry higher loads than the outer J-beams. The total self-weight of the J-beam was applied as a series of 27 equally spaced point loads (136 N at 295 mm spacing - blue arrows show a limited number these loads). Point loads were applied on the bottom flange, in line with the web. The direction of point loads remained constant during the analysis i.e. the load direction did not follow the rotation of the beam. The loading transferred by the channels has been applied as an additional 2 point loads (31.9 kN and 36.3 kN - red arrows).

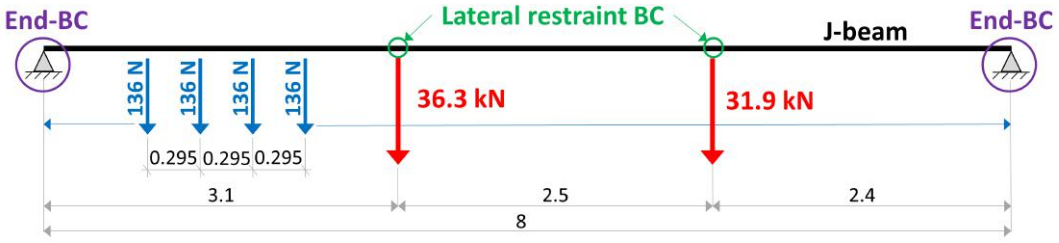

Figure 5.13: Elevation view of single J-beam model showing loads and boundary conditions

In the actual CBS, the channels and knee-braces provide lateral restraint to the J-beam. However, in the single element model these are included by providing a lateral restraint BC (green circles). Different end-BCs are provided (purple circles) to simulate the varying support conditions that primary beams (P-beams) could potentially provide, and what influence these have on structural behaviour. Four variations were tested: fixed-fixed (FF), fixed-roller (FR), pin-pin (PP) and pin-roller (PR), as illustrated in Figure 5.14.

In the Abaqus model, the end-BCs were applied at simulated reference points (RFs) that were kinematically constrained to the web of the J-beam (this process was previously discussed in Chapter 4, and shown in Figure 4.2). The

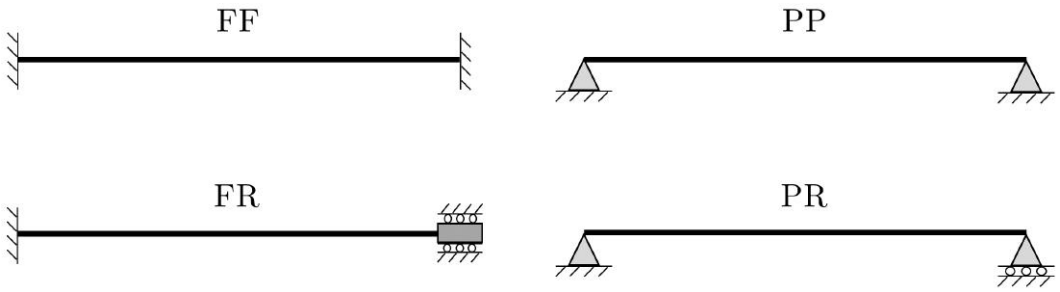

Figure 5.14: Diagram illustrating the four end boundary condition cases used for the J-beam model

RFs were placed at the same height as the centre bolt of the actual connection, and positioned to be flush with the web of the P-beam i.e. 76 *mm* from the edge of the J-beam web. Figure 5.15 shows a photo of the P-J connection, with the information above superimposed for clarity.

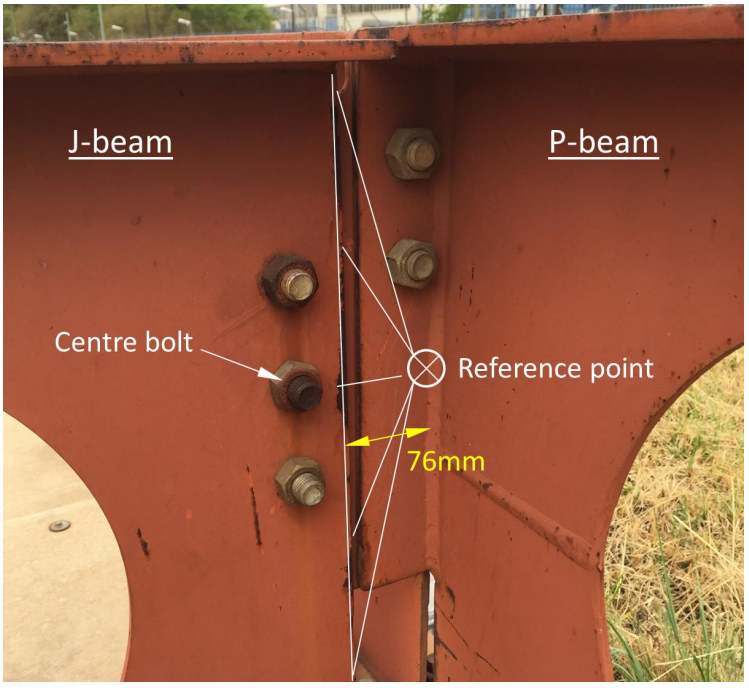

Figure 5.15: Reference point (RF) and kinematic constraint superimposed on a photo of a J- to P-beam connection

5.4.1.5 Solution procedure

The solution procedure used for the J-beam was equivalent to that of the Gillie (Section 4.2) and COST 1 (Section 4.3.2) benchmarks. In summary, there are three steps: (1) an initial step in which BCs are applied, (2) a mechanical step in which structural loads are applied, and (3) a thermal step in which

the steel temperature curves are applied over a normalised time period. An initial time increment size of 0.05 (3 minutes) was used for the StF-C and parametric fire analyses, whilst a smaller initial time increment of 0.01 (36 seconds) was used for the StF-NoC analysis. The smaller time increment was necessary as the steel starts heating up sooner. Thereafter, the automatic time incrementation feature of Abaqus was used, which adjusts the size of time increments based on the speed at which the solution converges (Abaqus, 2014). The parametric fire analysis utilised an initial increment size of 0.02 (2.4 minutes). The temperatures for the four steel segments (BF, LW, UW, TF) were specified as predetermined fields in the thermal step.

For the StF-NoC and parametric fire cases it was found that the solution procedure above did not converge for the PP J-beam. This was due to a local buckling event causing a momentary loss of equilibrium, during which a rapid transfer of strain energy from localised buckling zones to neighbouring parts of the model must take place. A simple way to understand this phenomenon is that the stiffness of elements becomes approximately zero, and displacements must occur before equilibrium is retained. However, a static solution method cannot solve a zero stiffness matrix. Hence, a dynamic analysis must be used or artificial damping can be applied (Abaqus, 2014). The latter supplies a small amount of damping to the system, which prevents a zero stiffness matrix from forming during instabilities. This allows matrices to be solved, deflections to occur and stability to be regained. Artificial damping was chosen in this research, for three reasons: (1) This approach has been successfully used in previous structural fire models (Yin and Wang, 2004; Najafi and Wang, 2016). (2) Abaqus has a built-in functionality that easily enables this. (3) The complexity and computational expense of a dynamic analysis is unwarranted.

Abaqus provides several options to apply artificial damping, also called *dissipated energy fraction*. This research utilised the *adaptive automatic stabilisation scheme*, which adjusts the size of the damping factor during an analysis. The adjustment is made based on the convergence history and the ratio of viscous damping energy to total strain energy. Thus, the damping factor is kept high enough to enable convergence, but low enough to not significantly affect the results. This scheme is preferred in relation to a constant value used throughout the analysis, as such an optimal damping factor can vary. The reader is referred to the *Abaqus Analysis User's Guide* (Abaqus, 2014) for further information. In this research, an initial damping factor of 2×10^{-5} was generally used, which was adjusted to 2×10^{-4} when further challenges to convergence were experienced. The default accuracy tolerance of 0.05 was consistently chosen. The artificial damping input screen is shown in Figure 5.16.

However, special precautions must be taken if artificial damping is applied. Firstly, the damping factor is problem-dependent, and thus a trial-and-error method is required to obtain an initial damping factor that works. Secondly,

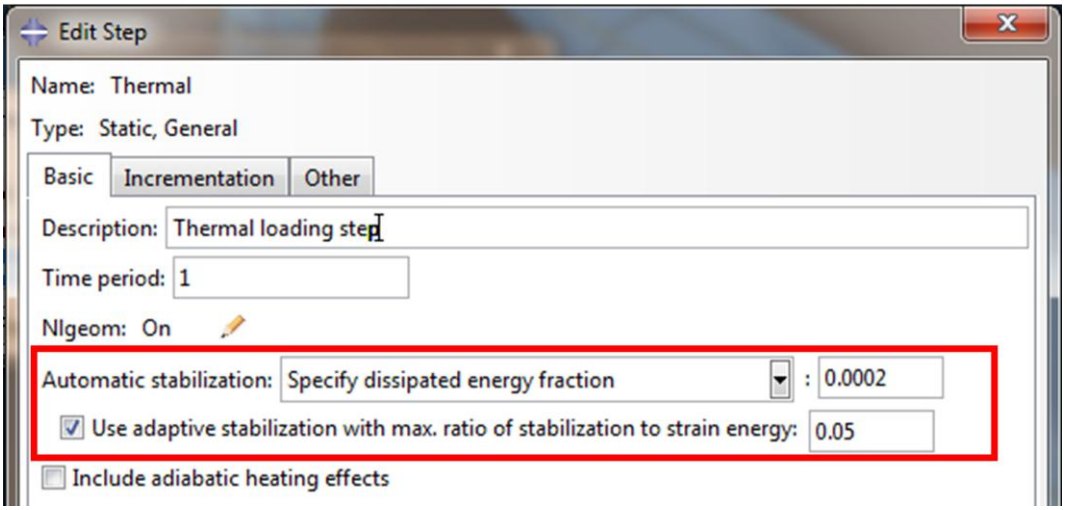

Figure 5.16: Abaqus artificial damping implementation

a damping factor that is too high can lead to inaccurate results. The adaptive stabilisation scheme helps to avoid this, but the Abaqus user manual still recommends a manual check. Thus, whenever damping was applied, the total strain energy was compared with the viscous damping energy. Abaqus recommends that this ratio should not exceed any "reasonable amount". Amongst all the single element models in this research, the viscous damping energy was at most 0.4% of the total strain energy, and was deemed satisfactory. Simply put, a maximum of 0.4% of the total load applied was effectively carried by the provided damping stiffness matrix.

5.4.1.6 Mesh sensitivity analysis

The chosen size of a mesh element can have a significant impact on the results of a FE model. Generally, a finer mesh will produce more accurate results (Cook *et al.*, 2002). However, this can greatly increase the time needed to run a model. Conversely, a coarse mesh is quick to run, yet can yield inaccurate results. Thus, a compromise between the two options is ideal, whereby sufficiently accurate results are achieved in an efficient way.

A sensitivity analysis has been performed to determine an optimal mesh element size. Three approximate mesh sizes were chosen: 50 mm, 40 mm and 25 mm. The 25 mm mesh is shown in Figure 5.12, whilst the 50 mm and 40 mm meshes can be seen in Figure 5.17. The J-beam model was used, for which the PP and PR end-BC test cases were chosen. The StF-NoC temperatures (Figure 5.5) were applied. As will be discussed in Section 5.4.2 below, the higher temperatures cause the top flange to buckle for the PP case. This highly non-linear outcome was specifically chosen, as the associated convergence complexity provided a rigourous testing ground.

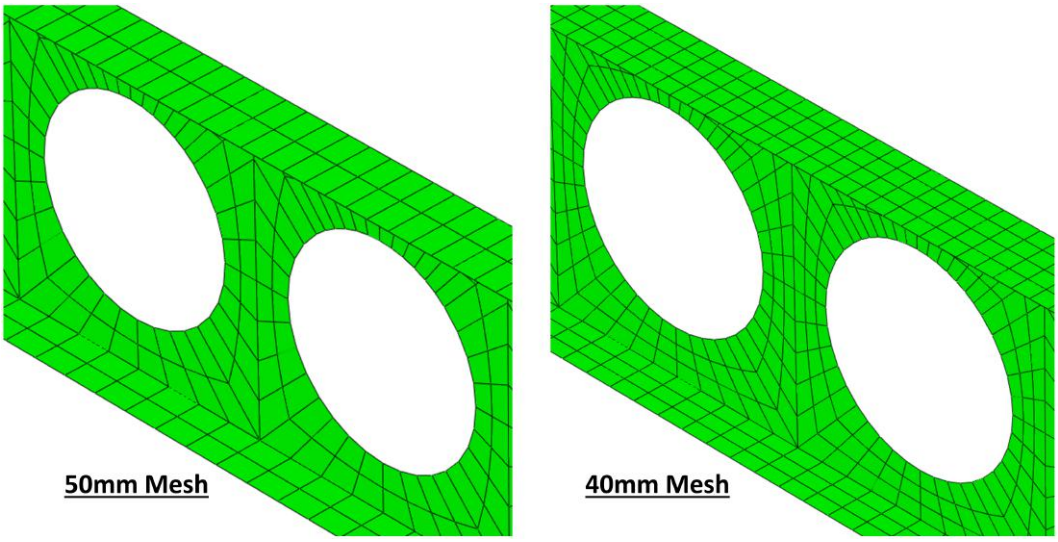

Figure 5.17: 50 *mm* and 40 *mm* meshes used in the mesh sensitivity analysis

The axial force and midspan deflection results of a PP J-beam with the different mesh sizes are given in Figure 5.18. A good correlation can be seen between the results, with slight differences in values. The refinement from 40 *mm* to 25 *mm* yielded maximum axial forces within approximately 0.6% of each other, and maximum midspan deflections of within 1% of each other. For the PR case, the same mesh refinement yielded midspan deflections within approximately 3.5% of each other (the PR graph has not been included for conciseness). Based on the above findings, further refinements in mesh size would have had a negligible effect on results.

5.4.2 Standard fire analyses

Figures 5.19 and 5.20 present the results from the StF and StF-NoC analyses respectively. The graphs show both the axial force and midspan deflection on separate axes for the four end-BC conditions. Axial forces are only present in the fixed-fixed (FF) and pin-pin (PP) cases, as the other two cases provided no axial restraint. A discussion and analysis of the results is presented below. The reader is encouraged to consult both the figures and text in conjunction, as the complicated structural behaviour is difficult to visualise based on only one set of details in isolation.

The standard fire with a ceiling analysis (StF-C) yielded the following findings:

- The 'lag effect' in steel temperatures causes a delayed reaction of the axial force and deflection, as they only begin to change significantly after approximately 20 minutes. This indicates that if a fire is quenched soon enough, the structural steel will have remained effectively unaffected.

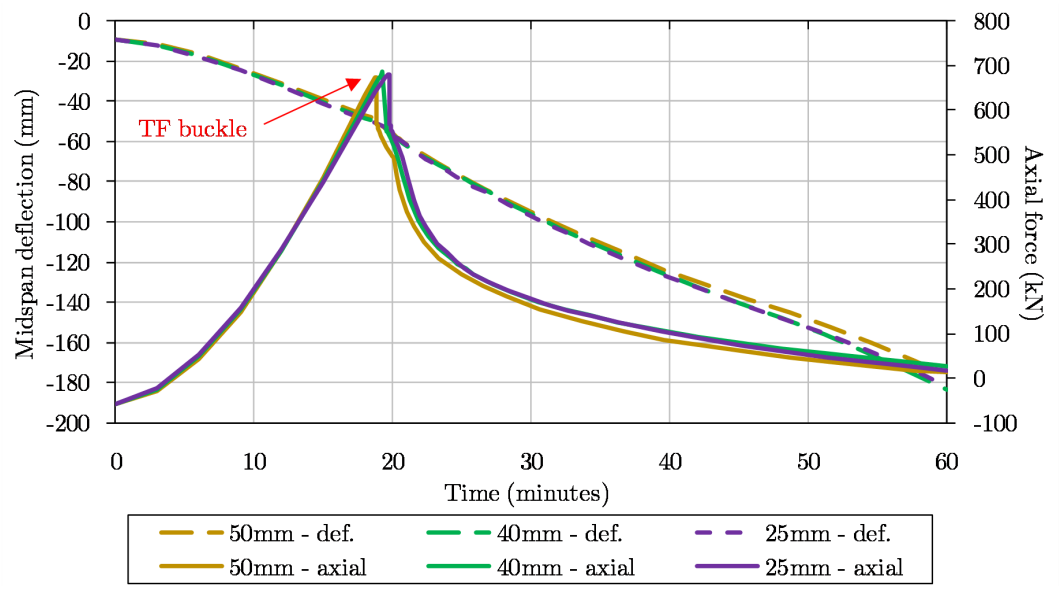

Figure 5.18: Mesh sensitivity analysis - axial force and midspan deflection of a pin-pin (PP) J-beam, during a standard fire analysis with no ceiling (StF-NoC). The time at which the top flange (TF) buckles is indicated.

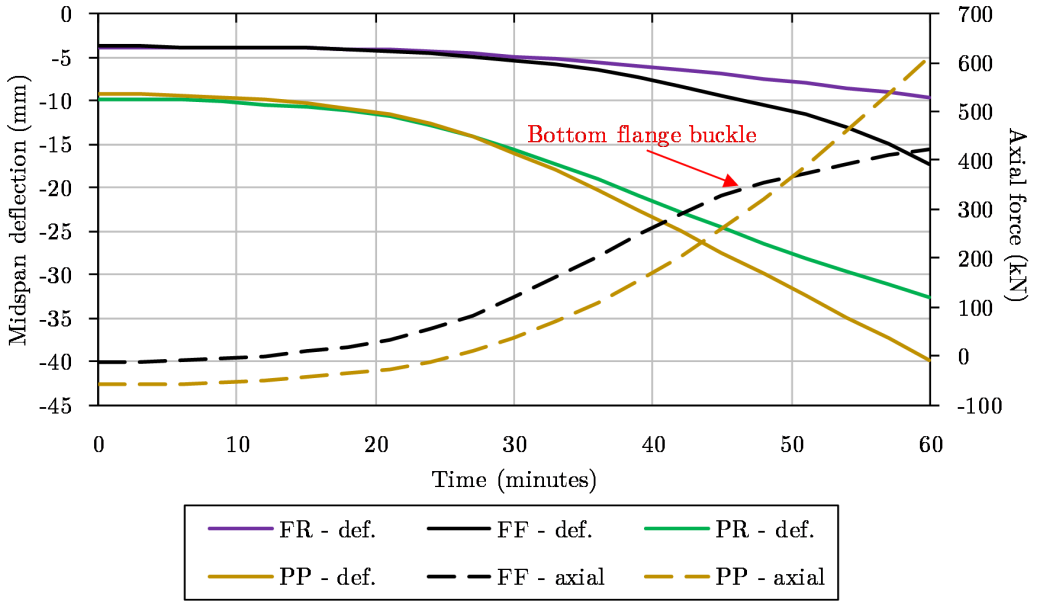

Figure 5.19: J-beam - axial force (axial) and midspan deflection (def.) during a standard fire the ceiling remaining intact (StF-C), with varying end boundary conditions

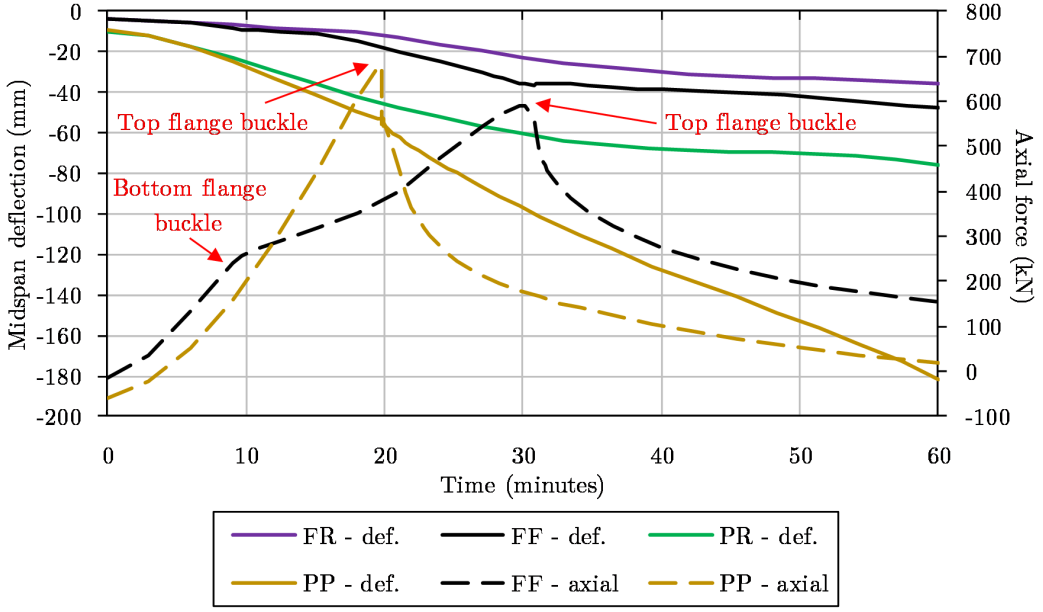

Figure 5.20: J-beam - axial force (axial) and midspan deflection (def.) during a standard fire with no ceiling (StF-NoC), with varying end boundary conditions

- Figure 5.19 shows that, as a general rule, axial restraint increases the midspan deflection. For instance, the FF deflection is 133% greater than the FR deflections, whilst the PP deflection is 75% higher than the PR deflections. These comparisons are based on offsetting the initial ambient temperature deflection i.e. only taking into account thermally induced deflection. This suggests that giving the beams room to freely expand can be beneficial to the structure, as it reduces midspan deflections. It was found that the maximum total longitudinal expansion was 6.4 mm and 7.5 mm, for the PR and FR cases respectively.

- Providing a moment restraint, as in the FF and FR cases, significantly stiffens the beams and reduces the midspan deflection. This can already be seen at ambient temperatures conditions i.e. 0 minutes, at which point the FF and FR beams have a midspan deflection approximately half that of the PP and PR beams. However, the difficulty in providing such a moment restraint in an actual connection is significant, especially under elevated temperatures.

- The PP case causes the greatest midspan deflection of 40 mm. This is due to the combination of axial restraint and lack of moment fixity. However, this worst case scenario deflection corresponds to a relatively low deflection ratio of span/200. This is ten times less than what is recommended by Part 20 of BS 476 (BSI, 2009), which limits the deflection of beams during fires to span/20.

- The asymmetry of the J-beam causes an unusual phenomenon, where the bottom flange bends outwards at higher temperatures. This event can can be seen in Figure 5.21, which shows a FF J-beam after a 60 minute standard fire (with ceiling). This can be attributed to an internal moment (about the weak axis of the J-beam) induced by the bottom flange being restrained by the cooler web on one side, and free to expand on the other. This is exacerbated by any axial restraint or moment fixity, which further hinders the expansion of the web. In the FF case, the induced moment is significant enough to buckle the bottom flange, which can be seen in a decrease in the rate of axial force (marked in Figure 5.19). The maximum lateral deflections in the bottom flange are summarised in Table 5.2. This table also includes the deflections from the StF-NoC and parametric fire analyses, which will be discussed further below.

Table 5.2: Maximum lateral deflection (in mm) of the bottom flange of the J-beam, under all fire and boundary condition scenarios

	PR	**PP**	**FR**	**FF**
StF-C	4.1	13.1	29.3	59.2
StF-NoC	5.6	23.6	94.4	247
Parametric fire	4.1	14.7	22.9	57.5

- Due to the asymmetry of the J-beam, it was found that introducing geometric imperfections based on an elastic buckling analysis was unnecessary. This approach was successfully used in the COST 2 benchmark (Section 4.3.3). However, the benchmark used a geometrically perfect I-beam, which required a user-defined initial imperfection to precipitate a non-linear reaction. In the case of the J-beam, the inherent asymmetry, which only increases with elevated temperatures, renders this measure unnecessary.

The standard fire with no ceiling analysis (StF-NoC) yielded further findings:

- The higher steel temperatures cause lateral torsional buckling in the top flange in both the PP and FF cases. This can be seen in Figure 5.22, which shows a PP J-beam after a 60 minute standard fire (no ceiling). The buckling can be attributed to the higher axial forces, as well as the significantly reduced material properties. In the FF case, the top flange buckling was preceded by bottom flange buckling caused by outward bending of the bottom flange. However, in both the PP and FF cases, buckling did not result in a runaway deflection. Rather, for the PP case,

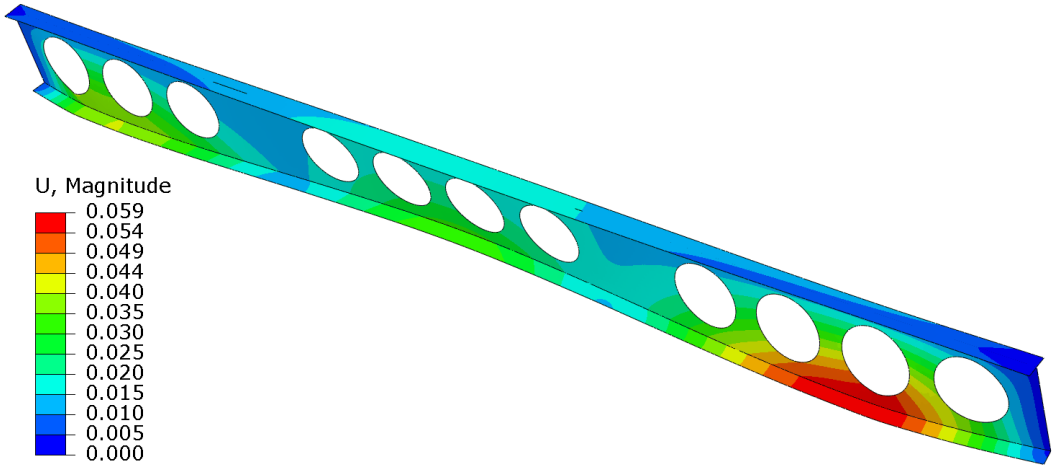

Figure 5.21: Fixed-fixed (FF) J-beam experiencing lateral deflection of the bottom flange caused by restrained thermal expansion. The total deflection is shown (in m), with a deformation scale factor of 2.

the rate of deflection merely increased, resulting in a maximum midspan deflection of 181 *mm* (span/44). In the FF case, the buckling actually *decreased* the rate of deflection. This may be counter-intuitive, but can be attributed to a release of stress following the buckling. This, when combined with the moment fixity, allows the beam to 'bounce back' slightly.

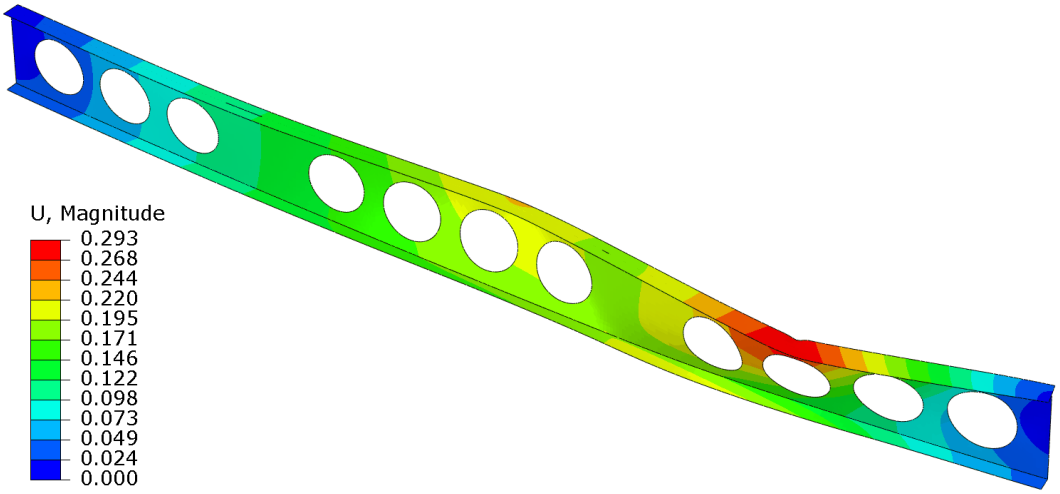

Figure 5.22: Pin-pin (PP) J-beam after the top flange has buckled. The total deflection is shown (in m), with a deformation scale factor of 1.

- Despite the significantly higher temperatures, the steel did not weaken enough for any major failure mechanism to develop in the J-beam for the FR and PR cases. However, the FR case did experience significant

lateral movement of the bottom flange (94 mm). Nevertheless, the midspan deflections remained relatively low, with the FR case resulting in a maximum deflection of 76 mm (span/105). This emphasises the effect that axial restraint can have in a fire, and further motivates ensuring the free expansion of beams. The maximum total expansion was 47.0 mm and 40.2 mm, for the PR and FR cases respectively.

To summarise, the important findings of both J-beam standard fire analyses are: (1) Preventing longitudinal expansion of the J-beam increases the midspan deflections. Furthermore, under higher temperatures the axial force can cause top flange lateral torsional buckling, leading to even greater deflections. (2) Conversely, allowing longitudinal expansion reduces the midspan deflection and prevents any significant failure mechanism from developing, even under the conservative 'no ceiling' temperatures. (3) The asymmetry of the J-beam causes significant lateral deflections of the bottom flange, posing a threat to the integrity of the ceiling system.

Considering all of the above, it follows that allowing thermal expansion is beneficial for the CBS. Whilst it has been shown that moment restraint further reduces vertical deflections, it also increases lateral deflections, and is thus not advisable. Ultimately, if the J-beams utilise connections that are slotted (i.e. enlarged bolt holes to allow expansion) and designed to be pinned, the behaviour would approach that of a PR beam. This is recommended, as a relatively low vertical deflection of 33 mm (span/242) is expected under standard fire conditions with the ceiling remaining intact (StF-C).

5.4.3 Parametric fire analyses

The parametric fire analysis serves two important roles: (1) to investigate if the higher maximum temperatures cause a significant structural failure and (2) to estimate possible tension forces during the cooling stage. However, when the parametric fire steel temperatures were first applied, it was found that the slow rate of cooling was preventing any tension forces from developing. Therefore, it was decided that a cooling stage would be manually enforced in this work. After 80 minutes, the temperatures of all four segments were linearly reduced to 20°C at 120 minutes, as shown in Figure 5.23. This is a reasonable assumption, as in reality the steel will always return to ambient temperature eventually, and thermal expansion is not dependent on the rate of changing temperature i.e. the length of the cooling period does not affect the analysis results. However, it appears that the thermal analysis model will need further refinement to accurately account for cooling conditions, as it may not be fully capturing the expected rate of cooling (Marx, 2018).

The axial force and midspan deflection of a J-beam in a parametric fire analysis are presented in Figure 5.24. The results yielded the following findings:

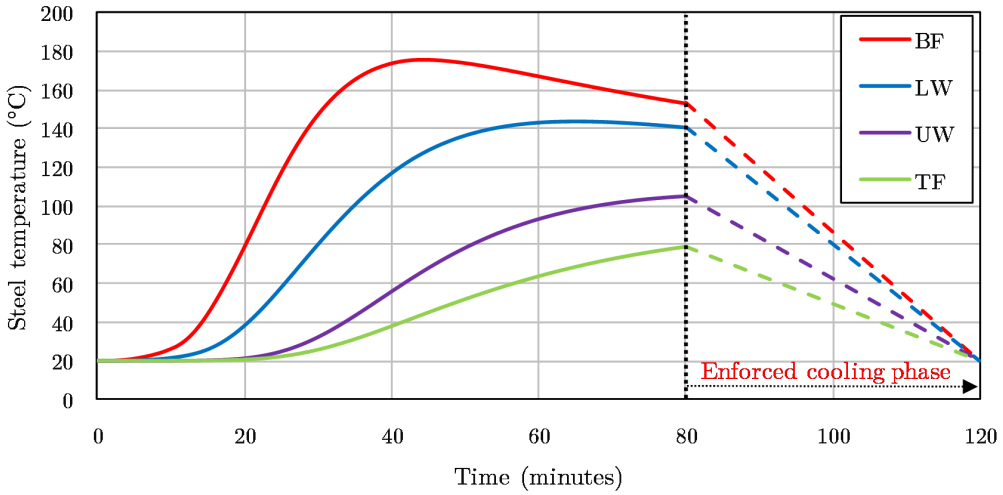

Figure 5.23: Expected steel temperatures in the J-beams during a 120 minute parametric fire, including the enforced linear cooling stage after 80 minutes

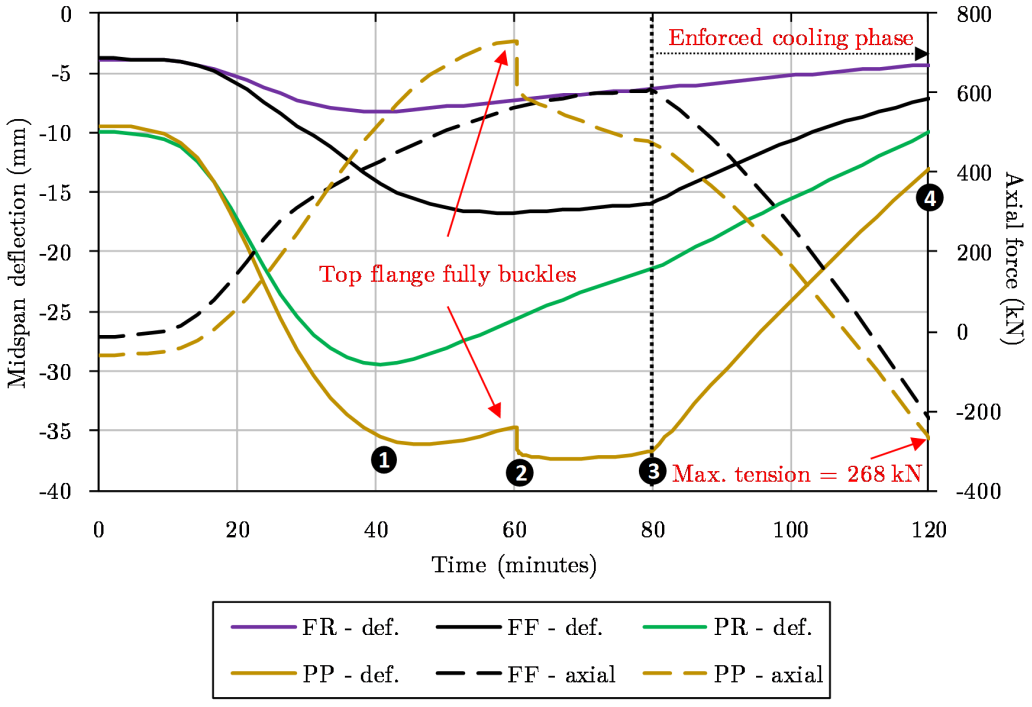

Figure 5.24: J-beam - axial force and midspan deflection during a parametric fire, with varying end boundary conditions. The numbers 1-4 correspond with Figure 5.25

- As in the standard fire analyses, the asymmetric bottom flange experienced lateral deflection as a result of restrained thermal expansion. The maximum lateral deflections are summarised in Table 5.2. This lateral movement relieves stresses and thus reduces the rate of axial force increase, as seen by the change in gradient after approximately 28 minutes in Figure 5.24. However, the cooling stage of the parametric fire allows the steel heam to recover elastic thermal deflections. The PR beam is able to recover all strain, whilst the PP, FR and FF beams return to within 8 mm, 5.1 mm and 37.6 mm of ambient deflection respectively. The permanent deformation is due to steel yielding causing plastic strain. This result indicates that a lack of both axial restraint and moment fixity, as in the PR case, reduces forces and effectively prevents any plastic strain from occurring. Such behaviour is advantageous, as it will aid any post-fire re-use of the structure.

- The parametric fire causes a complex series of events in the PP beam. This is best described in 5.25, which shows the progression of total deflection through the course of the parametric fire. There are four specific points in time that are highlighted: (1) After 43 minutes, the bottom flange has experienced enough lateral deflection to reduce the rate of increase of axial force increase, and thereby significantly prevent further midspan deflections. (2) After 61 minutes, the bottom flange has already started cooling down but the remaining segments are still heating up, thereby causing the top flange to buckle. A sudden drop in midspan deflection follows. (3) The top flange continues to deflect laterally until 80 minutes. (4) After 120 minutes, the return to ambient temperature has allowed the beam to contract and recover much of its thermal deflections. However, there is some amount of permanent deformation, most visible in the buckled top flange.

- In both 'roller' cases (FR and PR), the low stresses result in an almost pure elastic strain state i.e. little or no plasticity. As a result, the FR beam is able to return to within 0.5 mm of ambient midspan vertical deflection, whilst the PR beam shows negligible differences. However, the ceiling system must maintain its integrity during the fire, and thus the maximum midspan deflections are of interest. The PR beam experiences the greater deflection of the two, equal to 30 mm (L/267), at approximately 40 minutes.

- In contrast to the axially unrestrained beams, the FF and PP beams experienced higher stresses due to axial restraint. Thus, greater amounts of plastic strain were able to develop which led to greater permanent deformations (see No.4 in Figure 5.25). Nevertheless, the FF and PP beams were both able to return to within 3.5 mm of their respective ambient deflections. The PP beam experienced the greater midspan

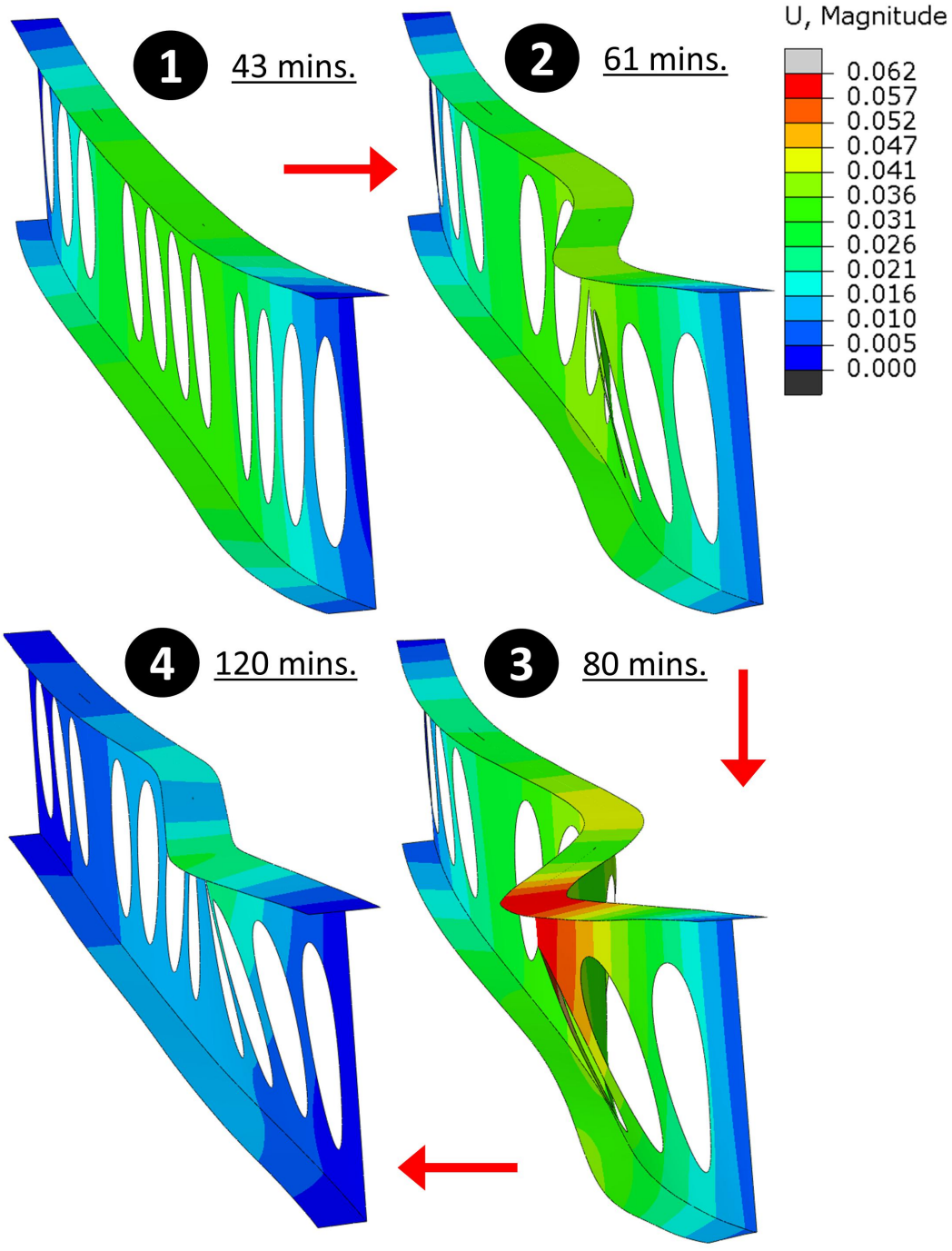

Figure 5.25: Deflection behaviour of a pin-pin (PP) J-beam through the course of a parametric fire. The total deflection is shown (in m), with a deformation scale factor of 5.

deflection during the fire, equal to 37 mm (L/216), at approximately 70 minutes.

- The enforced cooling stage caused the FF and PP beams to go into tension after approximately 110 minutes. Ultimately, the PP beam experienced the greater tension force of 268 kN after a full 120 minutes. The end connections of the J-beam should be designed with this in mind, as a sudden connection failure could be catastrophic. For instance, in the prototype CBS, the J- to P-beam connection (shown in Figure 5.15) has three M20 Class 8.8 bolts acting in shear. Each bolt has a factored shear capacity of 87.6 kN (SAISC, 2013), giving the connection an approximate total tensile capacity of $3 \times 87.6 = 263\ kN < 268kN$ i.e. failure. However, this corresponds with a perfect (theoretical) axial restraint, which is unrealistic in the case of the CBS. In reality, a situation between PR and PP can be expected, depending on the level of axial restraint provided by the P-beams. This will be discussed further in Section 6.3.1.

5.5 P-beam modelling

5.5.1 FEM input

The majority of FEM input for the primary beam (P-beam) is similar to that of the J-beam. Consequently, for conciseness a full description will not be repeated here. Rather, a brief summary of similar/common input is given: (1) The dimensions of the P-beam were based on the shop drawings (Appendix B) and are illustrated in Figure 5.26. (2) S4 elements with an approximate mesh size of 25 mm were utilised (see Figure 5.27). (3) An equivalent three-step solution procedure (initial, mechanical, thermal) was used. However, the loads and BCs were entirely P-beam-specific, and are elaborated below.

5.5.1.1 Loads and boundary conditions

The CBS is not a symmetric structure, and thus the magnitude of loads carried by the P1 and P2 beams differ slightly. The reader is referred back to Figure 3.5, which shows the structural layout and terminology used to describe the structural elements of the CBS. For the single P-beam analysis, P1 was chosen. It was not deemed necessary to model both, as the total loading is approximately equal. Figure 5.28 illustrates the loading and BCs applied to the P-beam.

The self-weight of the P-beam was combined with the contributing ceiling loading to form a single distributed loading. This was applied as a series of 42 equally spaced point loads (1212 N at 300 mm spacing - blue arrows show a limited number of these loads). The effect of J-beams was considered by

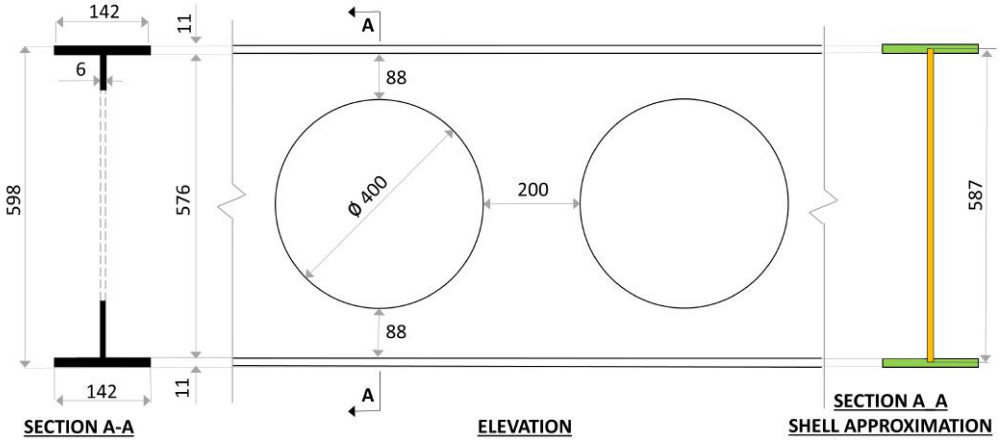

Figure 5.26: P-beam dimensions. The far right shows the shell approximation used. All dimensions in mm. Note: drawing not to scale

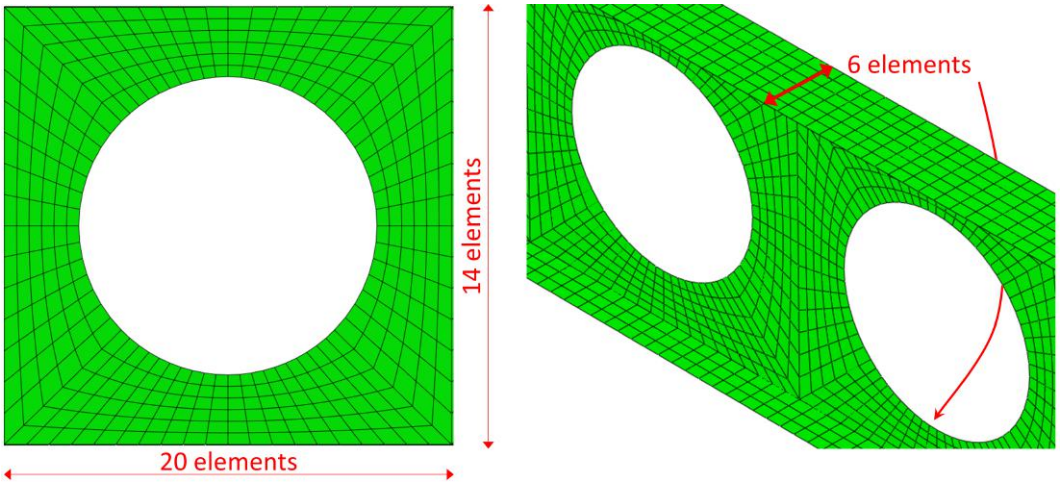

Figure 5.27: 25 *mm* mesh used for the single P-beam model

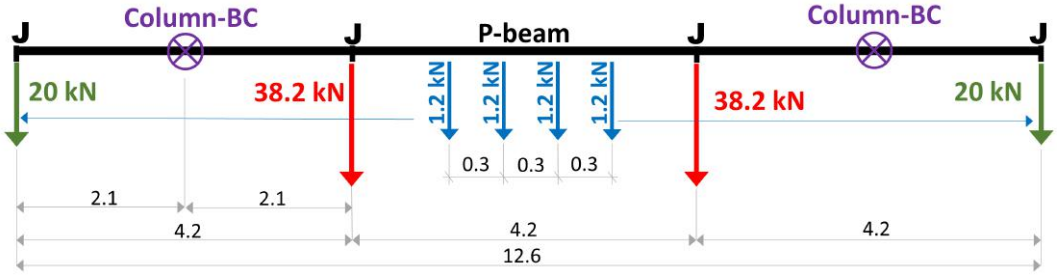

Figure 5.28: Elevation view of single P-beam model showing loads and boundary conditions

applying point loads at 4.2 m spacing. Internal J-beams carry higher loads (38.2 kN - red arrows), whilst external J-beams carry smaller loads (20 kN - green arrows). All point loads were applied to the bottom flange, in line with the web.

The expansion of the the P-beams will be resisted by the columns. This restraint was simplified and modelled using a spring element. An assumption was made that the columns are effectively fixed at the level of the floors immediately above and below, and that the floor-to-floor height is approximately 3 m. The analytical deflection of a fixed-fixed beam with a central point load is shown in Figure 5.29. Thus, based on weak-axis bending of the UC 254x254x74 columns and using the formula in Figure 5.29, the stiffness was calculated as $k = \frac{192EI}{l^3} = \frac{192 \times 200 \times 10^9 \times 38.7 \times 10^{-6}}{6^3} = 6.88 \times 10^6 \frac{N}{m}$. An alternative option would have been to include the columns in the structural model. However, it has been assumed that the columns will have sufficient passive fire protection based on the paper by Gebremeskel (2013), and will thus retain most of their ambient stiffness during a fire. Furthermore, this is conservative as higher steel temperatures would reduce the stiffness of the columns, and thus reduce the axial force, leading to reduced midspan deflections.

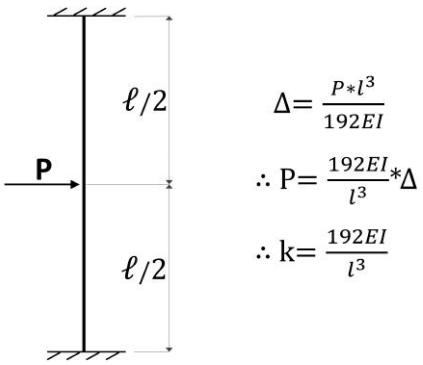

Figure 5.29: Analytical stiffness of a fixed-fixed beam with a central point load

The P-beams are attached to the columns with a connection plate and 8 bolts, at positions 2.1 m from the end of the beam, as previously shown in Figure 3.5. The connection plate is a 6 mm thick steel plate that is welded around its perimeter to the web of the P-beam, thereby stiffening the connection area. Figure 5.30 is a sketch of the connection, and illustrates the constraint used. Where the connection plate is welded onto the web, the web shell thickness was increased by 6 mm to 12 mm. The area between the bolts was fully constrained to a single reference point (RF), located at the centroid of the bolt group. The BCs were then applied to the RF. Vertical and lateral translation were fully fixed, but longitudinal translation (in the direction of the P-beam) was restrained by the spring element calculated above. Rotation about the

P-beam's strong and longitudinal axes were fixed, but weak-axis rotation was left free due to the negligible torsional capacity of the column.

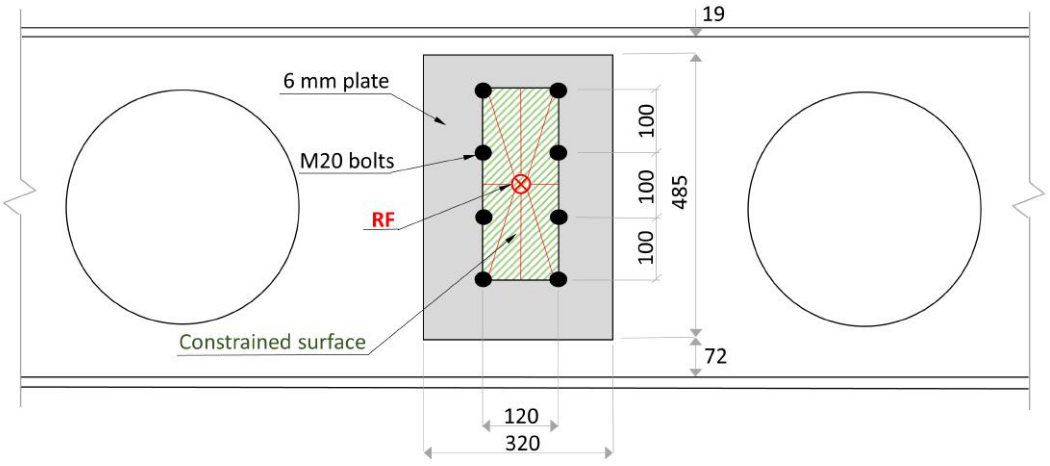

Figure 5.30: Reference point (RF) and constrained surface used to model the P-beam to column connection

The thermally expanding J-beams will exert an additional lateral force on the P-beams. However, this will be investigated further in Chapter 6, as these forces can only be accurately defined through global modelling of the structure.

5.5.2 Standard fire analyses

Figures 5.31 and 5.32 present the axial force and midspan vertical deflection results from the StF and StF-NoC analyses respectively. Moreover, the midspan lateral deflection for both the StF and StF-NoC are shown in Figure 5.33.

In the J-beam analysis, the midspan vertical deflection is calculated at the bottom of the web. However, the P-beam experienced lateral deflections large enough to affect the vertical deflection of the lower web, and thus the deflection at the top of the web was also extracted. This provides a more comprehensive overview of the behaviour of the P-beam. In Figures 5.31 and 5.32, the solid lines represent the midspan vertical deflection at the bottom of the web, whilst the dotted lines represent the top. Furthermore, the axial force (dashed lines) is shown for an an additional test case, in which the spring element was removed and translation was fixed i.e. the columns were assumed to provide full lateral restraint. This line is labelled "Axial - fixed", noting the axial restraint, although the weak-axis rotation is still left free at supports.

The StF-C and StF-NoC analyses yielded the following findings:

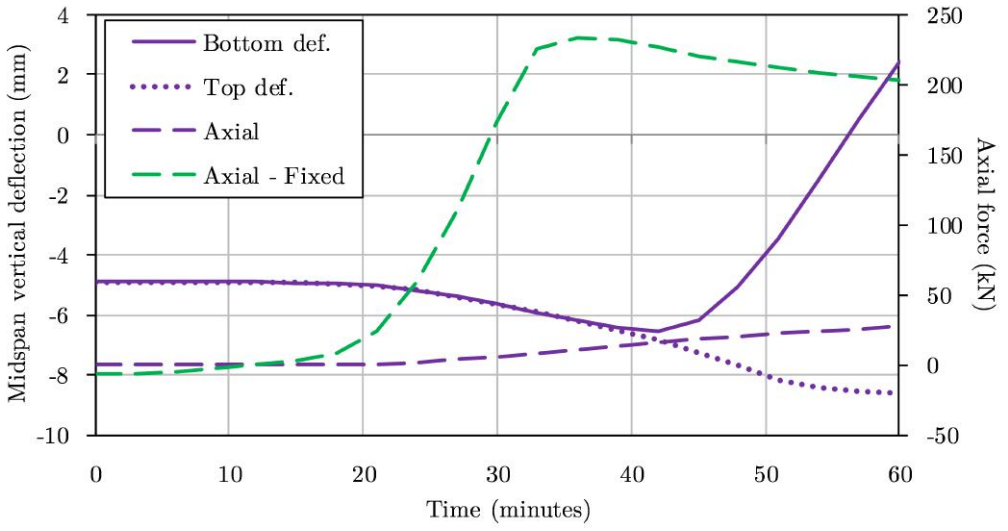

Figure 5.31: P-beam - axial force (axial) and midspan vertical deflection (def.) during a standard fire with a ceiling (StF-C)

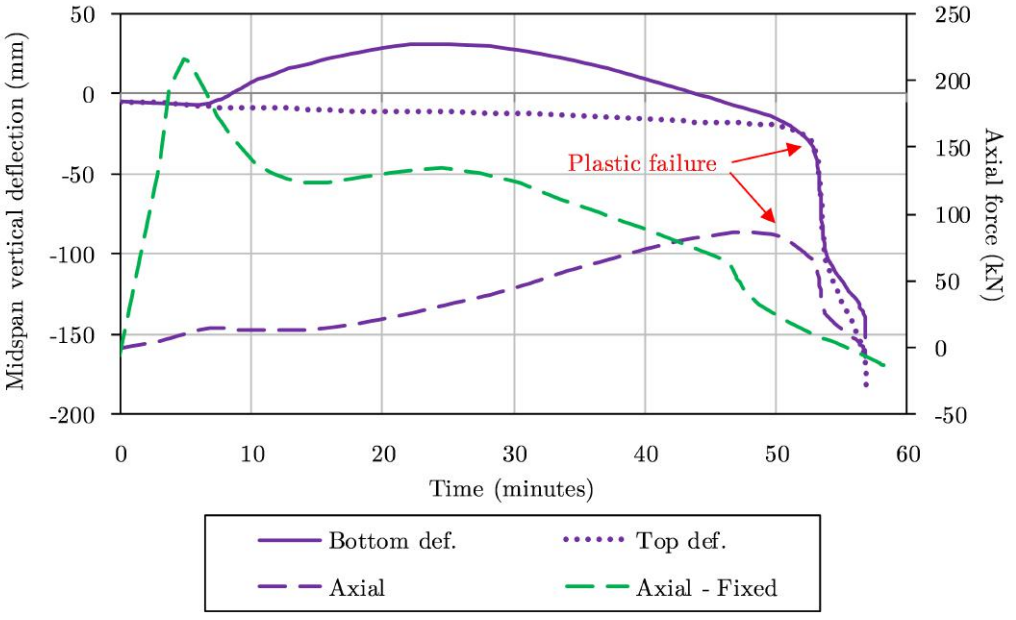

Figure 5.32: P-beam - axial force (axial) and midspan vertical deflection (def.) during a standard fire with no ceiling (StF-NoC)

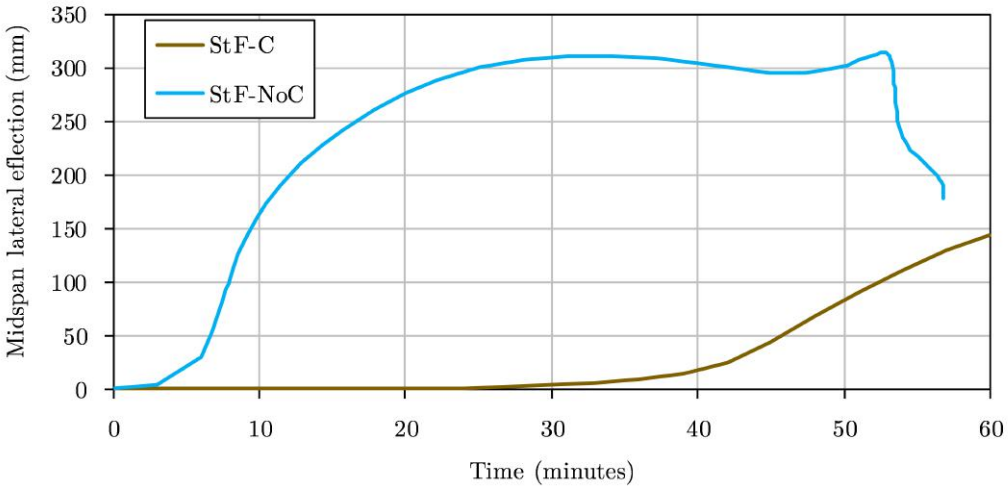

Figure 5.33: P-beam - midspan lateral deflection of bottom flange during a standard fire with and without a ceiling (StF-C and StF-NoC)

- Preventing longitudinal expansion at the columns has a substantial influence on the axial force in the P-beam. The maximum axial force in the StF-C analysis with a fixed restraint (234 kN) is 8.5 times greater than the spring equivalent (27.6 kN). For the StF-NoC analysis, it is 2.5 times greater (216.8 kN vs. 87 kN).

- The P-beams have a 40 mm deep notch in the top and bottom flanges, as shown in Figure 5.34, at the position of the columns to accommodate the connection. The asymmetry causes a twist in the P-beam due to a shift in the shear centre. Under ambient conditions the top flange experiences a lateral deflection of 3.3 mm. A twisted P-beam can be seen in Figure 5.35a. Whilst the lateral deflection is perhaps negligible at first, it introduces an imperfection that precipitates significant lateral deflections at elevated temperatures. As in the J-beam, this renders user-defined initial imperfections unnecessary. The lateral deflections are discussed further below.

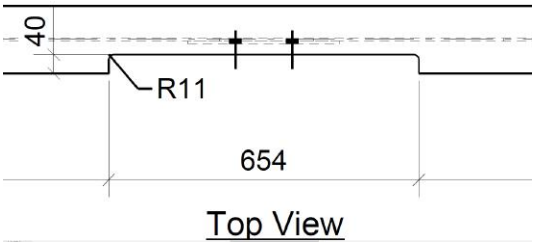

Figure 5.34: Extract from shop drawing A - CB49, showing a plan view of the notch in the P-beam flanges

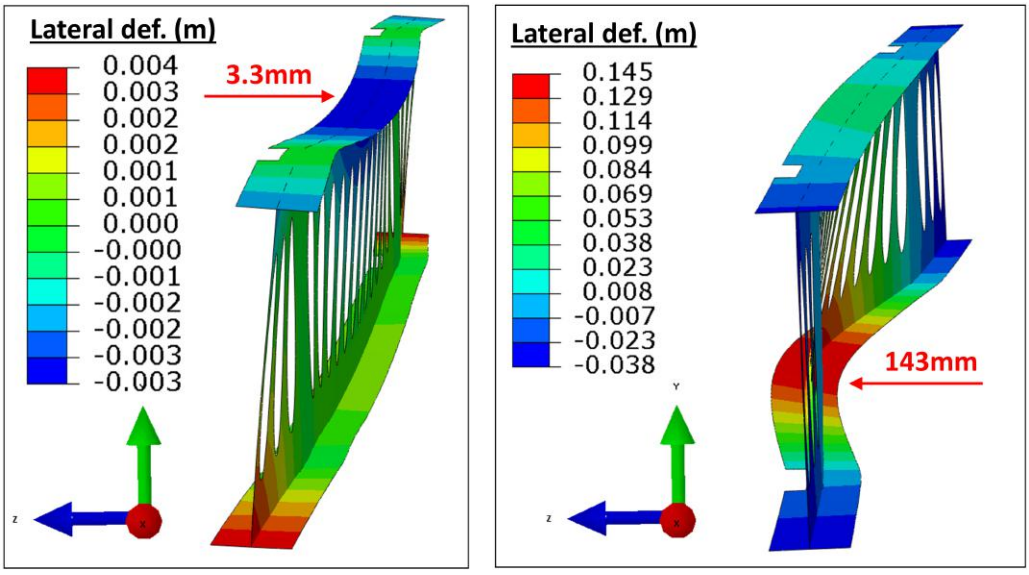

(a) Twisted P-beam under ambient loading conditions. Note: a large deformation scale factor of 10 was applied for visual clarity.

(b) Lateral deflections of a P-beam during a standard fire with a ceiling. Deformation scale factor = 1

Figure 5.35: P-beam experiencing lateral deflection under ambient and standard fire conditions.

- If one compares the vertical and lateral deflections of the P-beam under StF-C conditions, it is clear that the lateral deflections dominate. Whilst the top flange deflects downwards by 8.6 *mm*, the bottom flange deflects laterally by a significant 143 *mm* (almost 17 times greater). The lateral deflection can be seen in Figure 5.35b. As the flange deflects outwards, it is held back by the rest of the beam, thereby inducing a twisting action on the beam. This explains the *upward* deflection of the bottom flange, as the twist corresponds with an upward displacement of the bottom flange. The bottom flange deflections pose a threat to the integrity of the ceiling system, not just due to their significant magnitude but also the changing direction i.e. twisting. This kind of movement would be difficult to account for in the design of the ceiling system.

- In the StF-NoC analysis, a plastic failure occurred after 52 minutes, resulting in a runaway deflection failure. Furthermore, the maximum lateral deflection was 310 *mm* in the top flange. The plasticity is concentrated around the connections, as shown in Figure 5.36. Despite the application of artificial damping, the solution was not able to converge after 57 minutes. However, the result indicates that highly elevated temperatures can cause a serious structural failure in the P-beams. This contrasts with the the single J-beams models, in which the post-buckling behaviour is

coupled with reasonably stable deflection curves.

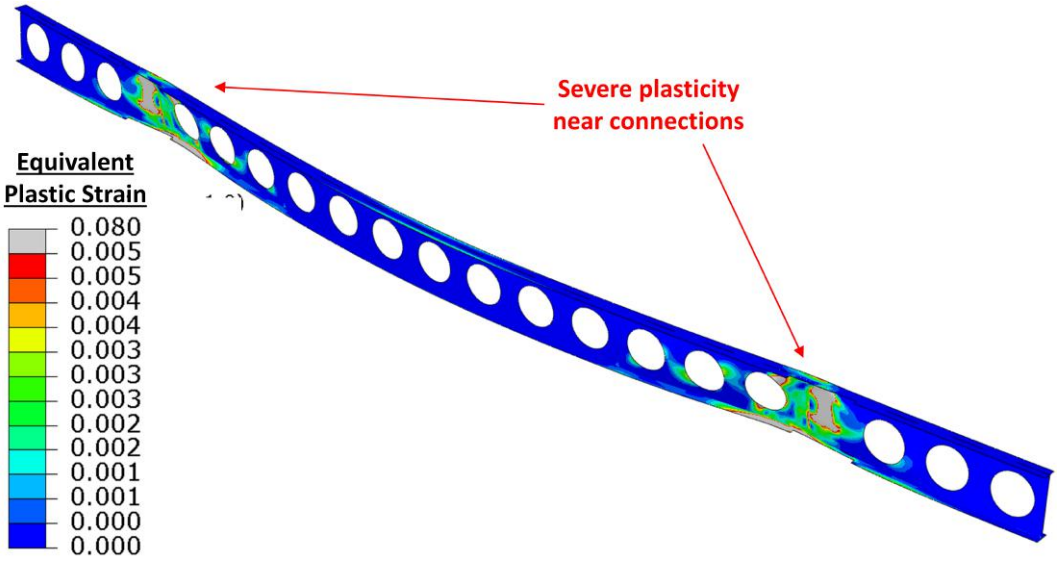

Figure 5.36: Plasticity near the P-beam connections that causes a runaway deflection under standard fire 'no ceiling' conditions (StF-C). The equivalent plastic strain is shown. Deformation scale factor = 1.

5.5.3 Parametric fire analyses

Figure 5.37 presents the axial force and midspan vertical deflection results from the parametric fire analysis, whilst Figure 5.38 shows the midspan lateral deflection.

Generally, the parametric fire had the same effects as the standard fires: (1) Markedly higher axial forces were present for the fixed column boundary condition case - 236 kN vs. 38 kN. (2) Lateral deflections are significantly higher than the vertical deflections - 114 mm bottom flange lateral vs. 8.5 mm top flange vertical (13.5 times greater). Again, this caused an upward deflection of the bottom flange.

However, the parametric fire was not severe enough to cause any major failure mechanism. Furthermore, a significant result of the parametric fire is that, despite the large deflections, the P-beam is able to rebound almost entirely during the cooling stage. This indicates that despite the reduced material properties of the steel, the yield stress is only exceeded in small areas, which minimises the plastic deformation. Thus, the vertical deflections return to within 0.4 mm of ambient deflections, whilst the lateral deflections return to within 5.2 mm. As for the J-beam, this is beneficial for the CBS as a lack of permanent deformation would reduce the long-term structural impact of a fire. Finally, if the flexibility of the columns is included, there are negligible tensile

forces in the P-beam. However, there is a maximum tensile force of 62 kN after 120 minutes for the axially fixed case. This suggests that the P-beam to column connection will most likely not experience high tension forces, and thus no extra connection design precautions are needed.

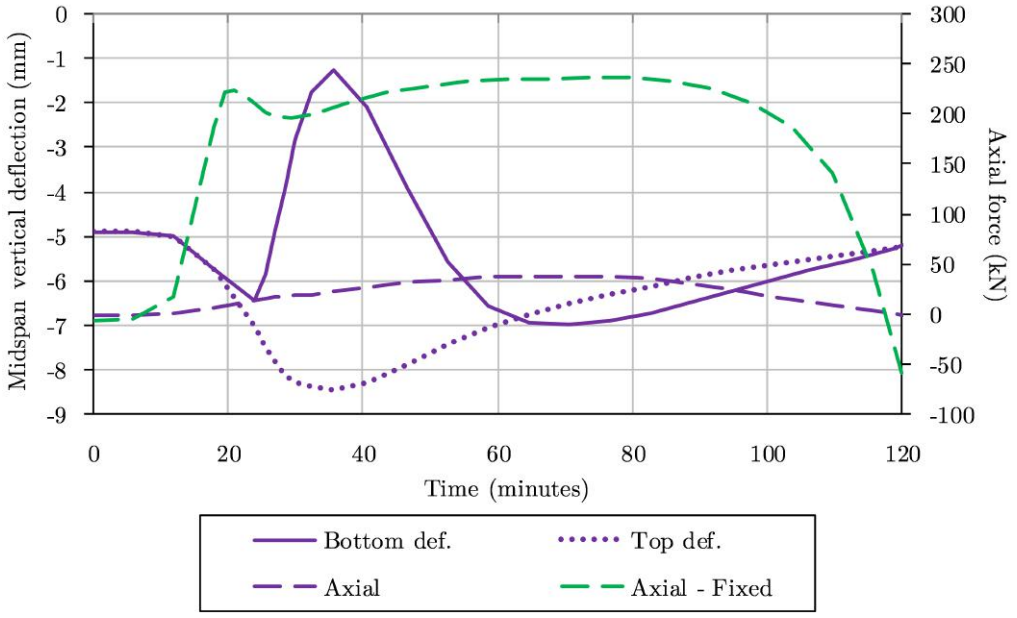

Figure 5.37: P-beam - axial force and midspan vertical deflection during a parametric fire

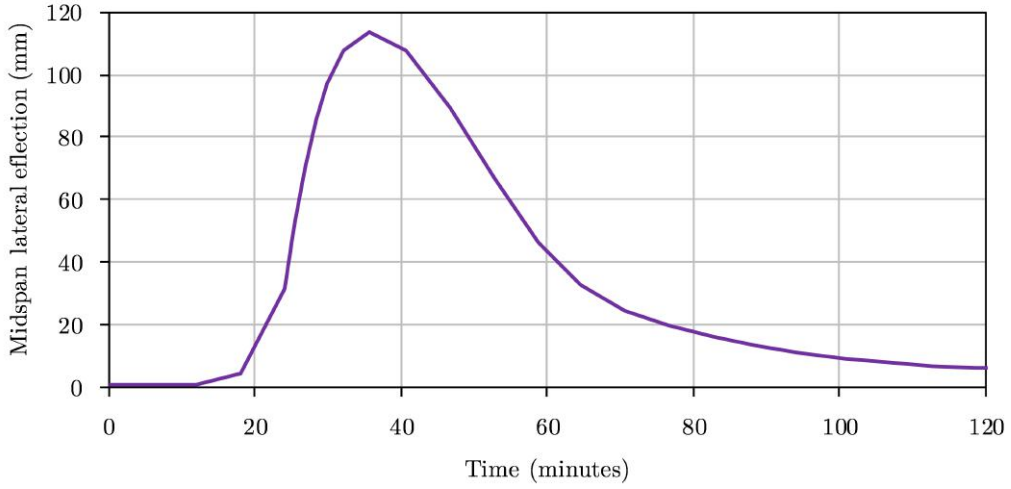

Figure 5.38: P-beam - midspan lateral deflection of bottom flange during a parametric fire

5.6 Conclusion

This chapter discussed the single element models that were used to investigate the structural behaviour of the CBS under fire conditions. Initially, an overview of the thermal analysis performed by Marx (2018) was given. The resultant output steel temperatures that became the thermal input for the structural models of this thesis are shown. Thereafter, the FEM input, results and analysis of the J-beam and P-beam models were presented. A summary of important findings is listed below:

1. Axial restraint increases the midspan vertical deflection of the J-beam. As the beams are already in a deflected state under ambient structural loading, the axial forces induced by preventing longitudinal thermal expansion cause an additional moment, which causes the J-beam to deflect downwards. In the StF-C, StF-NoC and parametric fire analyses, the deflection was between 27% and 161% greater. This indicates that wherever possible, the CBS should be designed to allow for thermal expansion of the J-beams. A possible option is to specify slotted bolt holes at the connections, which allows some thermal expansion of the beams, yet does not greatly affect the ambient performance.

2. In the StF-C analysis of the single J-beam, the greatest midspan vertical deflection of 40 *mm* (span/200) corresponded with the PP beam. To maintain the integrity of the ceiling system, the fire-resistant and fibre-cement boards could conservatively be designed to accommodate this deflection.

3. The asymmetry of the J-beam causes the lower flange to deflect laterally under elevated temperatures due to restrained thermal expansion. The maximum lateral deflection within the lower flange ranges between 4.1 *mm* and 59.2 *mm* for the StF-C analysis, 5.6 *mm* and 247 *mm* for the StF-NoC analysis, and 4.1 *mm* and 57.5 *mm* for the parametric fire analysis. It is recommended that any part of the ceiling system that may be attached to the lower flange of the J-beam should be designed with these deflections kept in mind.

4. The StF-NoC analysis showed that a J-beam can experience top flange lateral torsional buckling at high temperatures. However, it was only in the axially restrained beams (PP and FF) that buckling occurred. The PR and FR beam did not develop any failure mechanisms that caused sudden increases in deflection. This indicates that, if expansion is unhindered, the J-beam is robust under temperature conditions much higher than expected.

5. The cooling stage of the parametric fire allowed the steel beams to recover thermal deflections that remained in the elastic zone. However, depending on the magnitude of the stresses and weakened material properties, varying amounts of yielding caused permanent deformations. All vertical deflections for both the J- and P-beams returned to within a maximum of 3.5 mm of ambient deflections. P-beam lateral deflections returned to within 5.2 mm of ambient deflections. The PR J-beam recovered all lateral thermal strain, whilst the PP, FR and FF beams returned to within 6 mm - 37.6 mm of ambient deflections.

6. The parametric fire was used to predict tensile forces that may arise during the cooling period of a fire. The maximum tension in the J-beam was 268 kN for the PP case. The P-beam experienced a tensile force of 62 kN, but only when fully restrained against expansion i.e. ignoring the flexibility of the columns. It is recommended that the tensile capacity of the beam connections be checked against these values.

7. The notch in the P-beam flange shifts the shear centre, which results in a twisting action under vertical loading. Under ambient conditions the lateral deflection of the top flange is 3.3 mm. It was found that this imperfection exacerbated the thermally induced deflections.

8. Lateral deflections dominate the behaviour of the P-beam. In the StF-C and parametric fire analyses, the midspan lateral deflections were 17 and 13 times greater than the vertical deflection respectively. In the StF-NoC analysis, significant lateral deflections were also present (310 mm), yet at such high temperatures the beam ultimately failed due to excessive plasticity near the connections. It is unlikely that the remainder of the ceiling system i.e. the fibre-cement boards will be able to remain intact if such high lateral deflections are experienced, leading to even higher steel temperatures.

From the discussion above, one can conclude that the single element models generally indicate that the CBS performs well under fire conditions. Severe structural failure i.e. runaway deflection only occurred under the extreme temperature conditions corresponding with a complete lack of a fire-resistant board. In in all three fire cases it was found that reducing the axial restraint improves the structural performance by limiting the vertical and lateral deflections. Thus, it seems that the integrity of the ceiling system can be insured if it is designed to accommodate the expected deflections. This result will be relevant when considering the ceiling system details. However, single element models cannot take into account the interactions between different structural members. In order to address this, a global structural model of the prototype CBS has been created. The following chapter presents this work.

Chapter 6

Global structural modelling

6.1 Introduction

This chapter presents the results and analysis of the global structure models developed in this work that incorporate all the structural elements of a single cellular beam structure (CBS) sub-structure i.e. three connected bays. The global nature of the models capture the interactions between structural elements. This serves to give a better representation of the behaviour of the CBS under fire conditions, and to validate the single element models of the previous chapter. It has been shown in the literature that structural elements often perform much better when analysed as part of an entire structural system, rather than as isolated elements (Bisby *et al.*, 2013; Usmani *et al.*, 2001). However, in this chapter it is shown that due to the highly flexible nature of the entire structure, behaviour is much closer to that of a single element than would typically be expected.

This chapter begins by detailing the FEM input that was used to build the global model. The three possible fire scenarios (referred to as 'fire cases') that were considered are also introduced. Thereafter, the results and analyses of the three fire cases are given for each thermal load i.e. standard fire with a ceiling (StF-C), standard fire without a ceiling (StF-NoC), and parametric fire. Finally, the chapter concludes with a summary of significant findings.

6.2 FEM input

6.2.1 Geometry

The global model is made up of four different types of structural elements: primary beams (P-beams), secondary beams (J-beams), channels and knee-braces. Although the knee-braces are also channel sections, hereafter they will simply be referred to as 'knee-braces', whilst the load-bearing channels will be

referred to as 'channels'. The dimensions and terminology used for the various structural elements of the CBS, previously introduced in Chapter 3, are shown again in Figures 6.1 and 6.2 for clarity. The reader is encouraged to refer back to these figures during this chapter to understand the position of structural elements and how they interact with each other.

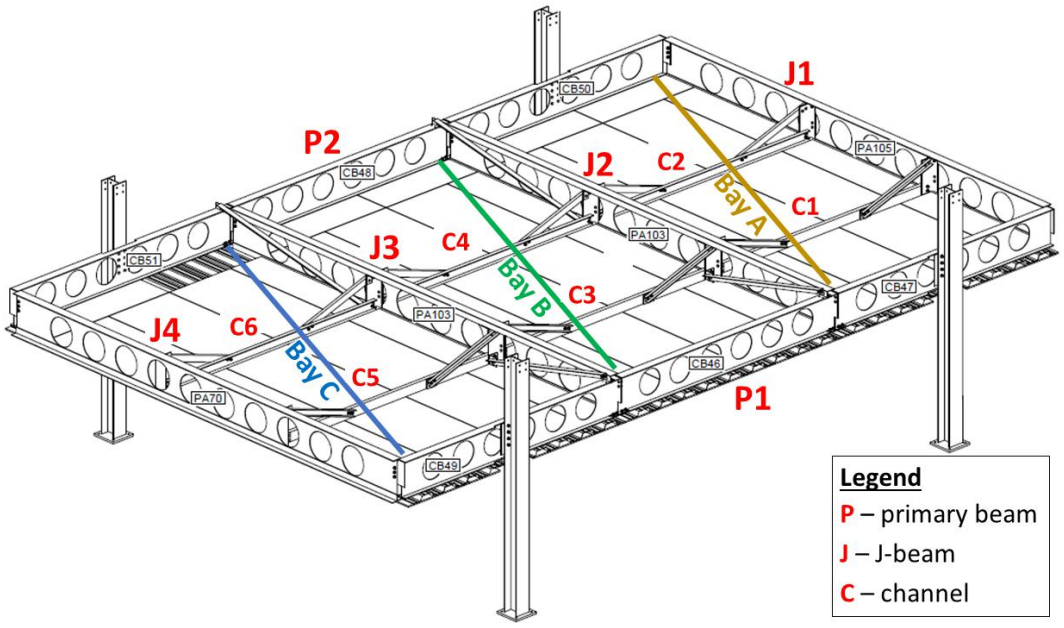

Figure 6.1: Structural layout used for the cellular beam structure (CBS) illustrating the terminology used for structural elements and bays

The J- and P-beam single element model geometry, as presented in Sections 5.4.1.1 and 5.5.1, has been re-used in the global model i.e. the individual parts were exported from the single element models, and imported into the global structure model. However, the channels and knee-braces were not previously modelled, and had to be defined. Consequently, the geometry is based on the standard hot-rolled channel sections: C160x65 for the channels that carry the ceiling, and C100x50 for the knee-braces, as specified in the shop drawings (Appendix B). A full description of section properties can be found in the SAISC Red Book (SAISC, 2013), but the essential dimensions are shown in Figure 6.3. For the tapered flanges of these channels the average flange thickness is used in models.

6.2.2 Elements and mesh

The elements and mesh used for the J- and P-beam single element models, as presented in Sections 5.4.1.2 and 5.5.1, were implemented in the global model. Thus, both beams utilise quadrilateral S4 shell elements, with an approximate mesh size of 25 mm. This mesh size was validated in the mesh sensitivity

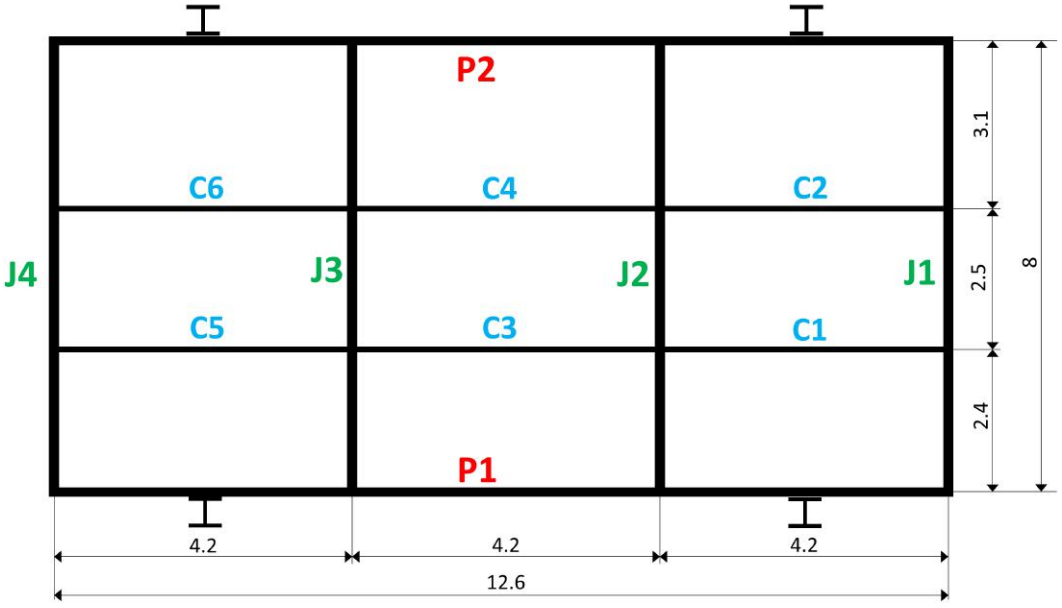

Figure 6.2: Plan view of the cellular beam structure (CBS) showing the main structural elements and dimensions (in m)

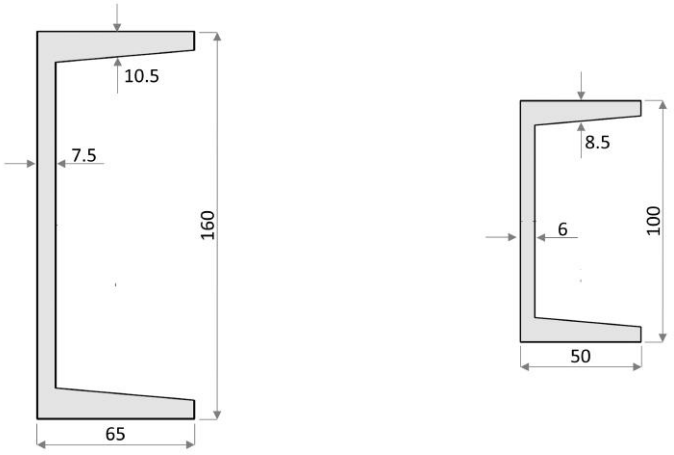

(a) C160×65 used to carry ceiling (b) C100×50 used as knee-brace

Figure 6.3: Dimensions (in mm) of channels used in the cellular beam structure (CBS)

analysis in Section 5.4.1.6. The channel used the same elements, but with an approximate mesh size of 30 mm. The channel mesh is shown in Figure 6.4.

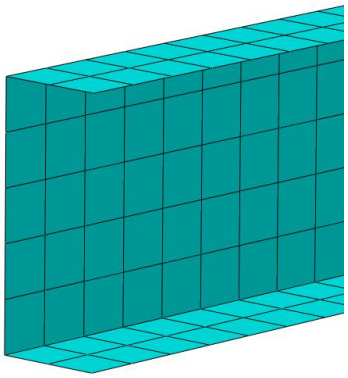

Figure 6.4: 30 mm mesh used for the C160x65 channel sections

The role of the knee-braces in the CBS is to support the channels and provide lateral restraint to the upper web of the J-beams, with the latter being of greater importance. The knee-braces do not carry any load along their length, and end connections have been designed to be pinned, and thus only axial forces are expected. Also, the self-weight of the C100x50 channel sections has been considered negligible. Considering the above, shell elements were not deemed necessary for the knee-braces, as no major stress distributions are expected within the cross-section. Therefore, beam elements were used to define the knee-braces, in order to lower the computational expense of the global model. A beam cross-section based on Figure 6.3b was assigned. A element length of approximately 140 mm was used i.e. 9 elements per knee-brace.

The thermal analysis of Marx (2018) did not include the knee-braces. This analysis has been used as the basis for the temperature of structural elements as discussed in Section 5.2. Thus, the temperature of the top flange of the channel has been applied to the knee-braces. This conservative assumption best describes the steel temperatures with the available data, as the knee-brace is connected to the channel, and along its entire length is situated within 400 mm of the top flange of the channel. However, the thermal analysis could possibly be refined to include the knee-braces.

6.2.3 Material models

The Eurocode material model (CEN, 2005) discussed in Section 4.3.1, and used throughout the single element modelling, was applied in the global model. An ambient Young's modulus of 200 GPa was used for steel, and a constant value of 1.4×10^{-5} was used as the coefficient of thermal expansion.

6.2.4 Interactions

The global model incorporates the entire CBS prototype i.e. one sub-structure made up of three connected modules, and consists of 24 single elements (4 J-beams, 2 P-beams, 6 channels and 12 knee-braces). Extensive use of kinematic coupling constraints between reference points (RFs) was made to connect the various elements to each other. The kinematic coupling constraints link degrees of freedom of a cross-section to a specific point, the RF, to ensure that an entire cross-section experiences uniform behaviour, as explained in Section 4.2. The connections specified for the CBS, as shown in Appendix B, have only been designed and detailed to transfer shear forces. Whilst a limited amount of moment restraint may occur, this is expected to be minimal, especially under elevated temperature conditions. Therefore, fully pinned connections between RFs were used throughout the model to ensure no moment restraint between sections. However, in future the moment resistance of the CBS connections could be investigated to refine the model. That said, the single element models indicate that allowing rotations at the connections is beneficial, and thus it would be advisable to detail connections to act as pins as much as possible.

Initially, the RFs at the end of the J-beams were defined on the web edge at the height of the centre bolt, as shown by the green circle in Figure 6.5a. However, after preliminary investigations it was found that the resultant eccentricity of 76 mm between the RF and the web of the P-beam induced a torsional force. This exacerbated the twisting action already prevalent due to the P-beam flange notches, as shown in Figure 5.34, resulting in the P-beam cross-section not being symmetrical at supports. Therefore, following a correspondence with the SAISC, it was decided to place the RF to be flush with the web of the P-beam i.e. half the width of the web (3 mm) away from the web centre, as shown in Figure 6.5c. This relies on the assumption that the connection will be able to simulate this behaviour, by rotating at the P-beam interface, and *not* at the J-beam interface. In the future the SAISC will modify the connection by using double angle cleats, which will provide the aforementioned structural behaviour. This has been shown to be a superior end connection under fire conditions in an experimental study by Wang *et al.* (2013), as discussed in Section 2.4.4. An example of this connection type is shown in Figure 6.6. The identification of this torsional behaviour, and proposal regarding how to address it, is an ancillary, but novel, contribution of this work.

The method of linking two elements used in Abaqus in this work incorporated two RFs and three constraints, and is illustrated in Figures 6.5b and 6.5c. The figure only shows a J-beam connected to a P-beam, but is representative of other connections between members e.g. J-beam to channel. Each element has its own RF linked to the relevant section area with a constraint. The third constraint connects the two RFs, effectively simulating a connection. As previously stated, all connections between elements were assumed to be fully

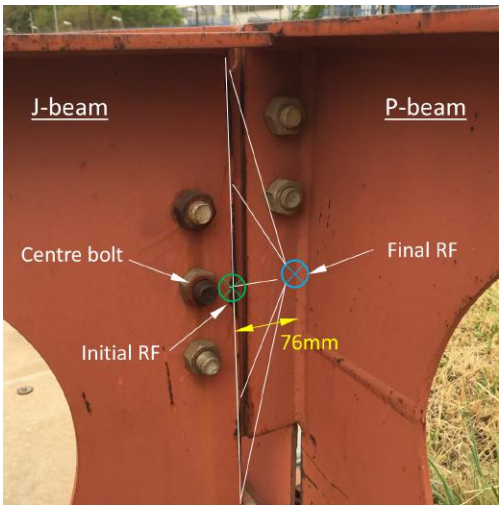

(a) Initial vs. final RF position and kinematic constraint superimposed on a photo of a J- to P-beam connection. This modification to connection specifications will be implemented in future CBS structures.

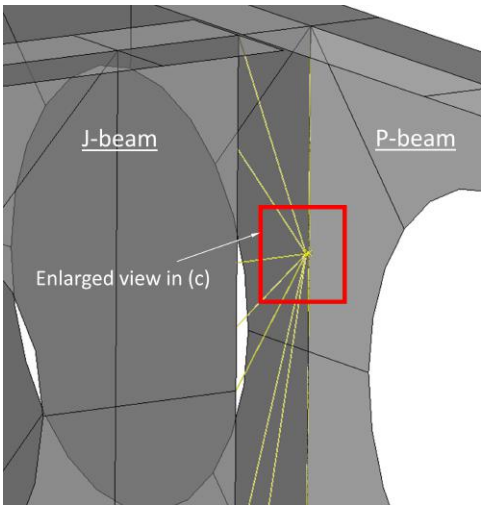

(b) RFs and kinematic constraints seen in Abaqus viewer

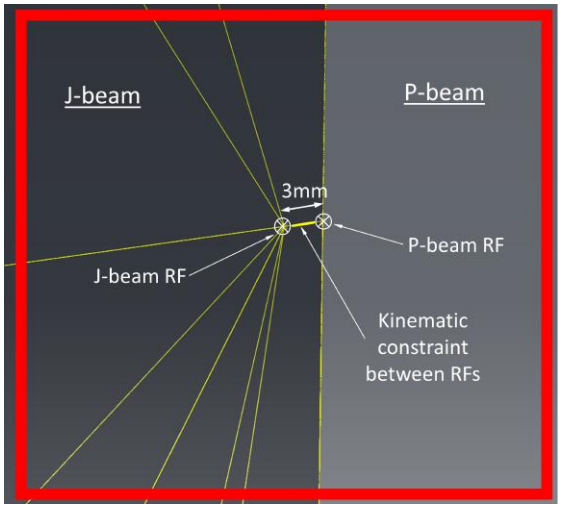

(c) Enlarged view of interaction between J- and P-beam RFs

Figure 6.5: Reference points (RFs) and kinematic constraints used to model the J- to P-beam connections

(a) Double angle cleats - side view (b) Double angle cleats - top view

Figure 6.6: Double angle cleat connection after being exposed to a fire (Wang *et al.*, 2013)

pinned, and the constraints were defined to represent this. It was ensured that constraints prevented torsional rotation.

6.2.5 Loads and boundary conditions

Figure 6.7 illustrates the loading and boundary conditions (BCs) applied to the global model. The addition of the channels necessitated minor adjustments to the single element loading discussed in Sections 5.4.1.4 and 5.5.1.1 in the previous chapter. As the channels carry the ceiling and decking loading, this longer needed to be approximated as point loads on the J-beams (red arrows in Figure 5.13). Rather, the total ceiling load was applied as a traction on the surface of the channel web. The traction was back-calculated using the area of the channel webs and total load, which resulted in a magnitude of 52 kPa for channels C1, C3 and C5, and 59.2 kPa for channels C2, C4 and C6. The downward direction of the traction was specified to remain constant, and the traction was always calculated based on the undeformed area i.e. changes in web area did not affect the total load. The traction is represented by the purple arrows in Figure 6.7.

As a result of the channels carrying the ceiling load, the only other load acting on the J-beams was the self-weight. This has been applied as in the single element model i.e. 27 point loads of magnitude 136 N at a spacing of 295 mm. For the P-beam, the point loads simulating the effect of the J-beams (green and red arrows in Figure 5.28) could be removed, as the J-beam elements themselves now transfer this loading. However, the self-weight of the P-beams combined with the contribution of the decking and ceiling loading has still been applied as 42 point loads of magnitude 1212 N at a spacing of 300 mm. The point loads acting on the J- and P-beams are shown as golden arrows in Figure 6.7

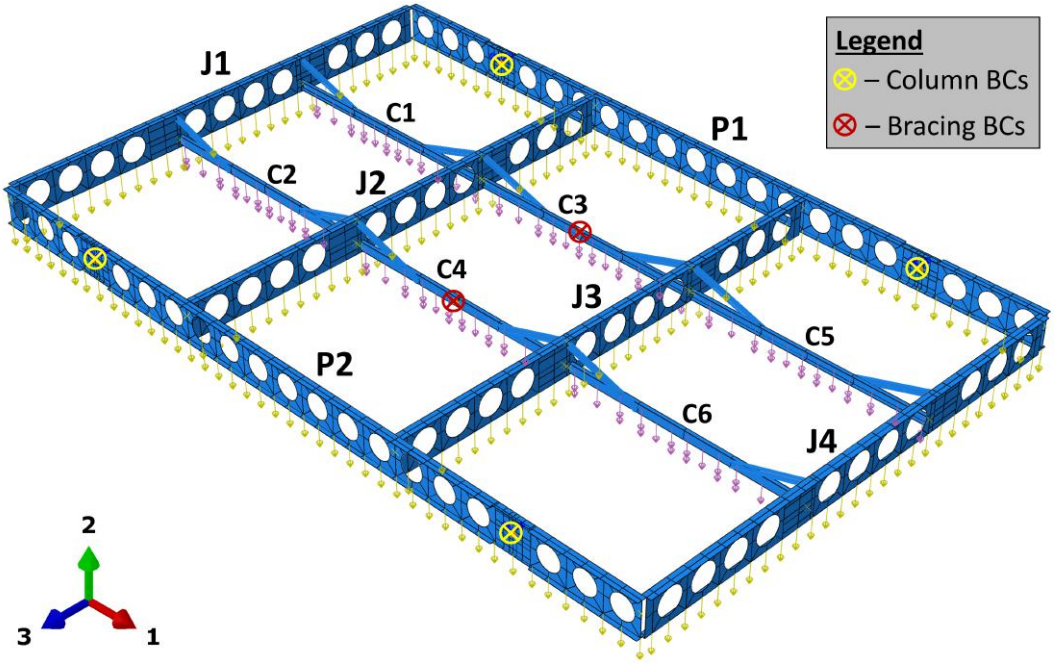

Figure 6.7: All loads and boundary conditions (BCs) in the global model

A BC has been applied at the columns (yellow circles in Figure 6.7). This is equivalent to the single P-beam model as discussed in Section 5.5.1.1, except for an additional spring element, which corresponds to the strong-axis bending of the columns. The spring has been added as the longitudinal expansion of the J-beams causes the P-beams to move laterally i.e. along the 3-axis of Figure 6.7. Thus, only the vertical deflection (2-axis) was fixed, whilst translation was allowed in both horizontal directions. For the additional spring, the formula from Figure 5.29 was used to calculate a stiffness of $k = \frac{192EI}{l^3} = \frac{192 \times 200 \times 10^9 \times 114 \times 10^{-6}}{6^3} = 20.27 \times 10^6 \frac{N}{m}$. As in the single P-beam model, rotation about the P-beam's strong and longitudinal axes were fixed, but weak-axis rotation has been left free.

An additional BC was applied at the centre of the channels in Bay B (red circles in Figure 6.7). The BC only prevents translation along the 1-axis. It was found that, without this BC, the entire floor system would act as a mechanism due to the lack of any moment-resisting connections between members. This has already been noted by the SAISC in the ambient design, and the combined decking and ceiling system has been specifically designed to act as a stiffening membrane (Gebremeskel, 2013). However, the system cannot necessarily be relied upon under fire conditions, as the thin steel sheeting will heat up very rapidly, thus losing stiffness, and the integrity of the boards is threatened if they are expected to carry large loads. Additional full-scale fire testing is required to identify to what extent the ceiling and decking can be relied upon during severe fires. Thus, the BC is provided here under the condi-

tion that a system providing lateral stability to the floor is maintained under fire conditions. If it is identified during testing that the existing system is insufficient, a possible solution would be to include additional steel members or wires that run diagonally across the bays.

An equilibrium check was performed in order to validate the global model reaction forces against the total loading. Based on the geometry of the CBS and the loads given in Table 5.1, the total factorised loading was calculated to be 334.22 kN. Under ambient conditions, summing the vertical reactions of the columns (in Abaqus) yielded 334.27 kN. The close correlation indicates that the loads were applied correctly to the Abaqus model.

6.2.6 Fire cases

Different 'fire cases' (FCs) were considered in order to characterise the behaviour of the global structure during a fire. These FCs aim to gauge the structure's reaction to possible fire scenarios. Although an infinite number of fire scenarios could be tested, three FCs were chosen based on them being considered worst-case scenarios:

FC1 A localised fire only heats up a single J-beam, whilst the rest of the structure remains at ambient temperature. The surrounding cooler, and thus stiffer, P-beams resist longitudinal expansion and induce axial forces.

FC2 A compartment fire occurs underneath Bay B, and heats all members within the bay. Thus, a greater number of elements is heated than in FC1, but the surrounding cooler structure still restrains expansion.

FC3 Compartmentation within the office has been completely lost, and the entire structure experiences the elevated temperatures. This is a conservative, worst-case scenario which would require a fully-developed fire acting over the entire 8 $m \times 12.6$ m area.

The three FCs are illustrated in Figure 6.8. The standard fire with the ceiling remaining intact (StF-C), standard fire 'no ceiling' (StF-NoC) and parametric fire steel temperatures were applied in each FC, with details as presented in Section 5.2. Consequently, a total of $3 \times 3 = 9$ global structure models were run.

6.2.7 Solution procedure

The three-step solution procedure (initial, mechanical, thermal) was used for the global structure. This approach has been validated in Chapter 4, and was successfully utilised throughout the previous chapter. Of the 9 models

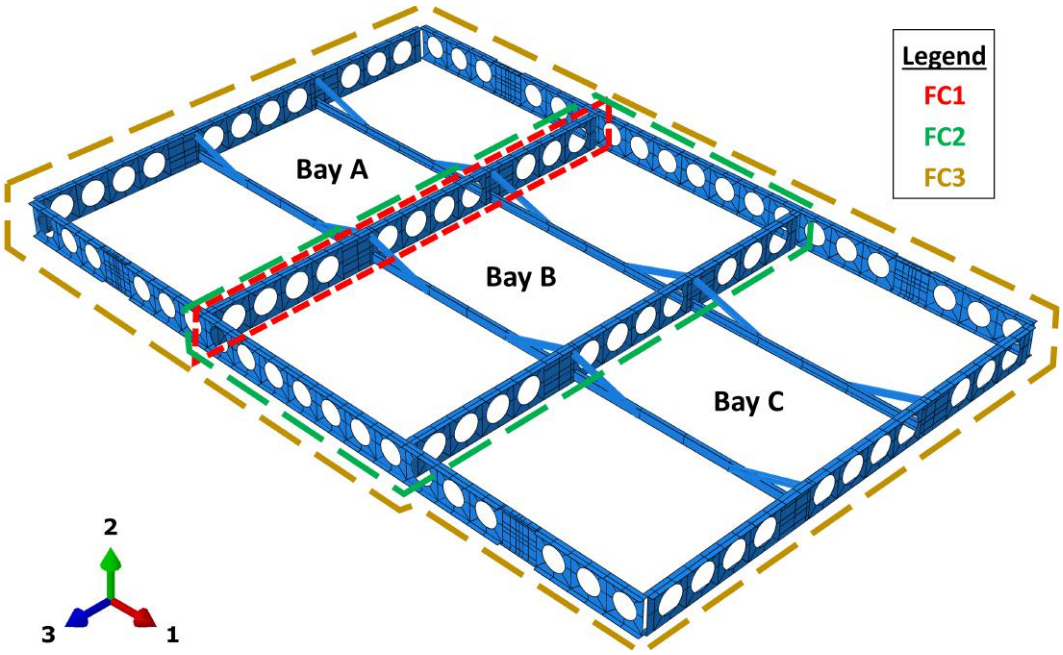

Figure 6.8: Diagram showing the three fire cases (FCs), and the corresponding structural elements that experience elevated temperatures

that were run, only FC3 under parametric fire conditions required artificial damping stabilisation, due to a temporary local instability. A damping factor of 2×10^{-5} was used. In this case, the viscous damping energy was at most 0.11 % of the total strain energy, which was deemed negligible.

6.3 Results and analysis

6.3.1 Fire case 1

This FC represents the possibility of a localised fire heating up only a single J-beam (J2). The rest of the structure remains at ambient temperature throughout the analysis. As the J-beam expands longitudinally, the colder and stiffer P-beams resist this expansion. This FC was chosen to simulate the greatest axial restraint that the P-beams could provide under fire conditions.

6.3.1.1 Standard fire with ceiling

Figure 6.9 shows the midspan vertical deflection of J2, an internal secondary beam, with it being subjected to a standard fire whilst the ceiling remains intact (StF-C). The deflection relative to the beam-end deflection is shown i.e. the result has been offset against the P-beam's vertical deflection. This relative deflection is what the ceilings must accommodate to maintain integrity. The results have been compared against the pin-roller (PR) and pin-pin (PP)

single J-beam model results, presented in Section 5.4. The fixed-roller (FR) and fixed-fixed (FR) results were not included, as the connections have been modelled as fully pinned i.e. there is no moment restraint, as explained in Section 6.2.4 above.

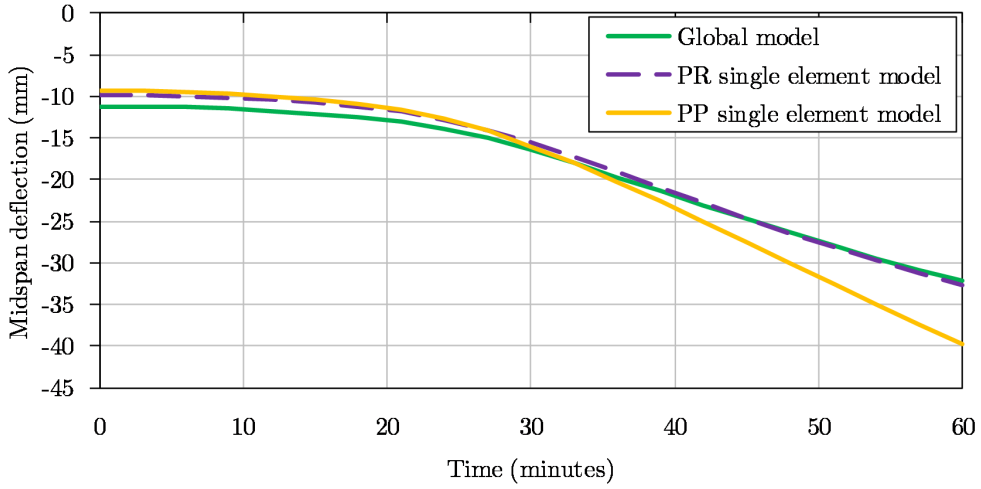

Figure 6.9: Fire case 1 (FC1) - midspan vertical deflection of J2 in the global model compared with single element J-beam models. The deflections are for the standard fire analysis whilst the ceiling remains intact (StF-C)

In the global model, behaviour somewhere between perfect PR and PP was initially expected. However, Figure 6.9 indicates that the J-beam shows a much stronger correlation with the PR beam, suggesting that there are very low axial forces present in the J-beam. There are minor differences between the global model and single PR J-beam results, such as the initial ambient deflection and the rate of deflection increase. However, these are likely due to the development of alternative load paths within the global structure as the fire progresses, and/or as a result of the difference in which lateral restraint was modelled i.e specified boundary condition (single element model) vs. channels and knee-braces (global model). These differences in predicted deflections are less than 1 mm throughout the analyses, and are deemed negligible. The correlation between the global model J2 behaviour and single model PR beam was confirmed by extracting the axial force from the global model, which yielded negligible forces of less than 10 kN throughout the analysis. Thus, the P-beams offer little axial restraint, as they bend about their weak-axis when the J-beams expand. The similarity between the global model and the PR single element model is significant, as it shows that the CBS is flexible enough to allow the J-beam end-restraint to be approximated as a roller. This important result may allow designers in the future to only consider single beams rather than global structures when considering fire behaviour.

The J2 maximum midspan vertical deflection, bottom flange lateral deflection and total expansion were extracted from the global model, and are summarised in Table 6.1. The bottom flange lateral deflection is due to the asymmetry of the J-beam, as identified in the previous chapter. The lateral deflections are included as they are important for investigating the deflections that decking and ceiling systems may need to accommodate. The maximum longitudinal expansion has been included to inform the design of connections to accommodate this movement. A visualisation of the global model, showing the deflection of J2, is provided in Figure 6.10. From Table 6.1 it can be observed that vertical deflections are significantly less than the limiting fire limit state requirement of span/20, even when there is no ceiling present. Hence, vertical deflection requirements will not be a governing factor except where they relate to maintaining ceiling integrity. It can be observed that there would be a significant change in longitudinal expansion if the ceiling fails, with the expansion increasing from 6.5mm to 46.5mm. Concurrently the maximum lateral deflection along the length of the beam increases from 4mm to 9mm.

Table 6.1: Fire case 1 (FC1) - maximum deflections (in mm) of J-beam J2

	Max. midspan def.	**Max. lateral def.**	**Max. expansion**
StF-C	32 (span/250)	4	6.5
StF-NoC	64 (span/125)	9	46.5
Par. Fire	28 (span/285)	5	9.3

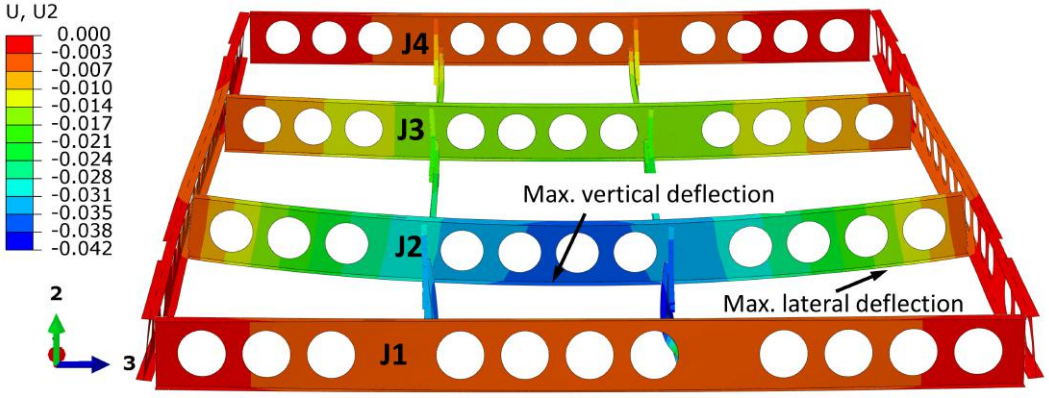

Figure 6.10: Fire case 1 (FC1) - global structure at 60 minutes in a standard fire with the ceiling remaining intact (StF-C) analysis, in which only J2 has been heated. This figure focuses on the deflection of J2. The total vertical deflection is shown i.e. no beam-end offset has been applied. Deformation scale factor = 10.

To maintain integrity, the ceiling must be able to deflect across the span of the J-beam, *and* across the span of the channels. A visualisation of the deflected channels is given in Figure 6.11. For FC1, it was found that that C2 deflected 4 *mm* more than C1, after 60 minutes under StF-C conditions. This is due to the asymmetry of the CBS, which causes C2 to carry a greater area of the ceiling. Thus, only the maximum midspan deflection results of C2 are summarised in Table 6.2, which can be used for design purposes. Once again the deflections are well within the span/20 requirement, with a maximum deflection of 25.6 *mm* (span/165), even with no ceiling present.

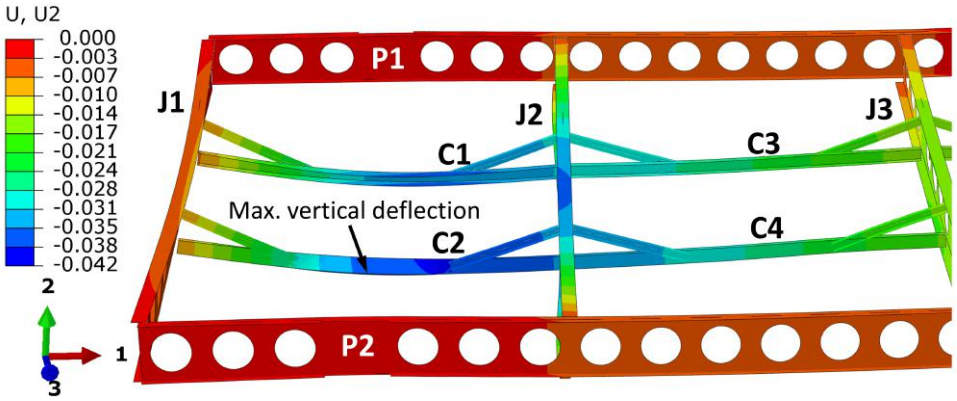

Figure 6.11: Fire case 1 (FC1) - global structure at 60 minutes in a standard fire with the ceiling remaining intact (StF-C) analysis, in which only J2 has been heated. This figure focuses on the deflection of C1 and C2. The total vertical deflection is shown i.e. no beam-end offset has been applied. Deformation scale factor = 10.

Table 6.2: Fire case 1 (FC1) - maximum midspan deflection (in mm) of channel C2

	Max. midspan deflection
StF-C	15.6 (span/270)
StF-NoC	25.6 (span/165)
Par. Fire	14.3 (span/295)

6.3.1.2 Standard fire with no ceiling and parametric fire

Overall, the behaviour of the global structure under 'no ceiling' and parametric fire conditions was similar to the StF-C analysis, except for the magnitudes of the axial forces and deflections. No failure mechanisms were detected in either case. The results are summarised in Tables 6.1 and 6.2. Significantly,

the cooling stage of the parametric fire allowed the J-beams and channels to recover all thermal strain i.e. no plasticity occured.

To conclude, FC1 suggests that the P-beams provide negligible axial restraint to an expanding J-beam, even if they remain cool throughout a fire. This is beneficial for the CBS, as the J-beams are thus free to expand, thereby preventing a build-up of axial forces and resulting in lower midspan deflections. Under worst-case 'no ceiling' conditions, the J-beam and channel deflection ratios are still low, at span/125 and span/165 respectively. Furthermore, if a more realistic parametric fire is used, the cooling stage allows the CBS to recover all thermally induced strain, thereby returning to its ambient deflection state. Therefore, the yield stress is never exceeded within the structure throughout the course of the fire. This is beneficial in that it illustrates the low stresses present in the CBS during the fire scenarios considered.

6.3.2 Fire case 2

This FC represents the possibility of a compartment fire occurring within the office space, which could heat up an entire bay. Bay B was chosen, as it will be restrained by the cooler bays on either side. This restraint increases the forces within the heated elements by resisting thermal expansion.

For FC2, similar behaviour was observed under all three thermal loads i.e. StF-C, StF-NoC and parametric fire: (1) Elevated temperatures in the P-beam cause it to expand longitudinally. However, this is restrained by the the columns and cooler external bays. The resultant axial force exacerbates the initial twist caused by the flange notches as identified in Section 5.5.2, and causes lateral deflections in both flanges, as shown in Figure 6.12a. (2) In FC2, both J-beams (J2 and J3) experience elevated temperatures. The corresponding expansion further increases the lateral deflection of the P-beams. (3) As the axial force in the P-beams continues to rise, they seek to buckle outwards to relieve the stresses. Outward is defined as away from the structure. However, the J-beams still provide some restraint, as they prevent the entire P-beam from deflecting outwards. At a certain point in time (shortly after 51 minutes for the StF-C analysis, as shown in Figure 6.12a), the outward force of P1 overcomes that of P2, allowing it to buckle outwards by pulling P2 along with it, as shown in Figure 6.12b. This means that initially the beams expand and rotate outwards in opposing directions, until P2 forces P1 to rotate the same way, leading to both P-beams rotating and deflecting in the same direction. This causes a significant lateral deflection that continues until 60 minutes (55 mm for the StF-C case).

The deflection results of FC2 are summarised in Table 6.3. The key findings are: (1) Of all the J-beams, J2 experiences the greatest vertical and lateral deflections, similarly to FC1. However, the vertical deflections are only 10%

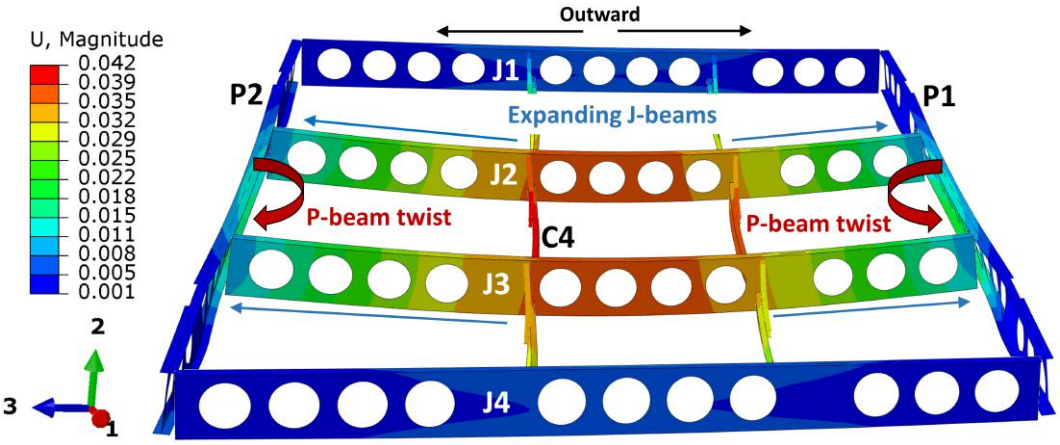

(a) 51 minutes - both P-beams are still rotating and deflecting outwards, in opposite directions relative to one another. P2 buckles shortly after 51 minutes, causing both P-beams to deflect as shown in (b).

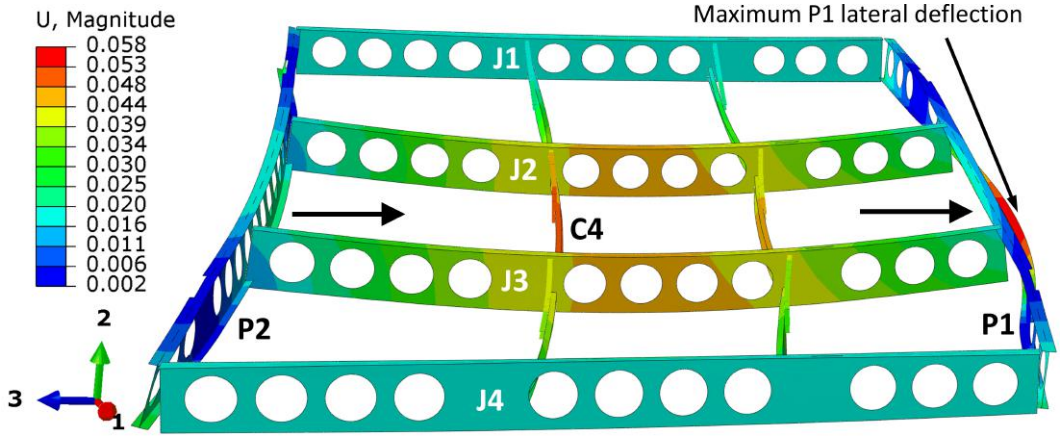

(b) 60 minutes - P2 has buckled, causing both P-beams deflect laterally to the right.

Figure 6.12: Fire case 2 (FC2) - global model at 51 and 60 minutes in the standard fire with the ceiling remaining intact analysis (StF-C). The total deflection is shown (in m), with a deformation scale factor of 10.

greater than FC1 under StF-C and parametric fire conditions, and 30% greater under StF-NoC conditions. This highlights that even though in this case a significantly larger portion of the structure has been heated, the behaviour observed for J-beams is still similar to that of a single beam in isolation. (2) Conversely, the lateral deflections are approximately double the FC1 results. This is most likely due to higher stresses in the bottom flange. (3) In FC2 the critical channel (C4) experiences deflections of 50%, 18% and 55% lower than in FC1, under StF-C, StF-NoC and parametric fire conditions respectively. This is due to the continuity of channels in internal bays i.e. knee-braces in adjacent channels prevent the internal J-beams from rotating, thus supporting the internal channels. (4) Importantly, the lateral deflection of P1 is significantly greater than that of J2 i.e. 7, 12 and 3.5 times greater for the StF-C, StF-NoC and parametric fire respectively. This indicates that the connections between the ceiling and P-beams will require more attention to insure that they remain intact during a fire. (5) As in FC1, the CBS recovers all thermal strain during the cooling stage of the parametric fire. This again highlights that low stresses are experienced in the structural elements.

Table 6.3: Fire case 2 (FC2) - maximum deflections (in mm) of critical elements

	J2		**C4**	**P1**
	midspan	**lateral**	**midspan**	**lateral**
StF-C	35 - L/229	8	7.7 - L/545	55
StF-NoC	84 - L/95	22	21 - L/200	266
Par. Fire	30 - L/267	7	6.4 - L/656	25

To conclude, it seems that the lateral deflections of the P-beams are more critical than those of the J-beams. Moreover, heating up greater areas of the CBS does not seem to worsen the J-beam or channel vertical deflection results, as a comparison between FC1 and FC2 shows. However, the J-beam maximum lateral deflection does approximately double. Finally, despite the significant lateral deflections of the P-beams, the steel does not yield throughout the more realistic parametric fire. Therefore, the entire structure is able to return to its ambient deflection state after the fire.

6.3.3 Fire case 3

This FC represents the possibility of compartmentation failing within the office space, which could lead to elevated temperatures throughout the CBS. This is a worst-case scenario and, especially when coupled with the 'no ceiling' temperatures, represents an extreme event. It has been included to test the ultimate fire resistance of the CBS, and locate possible failure zones.

Under StF-C, StF-NoC, and parametric fire behaviour, the same general behaviour was observed as in FC2. However, as the P-beams are now experiencing elevated temperatures over their entire length, the axial forces are greater, and the lateral deflection in a single direction of both P-beams begins sooner (39 minutes under StF-C conditions vs. 51 minutes in FC2). Thus, the outward deflection of P1 is significantly greater at 185 *mm* in FC3 vs. 55 *mm* in FC2. Figure 6.13 shows the lateral deflection of the global model after 60 minutes of a StF-C analysis. Furthermore, the figure also shows how the lateral movement of P1 and P2 causes the internal (J2 and J3) and external (J1 and J4) J-beams to deflect in opposite directions.

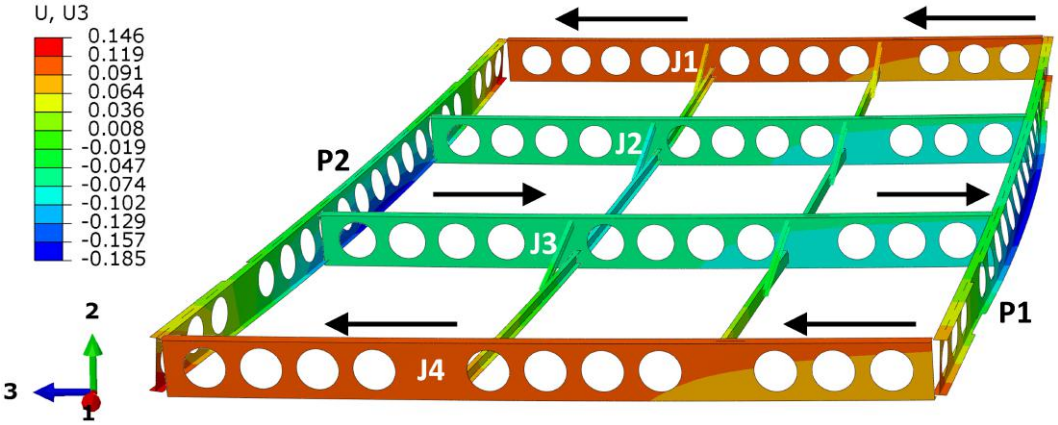

Figure 6.13: Fire case 3 (FC3) - lateral deflection under standard fire with a ceiling conditions (StF-C). The lateral deflection is shown. Deformation scale factor = 1.

Under StF-NoC conditions, it was found that severe yielding near the P-beam to column connections causes a runaway deflection failure. The plastic failure zones are shown in Figure 6.14. This result correlates with the single element P-beam model, as presented in Section 5.5, which identified the same failure mechanism. The midpoint deflection at the bottom flange of P1 under StF-NoC conditions is shown in Figure 6.15. The initial upward deflection seen in the graph is due to the twisting action forcing an upward displacement of the bottom flange, as in the single element analysis. However, as the steel begins to yield, the downward deflection dominates. This culminates in runaway deflection failure at approximately 31 minutes, which causes the entire structure to rapidly displace downwards. Thus, this occurrence corresponds with the ultimate fire resistance of the CBS. However, as stated previously, this failure only occurs under the extreme circumstances of a 'no ceiling' standard fire throughout the entire CBS.

The deflection results of FC2 are summarised in Table 6.4. The key findings are: (1) The midspan deflections for J2 are equivalent to those in FC2. This

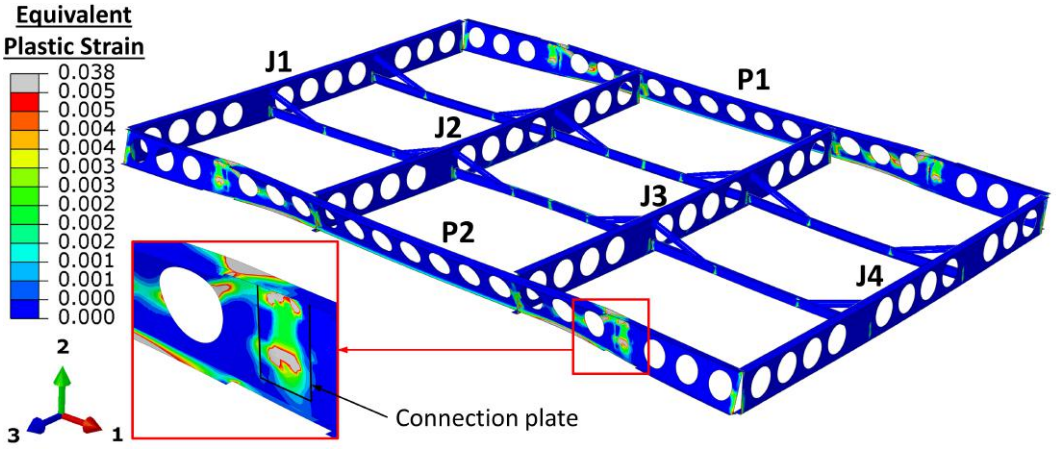

Figure 6.14: FC3 - severe plasticity near the column connections after 31 minutes of a standard fire 'no ceiling' analysis (StF-NoC). Collapse occurred shortly after this time. The plastic equivalent strain is shown. Deformation scale factor = 1.

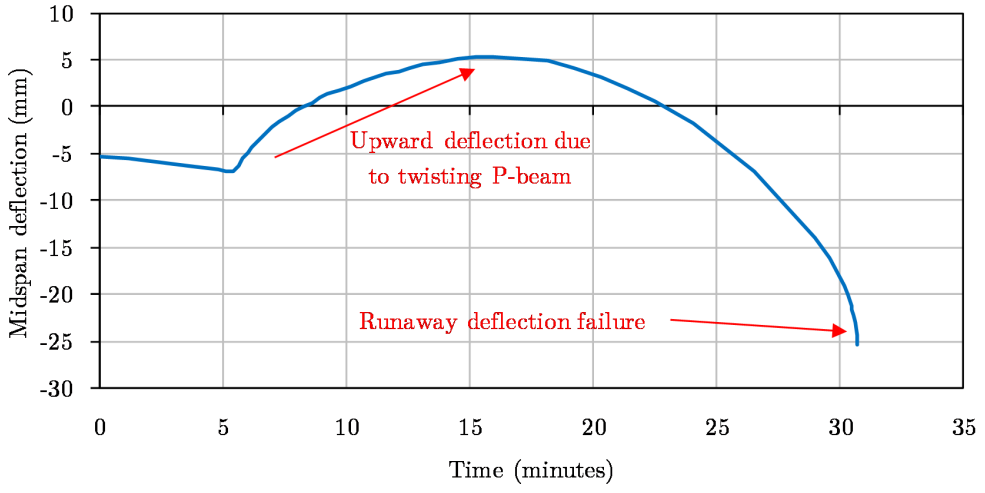

Figure 6.15: Fire case 3 (FC3) - midspan vertical deflection at bottom flange of P1, under standard fire 'no ceiling' conditions (StF-NoC)

suggests that the size of the fire (in terms of area of effect, not temperature) does not affect the deflections of the J-beams, as each one deflects independently of the others. (2) The maximum lateral deflections for the J-beams were found in J1, and not J2 as in FC2. However, they were only between 3 and 6 mm greater. (3) The critical channel in FC3, C2, deflects approximately twice as much as C4 in FC2. This indicates that the channels in external bays (bay A and C) are more sensitive to heightened temperatures. This is due to the channels lacking continuity i.e. at the perimeter of a structure there is no opposing knee-brace to prevent rotation of the external J-beam. Thus, the knee-brace is not able support the channel, resulting in greater vertical deflections. (4) As stated previously, the P-beam lateral deflections are significantly greater in FC3, due to the buckling of P2 causing both P-beams to deflect in the same directions. The maximum lateral deflection is 185 *mm* for P2 for the StF-C case. (5) As observed in FC1 and FC2, maximum midspan vertical deflections are within the requirement of span/20, except when runaway failure occurs. Therefore, they are only important relative to maintaining ceiling integrity. In this case the maximum deflection of J2 and C2 are 35 *mm* (L/229) and 30 *mm* (L/323) respectively for the StF-C case.

Figure 6.16 shows the global model at 0, 38 and 120 minutes in a parametric fire. As Figure 6.16b shows, the outward forces of either P-beam is not great enough to overcome the other. Thus, the deflections of the two P-beams shown in the Table 6.4 are both outward i.e. in opposite directions. However, it is possible that due to changes in input parameters or geometry, the lateral buckling phenomenon observed in FC2, and FC3 under both standard fires, could still occur. Figures 6.16a and 6.16c display the model before and after the fire, and show how the structure is able to achieve a near-return to the ambient deflection state after cooling. A limited amount of yielding results in a permanent lateral deformation of 2 *mm* in the bottom flanges of both P-beams.

Table 6.4: Fire case 3 (FC3) - maximum deflection (in mm) of critical elements

	J2	**J1**	**C2**	**P1**	**P2**
	midspan	**lateral**	**midspan**	**lateral**	**lateral**
StF-C	35 - L/229	11	13 - L/323	185	170
StF-NoC	*runaway*	25	*runaway*	293	276
Par. Fire	30 - L/267	13	13 - L/323	61	73

To conclude, the most significant finding of FC3 is the identification of a global failure mechanism. If the ceiling system were to lose all integrity, and the entire CBS were to experience elevated temperatures, it is possible that

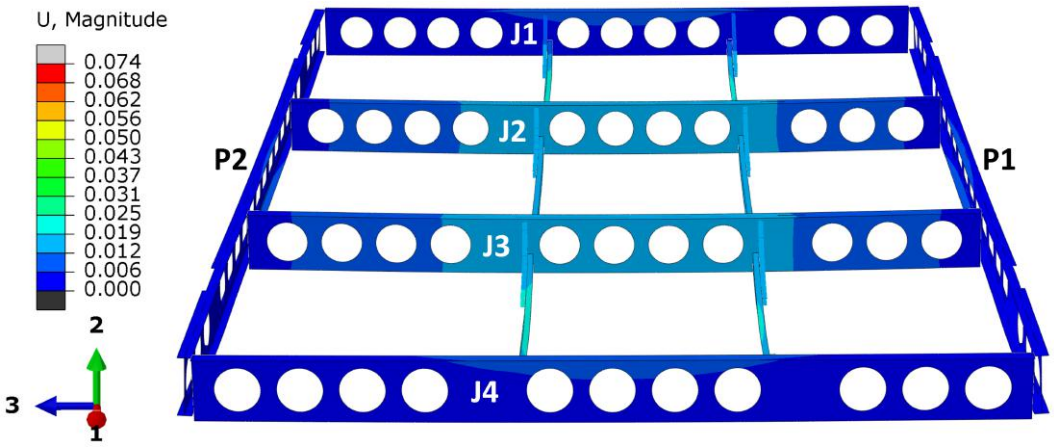

(a) 0 minutes - ambient deflection state

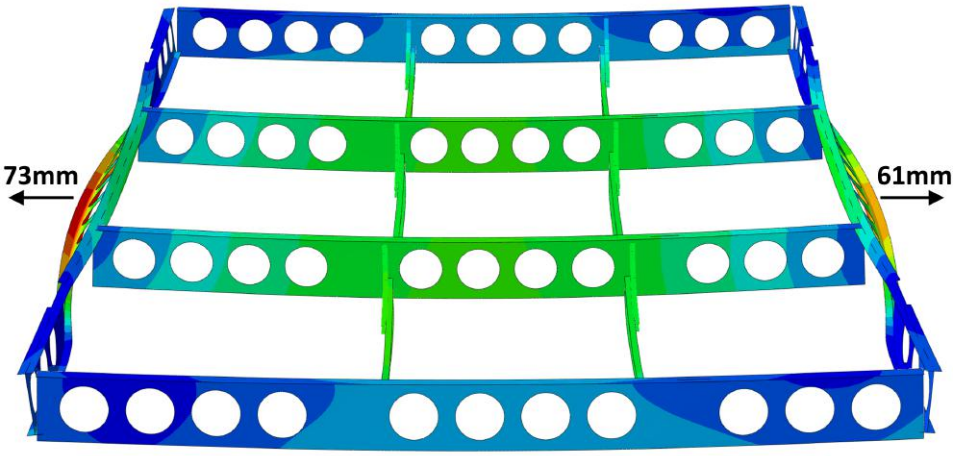

(b) 38 minutes - maximum lateral deflections of P-beams

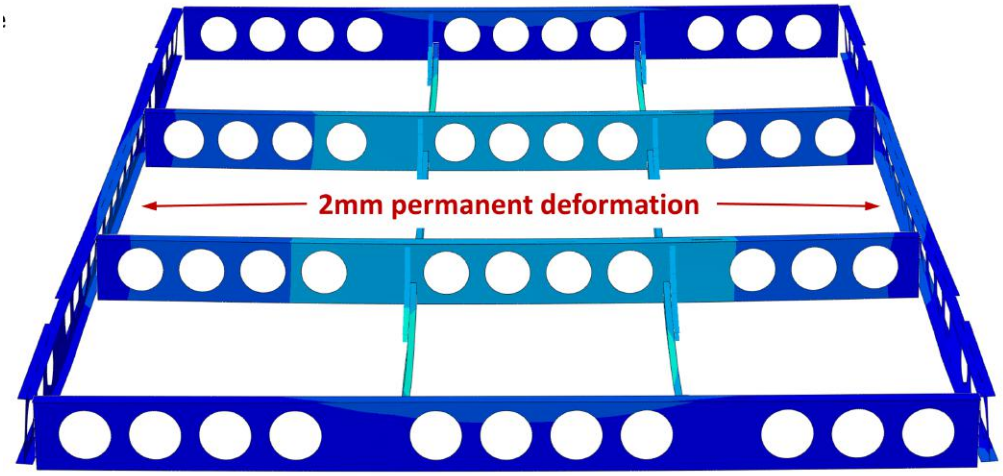

(c) 120 minutes - near return to ambient deflection state

Figure 6.16: Fire case 3 (FC3) - global model at 0, 38 and 120 minutes in a parametric fire analysis. The total deflection is shown. Deformation scale factor = 5.

severe plasticity near the P-beam to column connections can cause a runaway deflection failure. However, under the more realistic parametric fire conditions, the CBS does not experience such a failure, and is even able to return to a near-ambient deflection state upon cooling. Thus, if the integrity of the ceiling system can be ensured by allowing deflections, the CBS is flexible enough to withstand even a large fire across three bays. Furthermore, if the P-beam to column connection is detailed to allow some expansion i.e. by specifying oversized or slotted bolt holes, the stress near the connections will be reduced, along with the likelihood of a plastic failure. This aspect requires further research.

6.4 Conclusion

This chapter discussed the global structure modelling of a single CBS sub-structure. Thus, the interaction between structural elements was investigated in order to better predict the behaviour of the CBS under fire conditions. The chapter began by detailing the FEM input used, and includes a description of the three fire cases (FCs) considered. Thereafter, the results of the FCs were analysed. The important findings are:

- Fire case 1 (FC1), where only a single internal J-beam (J2) was heated, indicates that the P-beams provide nominal axial restraint to longitudinally expanding J-beams. A good correlation exists between the deflection behaviour of J2 in both FC1 and FC2, where an entire internal bay was heated, and the single PR J-beam model. This suggests that the P-beams act approximately like pin-roller supports. Therefore, a single element PR J-beam model could be used in the future for further fire resistance analyses, without resorting to the global model.

- FC2 shows that when the P-beams experience elevated temperatures, they undergo significant lateral deflections. These are between 3.5 and 12 times greater than those of the J-beams, depending on the fire conditions. This indicates that the connections between the ceilings and the P-beam should be carefully detailed in order to allow these deflections.

- FC3, where the entire structure was heated, identified a global failure mechanism, whereby yielding near the P-beam to column connections causes the entire structure to experience a runaway downward deflection. This only occurs under standard fire 'no ceiling' conditions, emphasising the importance of maintaining the integrity of the ceiling system. Once again, the behaviour of single elements analysed in isolation (in this case P-beams) are approximately the same as those predicted by the global model.

- In all three fire cases, the cooling stage under parametric fire conditions allowed the CBS to return to the ambient deflection state. Only in FC3 was there a small amount of yielding, leading to a permanent lateral deformation of 2 mm in the P-beams. However, this is deemed negligible, and suggests that the CBR performs well in a scenario that better simulates a real fire. Thus, the maximum deflections shown in Tables 6.1, 6.2, 6.3 and 6.4 can be used to design the connections between the ceiling system and the structural elements. This will serve to maintain the integrity in a real fire, and minimise the long-term effect of the fire on the structural steel.

Chapter 7

Conclusions and recommendations

7.1 Overview

This thesis has investigated the structural behaviour of a novel cellular beam structure (CBS) under fire conditions. Initially, Chapter 1 introduces the problem statement, and presents the objectives and scope of this research. Thereafter, Chapter 2 reviews the literature that provided the necessary knowledge to perform this research. Specifically, the important concepts of fire dynamics, structural fire engineering, steel in fire, physical fire testing and global modelling of structures in fire are discussed.

The CBS has been developed by the Southern African Institute of Steel Construction (SAISC) to meet the performance-based requirements of the building industry, which current construction methods are struggling to do. In response, a lightweight, versatile and cost-effective modular construction concept has been developed. As the focus of this research, and due to its unconventional nature, Chapter 3 presents a detailed discussion to familiarise the reader with the CBS. The chapter outlines the motive behind the innovation, an explanation of the structural design philosophy, and an introduction to the terminology used for the various structural elements.

Finite element (FE) modelling techniques have been the primary tool used in this thesis to characterise the structural behaviour of the CBS. However, under fire conditions such models become increasingly non-linear, and thus more complex. A rigorous validation process, detailed in Chapter 4, was undertaken to develop the modelling skills and techniques required to accurately model structures in fire. The validation study includes three benchmark FE models, and the development of a verified material model for structural steel under elevated temperatures.

Chapter 5 presents the FE models of single structural elements of the CBS. The chapter begins by giving an overview of the thermal analysis, performed by Marx (2018), used to specify the steel temperatures during a fire. Mul-

tiple models were run using different boundary conditions under three different thermal loads. In this way, the sensitivity of the CBS was tested, and the behaviour under a variety of possible scenarios was investigated.

Chapter 6 focuses on the global structure FE models that include all the elements of a single CBS sub-structure. In reality, stuctural elements do not act independently of each other. Therefore, as an assembly of connected single elements, the global model allows the elements to influence each other during the fire. Thus, the global model was able to provide a more holistic prediction of the behaviour of the CBS during a fire.

Chapter 7 provides a summary of the important findings of this research. Furthermore, practical design considerations are recommended to ensure the CBS performs well in a fire. Finally, suggestions are made for future research on the fire resistance of the CBS.

7.2 Summary of findings

In total, this thesis made use of 18 single element models and 9 global structure models. These yielded a substantial number of findings, that have been successively presented throughout the thesis. For conciseness, those results deemed most significant have been summarised and are listed in this section. For a complete list of findings, the reader is referred back to Chapters 5 and 6.

Axial restraint increases midspan deflections: In the single element models it was found that if the longitudinal thermal expansion of secondary beams (J-beams) was restrained, high axial forces can develop. This induces an additional moment due to the beam's ambient deflection state, which increases the midspan vertical deflection. For instance, under a standard fire with the ceiling remaining intact (StF-C), the midspan deflection of the J-beams is up to 133% higher if restrained.

Primary beams provide nominal axial restraint: In the global model, the J-beams are supported on either end by the primary beams (P-beams). A good correlation was found between the deflection results of the global model J-beam and single element J-beam with pin-roller supports. This indicates that the P-beams provide minimal axial restraint against the longitudinal expansion of the J-beams. This was confirmed when a negligible axial force was extracted from the global model. Ultimately, this is beneficial to the CBS, as the lack of axial restraint reduces the midspan deflections, and reduces the chance of buckling due to lower axial forces.

Low midspan deflection ratios: Under StF-C conditions, the greatest vertical deflection of 40 *mm* (span/200) was observed for the single element pin-pin J-beam, which could conservatively be used to design the ceiling system. However, as previously pointed out, the global model suggests that the J-beams are not axially restrained. Thus, the more realistic maximum midspan deflection of 35 *mm* (span/229) from the global models could be used for design purposes. In a design scenario engineers could use this information to consider different structural configurations in which axial restraint may be induced, such as when lift shafts or braced bays are present.

J-beam asymmetry causes lateral deflection: As the bottom flange of the J-beam heats up and expands, an internal moment is induced due to the restraint provided by the cooler web. This causes a lateral movement of the bottom flange, which could threaten the integrity of the ceiling system. The magnitude of the deflection is sensitive to the end boundary conditions, and ranges between 4 and 59 *mm* for the single element models under StF-C conditions. However, under the more realistic boundary conditions of the global model, the maximum lateral deflection for all fire cases was 11 *mm*. If the ceiling, or any other building feature, is connected to the bottom flange, this deflection should be accounted for.

High temperatures can cause lateral torsional buckling: Under the temperatures conditions of the standard fire 'no ceiling' analysis (StF-NoC), it was found that the top flange of the J-beam can buckle laterally. However, this did not result in a runaway deflection failure, as significant post-buckling strength was observed. At worst, the pin-pin J-beam experienced a 181 *mm* (span/44) midspan vertical deflection after 60 minutes of a StF-NoC analysis. That said, buckling only occurred if the the beam was axially restrained i.e. if free to expand no buckling occurs, even at extreme 'no ceiling' temperatures. Thus, this failure did not occur in any of the global models and is unlikely to occur in the CBS. However, it does further emphasise how any form of axial restraint should be avoided in the final design of the CBS.

P-beams experience significant lateral deflections: Whilst the vertical midspan deflections were relatively low i.e. less than 10 *mm*, the P-beams experience significantly higher lateral deflections. An initial twist due to notches in the flanges precipitates this lateral movement. The deflection is exacerbated by axial forces in the P-beam as a result of the axial restraint provided by the columns. In the global models, under fire cases 2 (only bay B heated) and 3 (entire model is heated), this behaviour ultimately causes one of the P-beams to buckle outwards, and pull the other one along. The resulting lateral deflections can be as high as 185 *mm*, under standard fire conditions with the ceiling remaining

intact. This deflection could be a major threat to the integrity of the ceiling system.

Plastic failure at P-beam to column connection: Under 'no ceiling' conditions, the P-beam experiences a runaway deflection, due to steel yielding near the column connections. This failure was detected in the single element model after 52 minutes, and in the global model after 31 minutes. However, in the global model the failure only occurred when the entire structure was heated. Thus, this failure is only expected to happen under extreme conditions i.e. if the entire fire-rated ceiling were to fail. Nevertheless, the event could cause a dangerous collapse, and stresses the importance of maintaining the integrity of the ceiling system.

Majority of steel deformation recovers upon cooling: Depending on the analysis, some amount of steel yielding during the fires resulted in permanent plastic deformations. However, the majority of thermally induced strain remained elastic, i.e. no yielding, and was thus recovered during the cooling stage of the parametric fire. Significantly, in the global models the CBS was able to recover *all* deflections, returning to the ambient deflection state. The only exception was a small 2 mm permanent lateral deflection of the P-beams, occurring when all three bays were heated. This highlights the flexibility of the CBS i.e. its ability to expand and deflect without causing major internal stresses. Thus, if the ceiling system is designed to withstand the predicted deflections, the results indicate that a real fire will have a minor long-term impact on the structural steel.

Tension force predicted by parametric fire: The parametric fire was used to estimate possible tension forces on end connections during the cooling stage. The pin-pin J-beam beam experienced the greatest tensile force of 268 kN. For the P-beams, a 62 kN force was detected, but only if the flexibility of columns was ignored. Therefore, both cases indicate that not only does axial restraint increase midspan deflections, but it also increases the likelihood of tensile forces upon cooling. Again, the flexibility of the CBS was beneficial, as negligible tensile forces were present in the global model.

It is important to note that the findings above are based on single element and global structural models that used the results of the thermal analysis of Marx (2018) as input. In the future, a validation of the predicted steel temperatures is critical. Further physical testing of the flooring system upon which the CBS relies is encouraged. The integrity of the fire-resistant boarding during a fire should receive special attention, as this work has shown that a global failure mechanism is possible if the fire-resistant boarding were to fail. In light of the

above, the findings of this work should not be seen as definitive, but rather as a first attempt to understand the structural behaviour of the CBS during a fire. Ultimately, a full-scale fire test of the prototype CBS could be used to validate the predicted steel temperatures and structural behaviour.

To conclude, in general the results suggest that the CBS performs well under fire conditions. The flexibility of the structure allows it to freely expand and deflect as the fire progresses, preventing the build-up of significant stresses. Although failure mechanisms were detected, these only occurred under extreme temperature conditions coinciding with a complete loss of the fire-resistant board. Furthermore, negligible yielding during the parametric fire analyses indicate that the CBS experiences relatively small permanent deformations. Finally, the integrity of the ceiling system can be ensured by allowing it to accommodate the predicted deflections. For design purposes, the maximum vertical and lateral deflections under StF-C conditions are 35 mm (span/229) and 185 mm respectively. Taking the above into consideration, it seems that the CBS will not only survive a fire, but the steel will return to its original state after cooling.

7.3 Design considerations

Based on the findings of this thesis, certain design considerations are recommended. Essentially, there are two main goals: keep the structure flexible i.e. allow it to deform, and keep the ceiling system intact. If the former cannot be attained it is still possible to design the structure considering the axial forces induced in members. However, the latter goal is consequently affected as greater deflections are experienced by beams.

To keep the structural system flexible, the following should be done: (1) Ensure that the connections between members act as pins i.e. provide negligible moment restraint. In light of this, it is recommended that the J-beam to P-beam connection be modified to use double angle cleats, which have been shown to perform well in fires. (2) Specify slotted bolt holes at connections to allow free thermal expansion. Under StF-C and parametric fire conditions, the J-beams expand a maximum of 9 mm i.e. 4.5 mm on each side. Thus, even if bolt holes are only oversized by 5 mm, the chance of axial forces developing is greatly diminished. The significant axial forces in the P-beams could also be reduced with the specification of slotted bolt holes.

Thereafter, it is essential that the ceiling system be designed with the expected deflections in mind. If this is not done, the ceiling might lose integrity, thereby losing its insulation properties and jeopardising the compartmentation function. Based on the global analysis under StF-C and parametric fire conditions, the ceiling boards must be able to withstand a maximum midspan deflection of 35 mm (span/229) underneath the J-beams, and 16 mm (span/270) un-

derneath the channels. Furthermore, a maximum lateral deflection of 13 *mm* is predicted for the J-beam bottom flange, and 185 *mm* for the P-beams. A possible solution is a suspended ceiling connection system, which allows the steel to deflect laterally independently of the ceiling. Alternatively, it would be necessary to include some form of floor bracing system, although this would induce axial forces which the CBS would have to withstand. It may also be possible to change the structural configuration to increase the stiffness of the bottom flange to reduce deflections. For the J-beam, this may be possible by ensuring sufficient connections between the J-beam and the additional angle that has been ignored in the structural analyses of this work, as discussed in Section 5.2 and shown in Figure 5.1.

7.4 Future research

This research has produced finite element models that aim to predict the behaviour of the CBS in a fire. However, as computer models, they remain a numerical approximation of reality, and cannot take into account all the complexities of a real fire. Therefore, it is recommended that physical fire testing be conducted. Initially, a furnace could be used to test isolated structural elements under standard fire conditions. If a furnace is not available, a real-fire test could also be performed on a single elements. Similarly to this thesis, the single element tests would be in preparation for a large-scale test, in which the existing prototype CBS is subjected to a real fire. This would be the ultimate test of the structure's resistance to fire, and would serve to validate/calibrate the computer models in this thesis.

The global structure models presented in this thesis consist of a single CBS sub-structure incorporating three modules/bays. Thus, the models could be expanded to include multiple floors, cross-bracing, different layouts and other such factors that influence the structural behaviour. Finally, further investigations could be carried out regarding how to ensure that the ceiling remains intact during fires.

List of References

Abaqus (2014). *Abaqus 6.14 Analysis User's Guide*. Dassault Systèmes Simulia, Providence. (Cited on pages 29, 43, 46, and 70.)

AISC (2010). *Specification for Structural Steel Buildings*. American Institute of Steel Construction, Chicago. (Cited on page 14.)

Al-Jabiri, K. (1999). *The behaviour of steel and composite beam-to-column connections in fire*. Ph.D. thesis, University of Sheffield. (Cited on page 22.)

Bailey, C.G., Lennon, T. and Moore, D. (1999). The behaviour of full-scale steel-framed buildings subjected to compartment fires. *The Structural Engineer*, vol. 77, no. 8, pp. 15–21. (Cited on page 26.)

Bisby, L., Gales, J. and Maluk, C. (2013). A contemporary review of large-scale non-standard structural fire testing. *Fire Science Reviews*. (Cited on pages 12, 25, 26, and 92.)

BSI (2009). *BS 476: Fire tests on building materials and structures*. British Standards Institute, London. (Cited on page 74.)

Buchanan, A. and Abu, A. (2017). *Structural Design for Fire Safety*. John Wiley & Sons Ltd, Chichester. (Cited on pages 6, 7, 9, 10, 11, 22, 24, 25, 27, and 61.)

Burgess, I.W., El Rimawi, J. and Plank, R.J. (1991). Studies of the Behaviour of Steel Beams in Fire. *Journal of Construction Research*, vol. 19, pp. 285–312. ISSN 0143974X. (Cited on pages 22 and 60.)

CEN (2002). *Eurocode 1: Actions on structures - Part 1-2: General actions - Actions on structures exposed to fire*. European Committee for Standardization, Brussels. (Cited on pages 11, 13, 58, and 125.)

CEN (2005). *Eurocode 3: Design of steel structures - Part 1-2: General rules - Structural fire design*. European Committee for Standardization, Brussels. (Cited on pages x, xi, 14, 15, 16, 17, 46, 47, 48, and 95.)

CEN (2009*a*). *Eurocode 3: Design of steel structures - Part 1-1: General rules and rules for buildings*. European Committee for Standardization, Brussels. (Cited on page 53.)

CEN (2009*b*). *Eurocode 3: Design of steel structures - Part 1-5: Plated structural elements*. European Committee for Standardization, Brussels. (Cited on page 53.)

Cook, R., Malkus, D., Plesha, M. and Witt, R. (2002). *Concepts and Applications of Finite Element Analysis*. John Wiley & Sons Ltd, Chichester. (Cited on pages 41 and 71.)

COST (2014). *Benchmark studies: Verification of numerical models in fire engineering*. CTU Publishing House, Prague. ISBN 978-80-01-05442-0. (Cited on pages xi, 41, 42, 46, 53, and 60.)

CSA (2009). *CSA S16-09 Design of steel structures*. Canadian Standards Association, Toronto. (Cited on page 11.)

Drysdale, D. (2011). *An Introduction to Fire Dynamics*. John Wiley & Sons Ltd, Chichester. (Cited on pages 6, 7, 8, and 9.)

ECCS (2001). *Model Code on Fire Engineering*. European Convention for Constructional Steelwork, Brussels. (Cited on pages 11, 17, and 47.)

Gebremeskel, A. (2013). Modular access floor building system (white paper). *Steel Future Conference*. (Cited on pages 33, 83, and 99.)

Gillie, M. (2009). Analysis of heated structures: Nature and modelling benchmarks. *Fire Safety Journal*, vol. 44, no. 5, pp. 673–680. ISSN 03797112. (Cited on pages xi, 13, 27, 29, 32, 41, 42, and 44.)

Hicks, S., Feeney, M. and Clifton, G.C. (2012). Fire Performance of an Office Building with Long-span Cellular Floor Beams - Britomart East, Auckland. *Structural Engineering International*, vol. 22, no. 4, pp. 533–540. (Cited on pages xi, 14, 24, 31, and 32.)

ISO (1999). *ISO 834-1:1999: Fire Resistance Tests - Elements of Building Construction - Part 1: General Requirements*. International Organization for Standardization, Geneva. (Cited on pages 11 and 25.)

Kerdal, D. and Nethercott, D.A. (1984). Failure Modes for Castellated Beams. *Journal of Constructional Steel Research*, vol. 4, pp. 295–315. (Cited on pages x, 18, 19, 20, and 21.)

Kuchta, K. and Maślak, M. (2015). Failure Modes Determining the Resistance and the Stability of Steel Cellular Beams. *Journal of Civil Engineering, Environment and Architecture*, vol. 62, pp. 263–280. (Cited on pages x, 19, 20, and 21.)

Lamont, S. (2001). *The Behaviour of Multi-storey Composite Steel Framed Structures in Response to Fires*. Ph.D. thesis, University of Edinburgh. (Cited on pages x and 14.)

Lawson, R. and Hicks, S. (2011). *Design of composite beams with large web openings*. Steel Constuction Institute, Ascot. ISBN 9781859421970. (Cited on page 21.)

Lennon, T. (2011). *Structural Fire Engineering*. ICE Publishing, London. (Cited on pages 10, 25, and 61.)

Li, G.Q. and Guo, S.X. (2008). Experiment on restrained steel beams subjected to heating and cooling. *Journal of Constructional Steel Research*, vol. 64, no. 3, pp. 268–274. ISSN 0143974X. (Cited on page 18.)

Liu, T.C.H., Fahad, M.K. and Davies, J.M. (2002). Experimental investigation of behaviour of axially restrained steel beams in fire. *Journal of Constructional Steel Research*, vol. 58, no. 9, pp. 1211–1230. ISSN 0143974X. (Cited on pages 18 and 24.)

Marx, H. (2018). *Thermal behaviour of a novel cellular beam structural system in fire*. Master's thesis, Stellenbosch University. (Cited on pages xi, xii, xvi, 3, 36, 57, 58, 59, 61, 62, 63, 64, 65, 77, 90, 95, 114, 117, 125, and 126.)

Nadjai, A., Vassart, O., Ali, F., Talamona, D., Allam, A. and Hawes, M. (2007). Performance of cellular composite floor beams at elevated temperatures. *Fire Safety Journal*, vol. 42, pp. 489–497. (Cited on page 21.)

Najafi, M. and Wang, Y.C. (2016). Axially restrained steel beams with web openings at elevated temperatures, part 1: Behaviour and numerical simulation results. *Journal of Constructional Steel Research*, vol. 128, pp. 745–761. ISSN 0143974X. (Cited on pages 14, 18, 21, 29, 32, 60, 67, 68, and 70.)

NIST (2005). Final Report on the Collapse of the World Trade Center Towers. Tech. Rep., National Institute of Standards and Technology. (Cited on page 22.)

NIST (2010). Technical Note 1681 - Best Practice Guidelines for Structural Fire Resistance Design of Concrete and Steel Buildings. Tech. Rep., National Insititute of Standards and Technology. (Cited on page 10.)

Powell, W. (2017). The fire triangle. Available at: `www.donleyinc.com/news-events/post/what-you-need-to-know-about-the-fire-triangle` (Cited on pages x and 7.)

SABS (2011*a*). *SANS 10160-2:2011 - Basis of structural design and actions for buildings and industrial structures Part 2: Self-weight and imposed loads*. South African Bureau of Standards, Pretoria. (Cited on page 65.)

SABS (2011*b*). *SANS 10400-T:2011 The application of the National Building Regulations Part T : Fire*. South African Bureau of Standards, Pretoria. ISBN 9780626251932. (Cited on pages 1 and 58.)

SAISC (2013). *The Red Book: Southern African Steel Construction Handbook*. Southern African Institute of Steel Construction. (Cited on pages 68, 81, and 93.)

University of Edinburgh (2000). Final Report of the DETR-PIT Project: Behaviour of Steel Framed Structures under Fire Conditions. Tech. Rep., Building Research Establishment. (Cited on pages 13, 14, 24, 26, 30, and 32.)

Usmani, A., Rotter, J.M., Lamont, S., Sanad, A. and Gillie, M. (2001). Fundamental principles of structural behaviour under thermal effects. *Fire Safety Journal*, vol. 36, no. 8, pp. 721–744. ISSN 03797112. (Cited on pages 27 and 92.)

van Jaarsveldt, W. (2016). *Predicting the failure load of steel columns weakened to facilitate demolition of structures*. Master's thesis, Stellenbosch University. (Cited on page 66.)

Vassart, O., Hawes, M., Simms, I., Zhao, B., Franssen, J. and Nadjai, A. (2010). Fire resistance of long span cellular beam made of rolled profiles (FICEB). Tech. Rep., Euroopean Commision: Resarch Fund for Coal and Steel Unit. (Cited on page 21.)

Walls, R. (2016). *A beam finite element for the analysis of structures in fire*. Ph.D. thesis, Stellenbosch University. (Cited on pages x and 9.)

Walls, R. and Botha, M. (2016). Towards a Structural Fire Loading Code for Buildings in South Africa. *Insights and Innovations in Structural Engineering, Mechanics and Computation*, pp. 1761–5. (Cited on page 11.)

Walls, R., Viljoen, C., de Clercq, H. and Retief, J. (2014). A critical review on current and proposed structural fire engineering codes for steelwork in South Africa. *Construction Materials & Structures*, pp. 1134–1140. (Cited on pages 11 and 65.)

Walls, R.S., Viljoen, C., de Clercq, H. and Clifton, G.C. (2017). Reliability Analysis of the Slab Panel Method (SPM) for the Design of Composite Steel Floors in Severe Fires. *Journal of Structural Fire Engineering*, vol. 8, no. 1, pp. 84–103. ISSN 20402325. (Cited on page 31.)

Wang, P., Ma, N. and Wang, X. (2014). Numerical studies on large deflection behaviors of restrained castellated steel beams in a fire. *Journal of Constructional Steel Research*, vol. 100, pp. 136–145. ISSN 0143974X.
Available at: `http://dx.doi.org/10.1016/j.jcsr.2014.04.026` (Cited on page 67.)

Wang, Y., Burgess, I., Wald, F. and Gillie, M. (2013). *Performance-Based Fire Engineering of Structures*. Boca Raton, CRC Press. (Cited on pages x, xiv, 8, 12, 13, 15, 22, 23, 25, 26, 27, 28, 29, 31, 57, 96, and 98.)

Yin, Y.Z. and Wang, Y.C. (2004). A numerical study of large deflection behaviour of restrained steel beams at elevated temperatures. *Journal of Constructional Steel Research*, vol. 60, no. 7, pp. 1029–1047. ISSN 0143974X. (Cited on pages 18, 29, 32, 67, and 70.)

Appendices

Appendix A

Parametric fire

The parametric fire used in this thesis was calculated according to EN 1991-1-2 CEN (2002), based on the assumptions given in Table A.1 (Marx, 2018). Using the table, the reader should be able to reproduce the fire curve.

Table A.1: Assumptions made for parametric fire calculations (Marx, 2018)

Basic assumptions for parametric fire calculations			
Occupancy Type:	Office		
Fire load density: $q_{f,k}$ =	511	MJ/m^2	(80% Fractile)
Fire growth rate / Medium	t_a (s) / 300	RHR_f / 250	EN1991-1-2 Table E.5
Factor (γ_n) =	1.0	(Active safety measures)	
Activity factor (γ_{q2}) =	1.0	(Office)	
Combustion factor:	Cellulosic material (m = 0.8)		

Dimensions of compartment			
Floor length	L =	12.75	m
Floor width	B =	8.5	m
Floor height	H =	2.56	m

Ventilation openings			
Opening type	**Window**	**Door**	**Other**
Quantity	4	1	0
Width (m)	3.85	1	0
Height (m)	1.54	2	0

Compartment boundaries				
Boundary	**Material**	**ρ (kg/m³)**	**k (W/mK)**	**c_p (J/kgK)**
Floor	FCB	1260	0.17	2500
Ceiling	Gypsum	1440	0.48	840
Walls	Gypsum	1440	0.48	840

Appendix B

Shop drawings

This appendix includes only the shop drawings used in this thesis to define the geometry of the finite element models. For a complete set of shop drawings, please contact Amanuel Gebremeskel of the SAISC. All drawings are supplied courtesy of the SAISC.

As well as the General Arrangement drawing, the shop drawings included are:

CB46 - P-beam

CB47 - P-beam

CB48 - P-beam

CB49 - P-beam

CB50 - P-beam

CB51 - P-beam

PA70 - J-beam

PA103 - J-beam

PA105 - J-beam

M116 - Channel

A125 - Knee-brace

P153 - P-beam connection plate

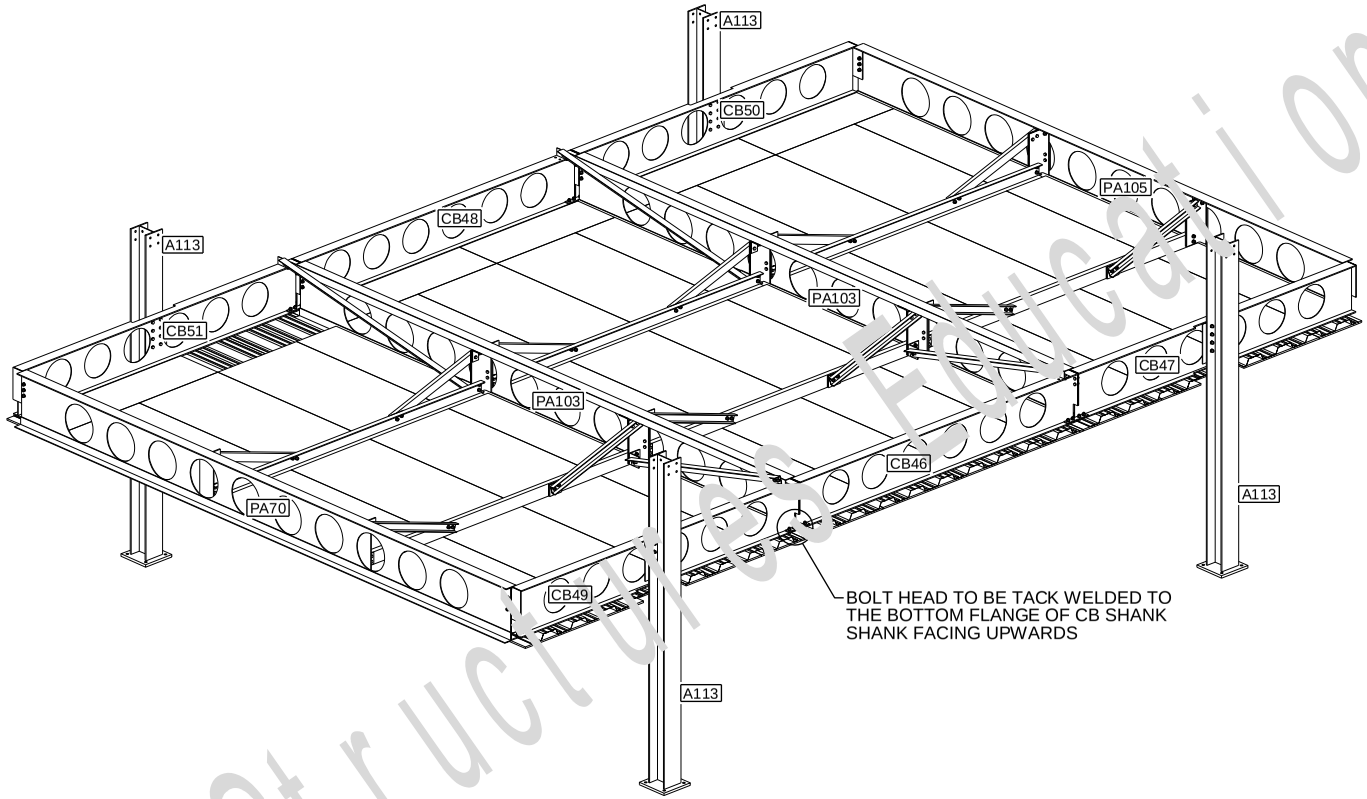

Standard rendered

Model :- New model 4

Rev	Mark	Revision Description	Date

SAISC
Dry Floor Panel and Modular Access Floor
Research
Power Street Germiston

Drawing title
A3 General Arrangement Drawing

Drawn C Schoeman &
Scale 1:50
Issued
Revised
Project Number 1
Drawing G [2]
Rev 0

Supplied by
Cadex SA (Tekla's SA Reseller)
Tel +27 11 463 1857/3641 Fax +27 11 463 9445
P O Box 411340
Craighall 2024, South Africa
info@CadexSA.com

POWERED BY TEKLA A TRIMBLE COMPANY

Tekla Structures

Phase number & name	Qty
1 Phase 1	1

Prepared using Tekla Structures® (www.tekla.com)

Model :- New model 4

General Notes: All steelwork to comply with SANS 2001:CS1 & SANS 1921-3
All welds 6mm continuous fillet welds unless noted otherwise
All butt welds full penetration welds unless noted otherwise
Mark assembly at position shown for correct site orientation
All holes to be 22DIA for M20 bolts unless noted otherwise

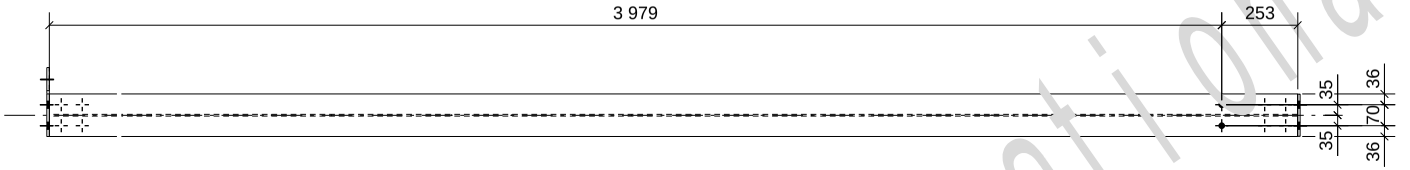

Top View

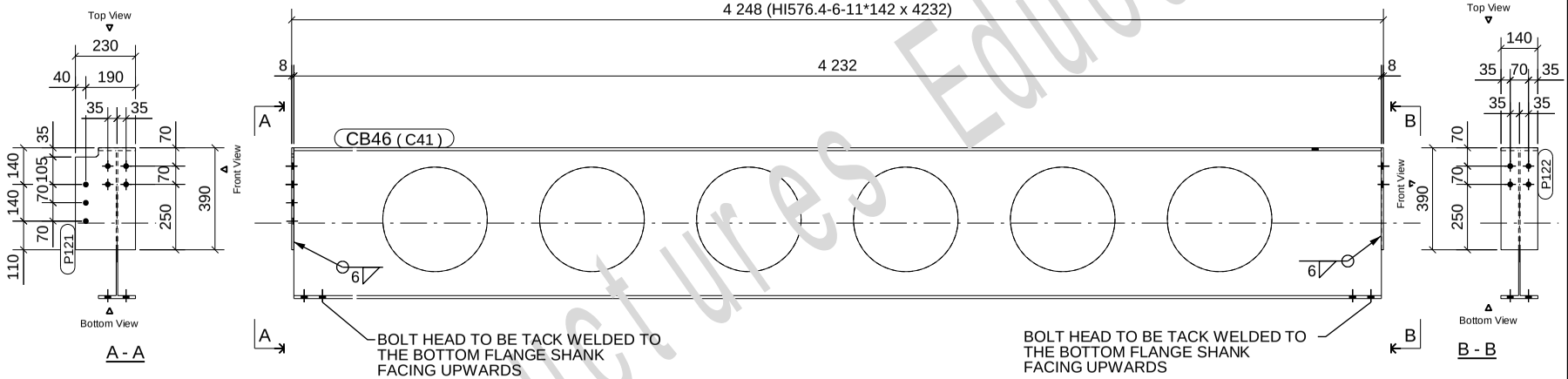

Front View

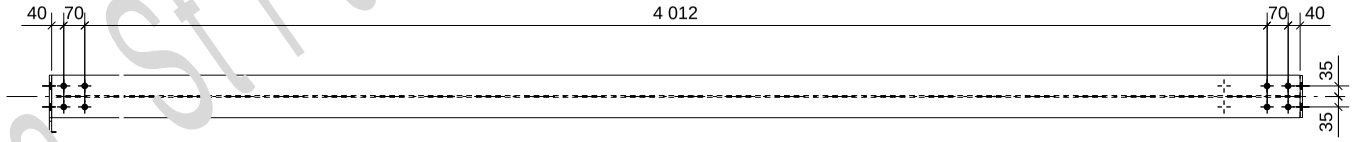

Bottom View

Material list for 1 BEAM assembly marked CB46 - only 1 is required						
Mark	No	Profile	Length	Grade	Paint area	Mass
C41	1	HI576.4-6-11*142	4232	S355JR	5.8	214.3
P121	1	PLT8*230	390	S355JR	0.2	5.6
P122	1	PLT8*140	390	S355JR	0.1	3.4
Total for 1 assembly					6.1	223.4

Tekla Structures

1 'BEAM' required marked CB46

Rev	Mark	Revision Description	Date

SAISC
Dry Floor Panel and Modular Access Floor Research
Power Street Germiston

POWERED BY TEKLA A TRIMBLE COMPANY

Draw C Schoeman &
Scale 1:15
Issued
Revised
Project Number 1

Supplied by
Cadex SA (Tekla's SA Reseller)
Tel +27 11 463 1857/3641 Fax +27 11 463 9445
P O Box 411340
Craighall 2024, South Africa
info@CadexSA.com

Assembly Drawing A [CB.46] Rev 0

Phase number & name	Qty
1 Phase 1	1

Prepared using Tekla Structures® (www.tekla.com)

Model :- New model 4

General Notes: All steelwork to comply with SANS 2001:CS1 & SANS 1921-3
All welds 6mm continuous fillet welds unless noted otherwise
All butt welds full penetration welds unless noted otherwise
Mark assembly at position shown for correct site orientation
All holes to be 22DIA for M20 bolts unless noted otherwise

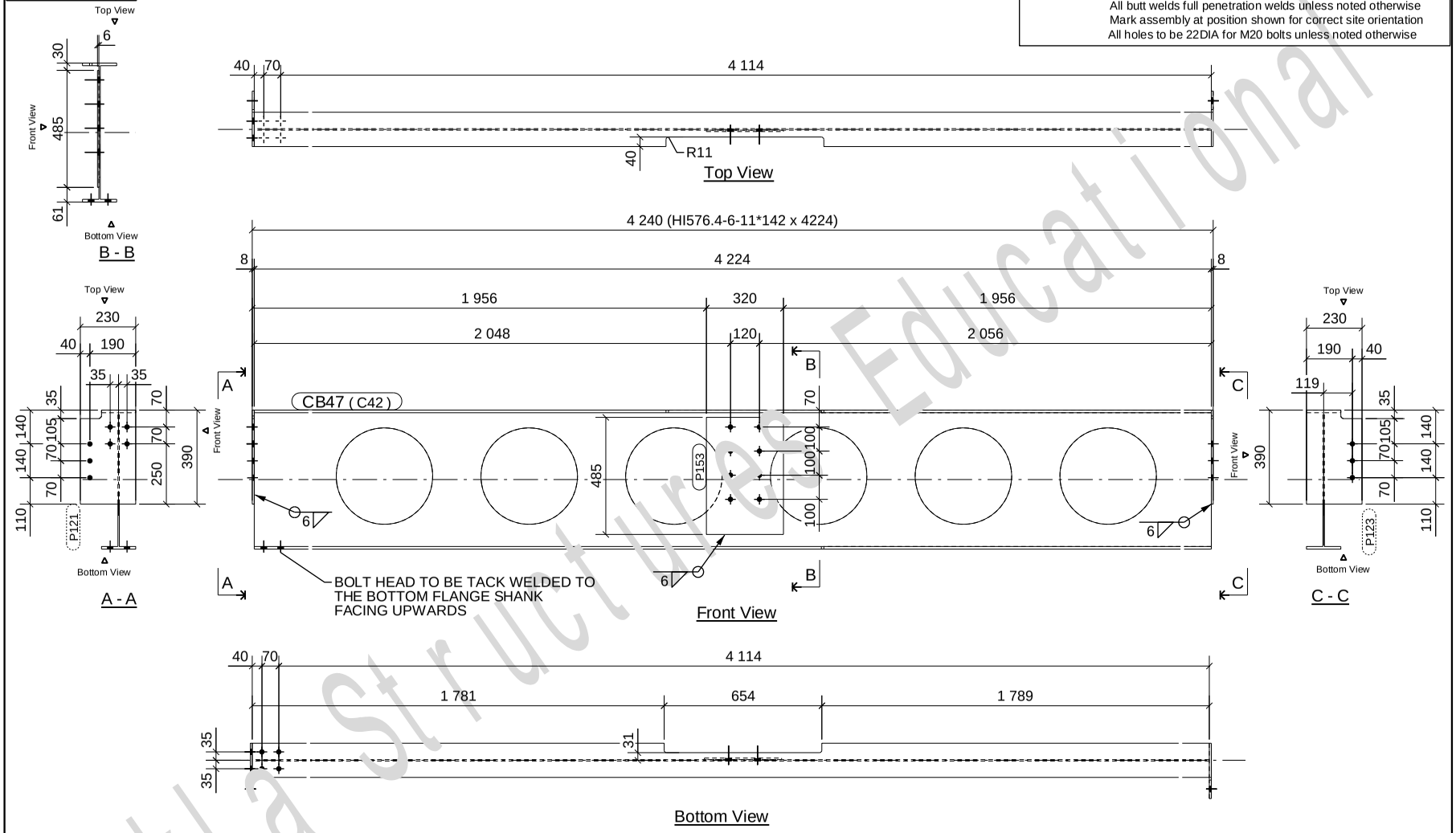

Material list for 1 BEAM assembly marked CB47 - only 1 is required

Mark	No	Profile	Length	Grade	Paint area	Mass
C42	1	HI576.4-6-11*142	4224	S355JR	5.7	213.9
P121	1	PLT8*230	390	S355JR	0.2	5.6
P123	1	PLT8*230	390	S355JR	0.2	5.6
P153	1	PLT6*320	485	S355JR	0.3	7.3
Total for 1 assembly					6.4	232.5

1 'BEAM' required marked CB47

Rev	Mark	Revision Description	Date

SAISC
Dry Floor Panel and Modular Access Floor Research
Power Street Germiston

Supplied by
Cadex SA (Tekla's SA Reseller)
Tel +27 11 463 1857/3641 Fax +27 11 463 9445
P O Box 411340
Craighall 2024, South Africa
info@CadexSA.com

POWERED BY TEKLA A TRIMBLE COMPANY

Drawn C Schoeman &
Scale 1:15
Issued
Revised
Project Number 1
Assembly Drawing A [CB.47]
Rev 0

Tekla Structures

Phase number & name	Qty
1 Phase 1	1

Prepared using Tekla Structures® (www.tekla.com)

Model :- New model 4

General Notes: All steelwork to comply with SANS 2001:CS1 & SANS 1921-3
All welds 6mm continuous fillet welds unless noted otherwise
All butt welds full penetration welds unless noted otherwise
Mark assembly at position shown for correct site orientation
All holes to be 22DIA for M20 bolts unless noted otherwise

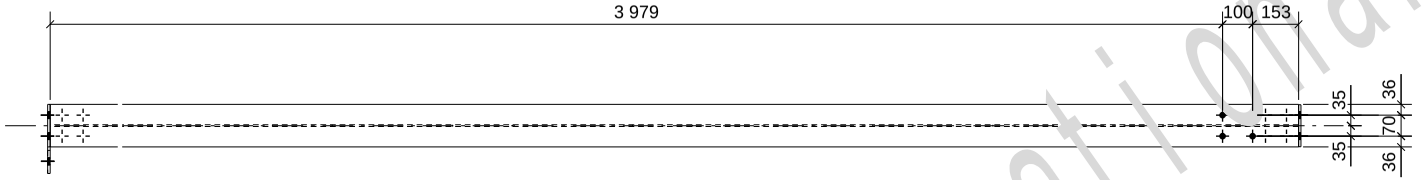

Top View

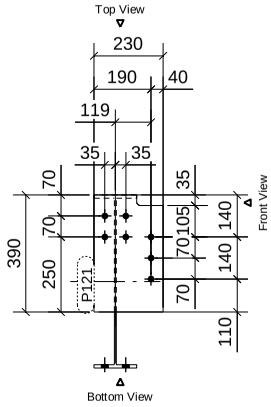

A - A

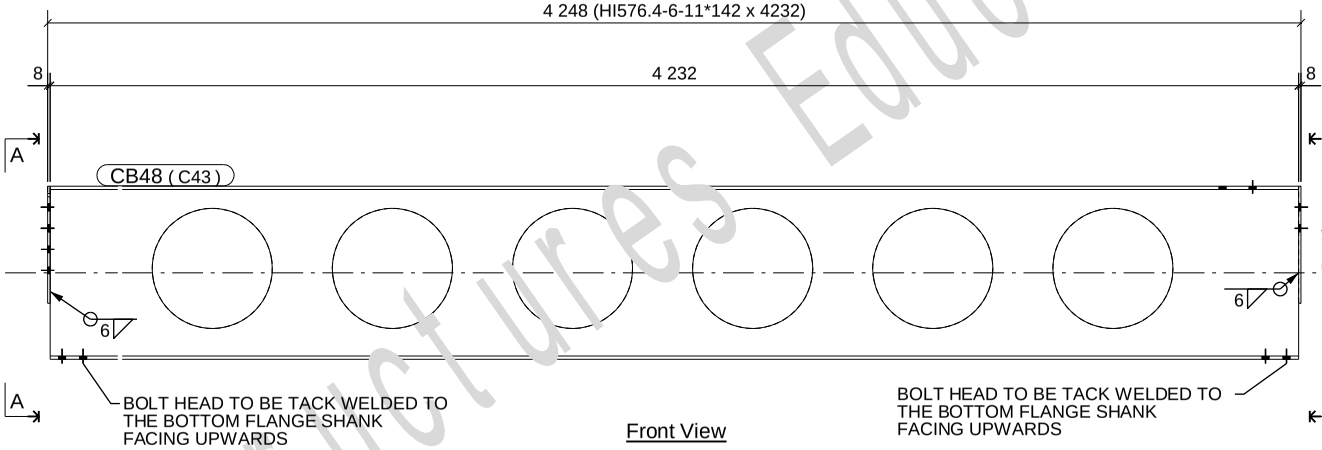

Front View

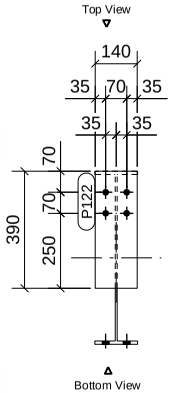

B - B

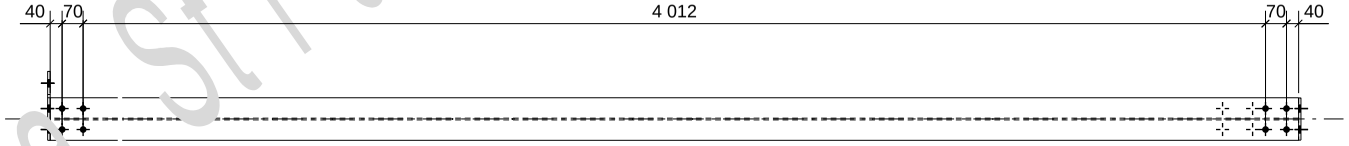

Bottom View

Material list for 1 BEAM assembly marked CB48 - only 1 is required						
Mark	No	Profile	Length	Grade	Paint area	Mass
C43	1	HI576.4-6-11*142	4232	S355JR	5.8	214.3
P121	1	PLT8*230	390	S355JR	0.2	5.6
P122	1	PLT8*140	390	S355JR	0.1	3.4
Total for 1 assembly					6.1	223.4

Tekla Structures

1 'BEAM' required marked CB48

Rev	Mark	Revision Description	Date

SAISC
Dry Floor Panel and Modular Access Floor Research
Power Street Germiston

Supplied by
Cadex SA (Tekla's SA Reseller)
Tel +27 11 463 1857/3641 Fax +27 11 463 9445
P O Box 411340
Craighall 2024, South Africa
info@CadexSA.com

POWERED BY TEKLA A TRIMBLE COMPANY

Drawn C Schoeman &
Scale 1:15
Issued
Revised
Project Number 1

Assembly Drawing A [CB.48] Rev 0

Phase number & name	Qty
1 Phase 1	1

Prepared using Tekla Structures® (www.tekla.com)

Model :- New model 4

General Notes: All steelwork to comply with SANS 2001:CS1 & SANS 1921-3
All welds 6mm continuous fillet welds unless noted otherwise
All butt welds full penetration welds unless noted otherwise
Mark assembly at position shown for correct site orientation
All holes to be 22DIA for M20 bolts unless noted otherwise

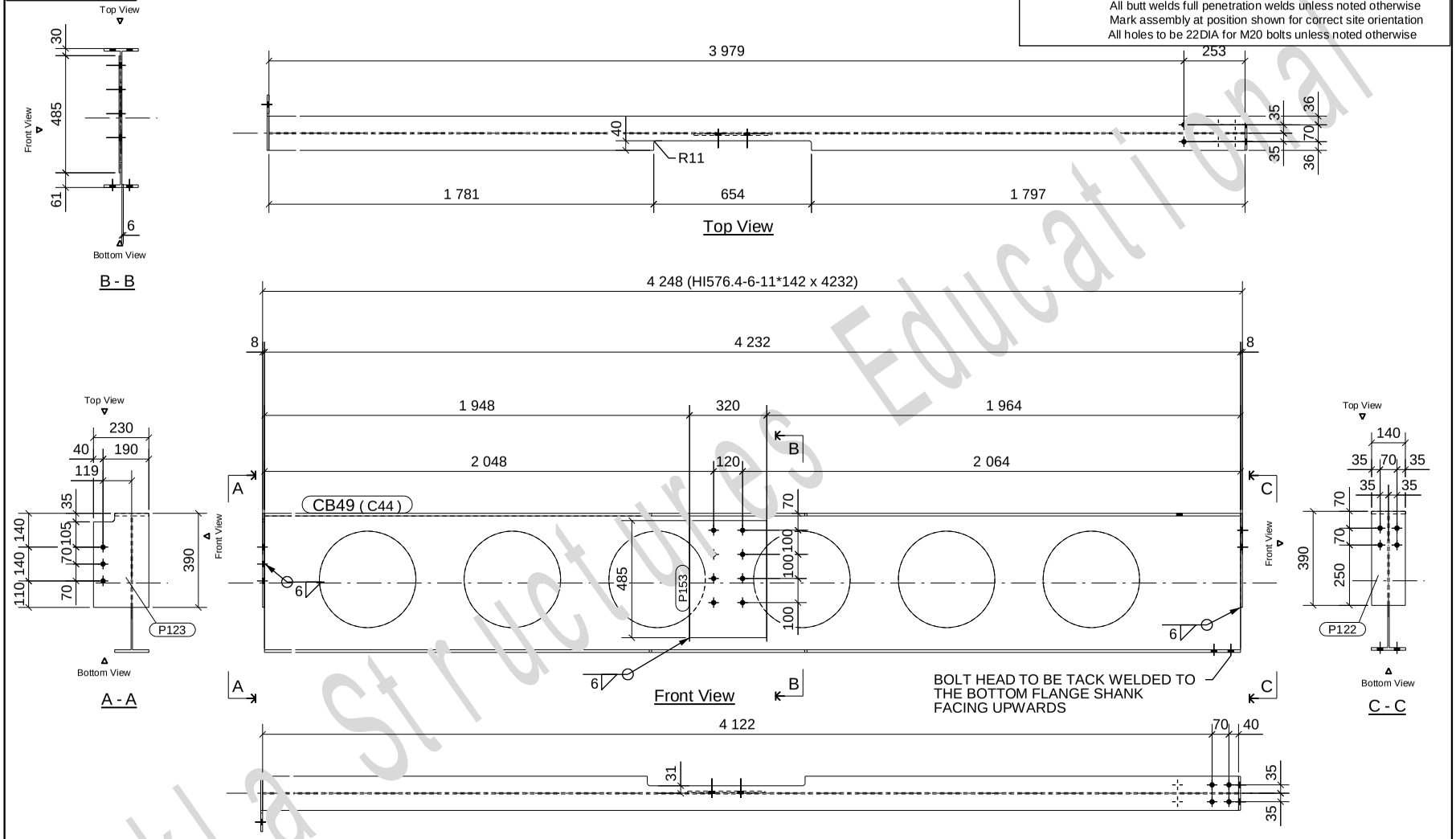

Material list for 1 BEAM assembly marked CB49 - only 1 is required

Mark	No	Profile	Length	Grade	Paint area	Mass
C44	1	HI576.4-6-11*142	4232	S355JR	5.7	214.3
P122	1	PLT8*140	390	S355JR	0.1	3.4
P123	1	PLT8*230	390	S355JR	0.2	5.6
P153	1	PLT6*320	485	S355JR	0.3	7.3
Total for 1 assembly					6.3	230.7

1 'BEAM' required marked CB49

Rev	Mark	Revision Description	Date

SAISC
Dry Floor Panel and Modular Access Floor Research
Power Street Germiston

Supplied by
Cadex SA (Tekla's SA Reseller)
Tel +27 11 463 1857/3641 Fax +27 11 463 9445
P O Box 411340
Craighall 2024, South Africa
info@CadexSA.com

POWERED BY TEKLA A TRIMBLE COMPANY

Draw C Schoeman &
Scale 1:15
Issued
Revised
Project Number 1
Assembly Drawing A [CB.49]
Rev 0

Tekla Structures

Phase number & name	Qty
1 Phase 1	1

Prepared using Tekla Structures® (www.tekla.com)

Model :- New model 4

General Notes: All steelwork to comply with SANS 2001:CS1 & SANS 1921-3
All welds 6mm continuous fillet welds unless noted otherwise
All butt welds full penetration welds unless noted otherwise
Mark assembly at position shown for correct site orientation
All holes to be 22DIA for M20 bolts unless noted otherwise

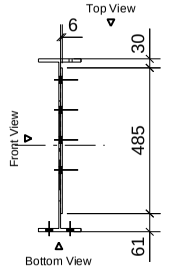

B - B

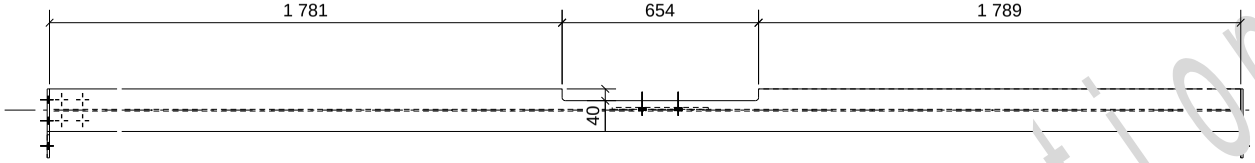

Top View

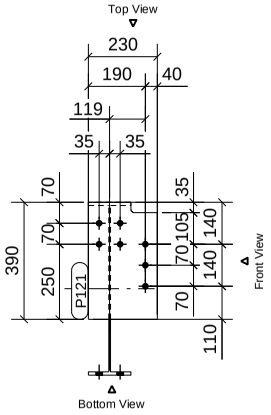

A - A

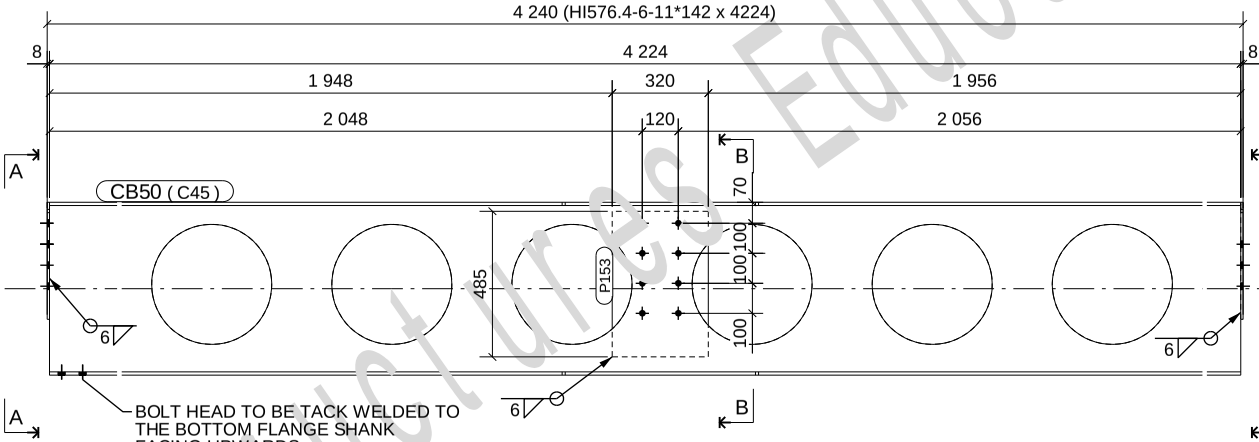

Front View

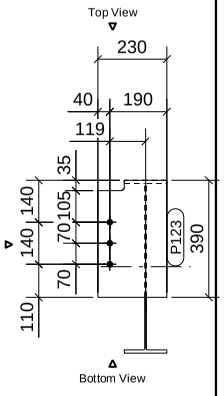

C - C

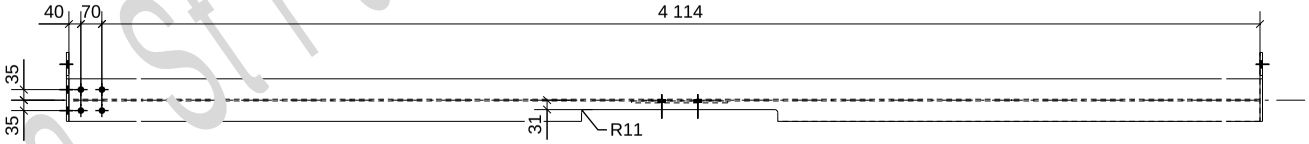

Bottom View

Material list for 1 BEAM assembly marked CB50 - only 1 is required

Mark	No	Profile	Length	Grade	Paint area	Mass
C45	1	HI576.4-6-11*142	4224	S355JR	5.7	213.9
P121	1	PLT8*230	390	S355JR	0.2	5.6
P123	1	PLT8*230	390	S355JR	0.2	5.6
P153	1	PLT6*320	485	S355JR	0.3	7.3
Total for 1 assembly					6.4	232.5

1 'BEAM' required marked CB50

Rev	Mark	Revision Description	Date

SAISC
Dry Floor Panel and Modular Access Floor Research
Power Street Germiston

POWERED BY TEKLA A TRIMBLE COMPANY

Drawn C Schoeman &
Scale 1:15
Issued
Revised
Project Number 1

Supplied by
Cadex SA (Tekla's SA Reseller)
Tel +27 11 463 1857/3641 Fax +27 11 463 9445
P O Box 411340
Craighall 2024, South Africa
info@CadexSA.com

Assembly Drawing A [CB.50] Rev 0

Tekla Structures

Phase number & name	Qty
1 Phase 1	1

Prepared using Tekla Structures® (www.tekla.com)

Model :- New model 4

General Notes: All steelwork to comply with SANS 2001:CS1 & SANS 1921-3
All welds 6mm continuous fillet welds unless noted otherwise
All butt welds full penetration welds unless noted otherwise
Mark assembly at position shown for correct site orientation
All holes to be 22DIA for M20 bolts unless noted otherwise

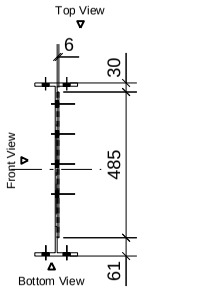

B - B

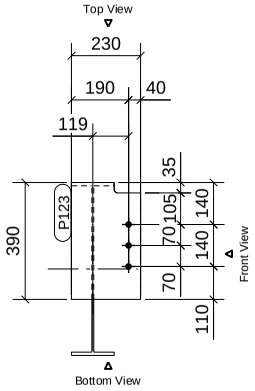

A - A

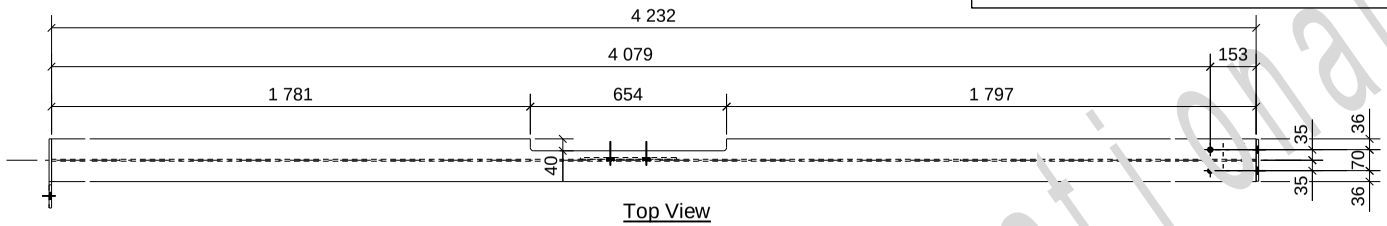

Top View

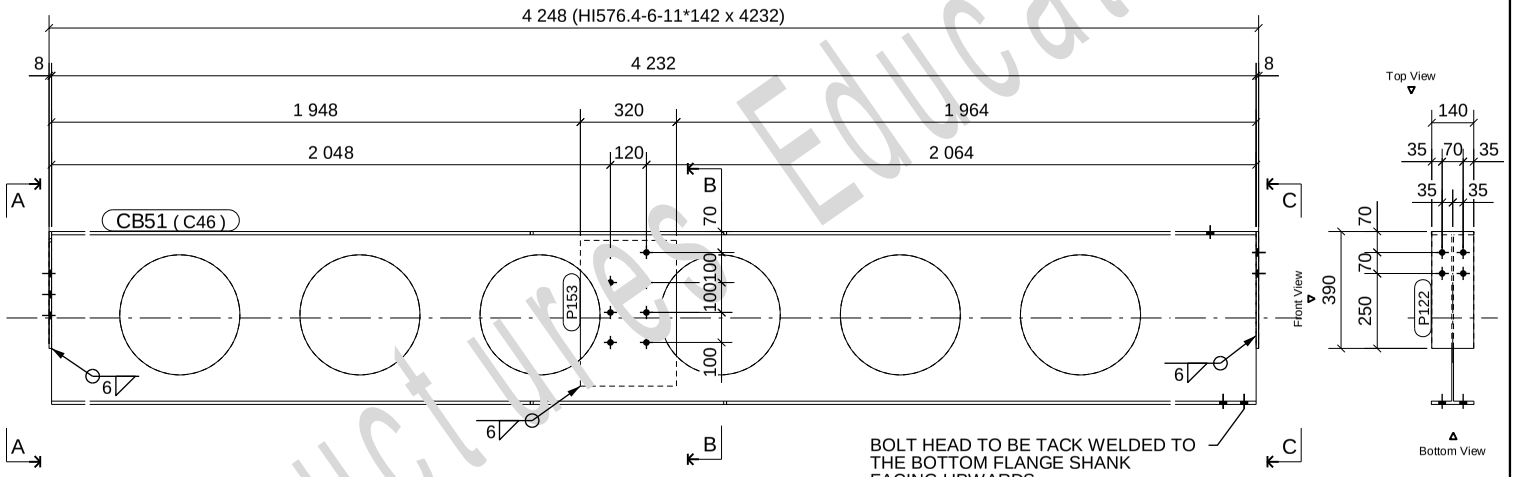

Front View

C - C

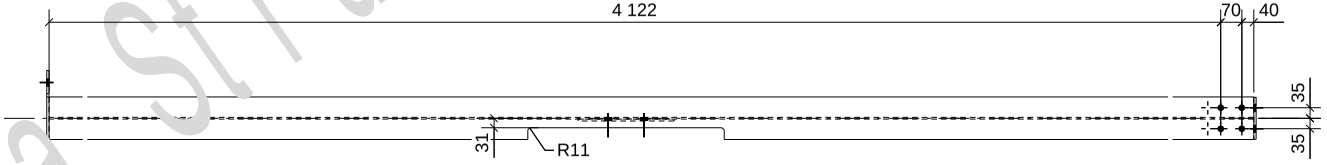

Bottom View

Material list for 1 BEAM assembly marked CB51 - only 1 is required

Mark	No	Profile	Length	Grade	Paint area	Mass
C46	1	HI576.4-6-11*142	4232	S355JR	5.7	214.3
P122	1	PLT8*140	390	S355JR	0.1	3.4
P123	1	PLT8*230	390	S355JR	0.2	5.6
P153	1	PLT6*320	485	S355JR	0.3	7.3
Total for 1 assembly					6.3	230.7

Tekla Structures

1 'BEAM' required marked CB51

Rev	Mark	Revision Description	Date

SAISC
Dry Floor Panel and Modular Access Floor Research
Power Street Germiston

POWERED BY TEKLA A TRIMBLE COMPANY

Draw C Schoeman &
Scale 1:15
Issued
Revised
Project Number 1

Supplied by
Cadex SA (Tekla's SA Reseller)
Tel +27 11 463 1857/3641 Fax +27 11 463 9445
P O Box 411340
Craighall 2024, South Africa
info@CadexSA.com

Assembly Drawing A [CB.51] Rev 0

Phase number & name	Qty
1 Phase 1	1

Prepared using Tekla Structures® (www.tekla.com)

Model :- New model 4

General Notes: All steelwork to comply with SANS 2001:CS1 & SANS 1921-3
All welds 6mm continuous fillet welds unless noted otherwise
All butt welds full penetration welds unless noted otherwise
Mark assembly at position shown for correct site orientation
All holes to be 22DIA for M20 bolts unless noted otherwise

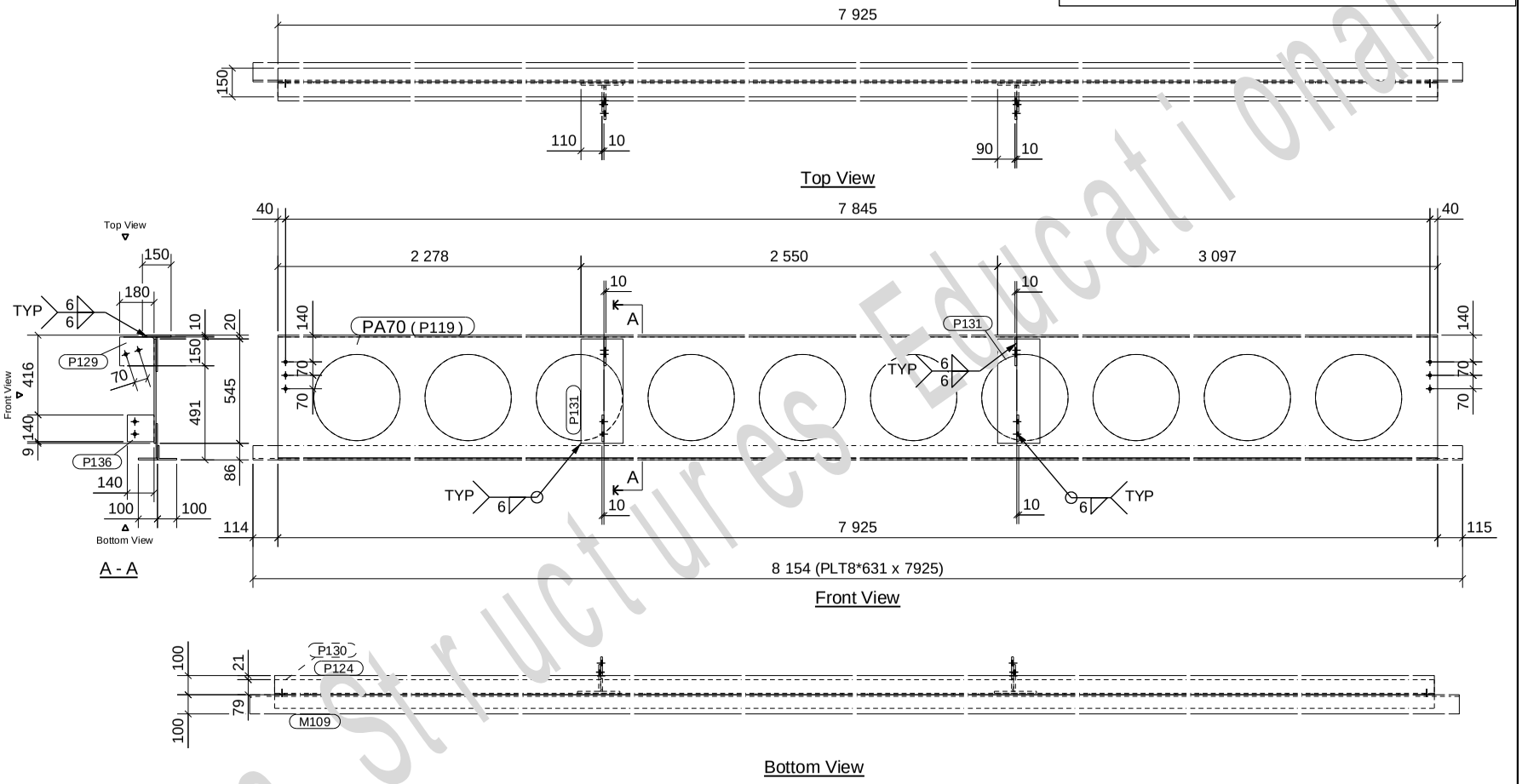

Material list for 1 Plate assembly marked PA70 - only 1 is required

Mark	No	Profile	Length	Grade	Paint area	Mass
M109	1	L100*75*8	8154	S355JR	2.9	86.4
P119	1	PLT8*631	7925	S355JR	7.1	314.0
P124	1	FL10*100	7925	S355JR	1.7	62.2
P129	2	FL10*150	180	S355JR	0.1	4.2
P130	1	FL10*150	7925	S355JR	2.5	93.3
P131	2	PLT10*220	545	S355JR	0.5	18.8
P136	2	PLT10*140	140	S355JR	0.1	3.1
Total for 1 assembly					14.9	582.1

1 'Plate' required marked PA70

Rev	Mark	Revision Description	Date

SAISC
Dry Floor Panel and Modular Access Floor Research
Power Street Germiston

Supplied by
Cadex SA (Tekla's SA Reseller)
Tel +27 11 463 1857/3641 Fax +27 11 463 9445
P O Box 411340
Craighall 2024, South Africa
info@CadexSA.com

POWERED BY TEKLA A TRIMBLE COMPANY

Drawn C Schoeman &
Scale 1:20
Issued
Revised
Project Number 1
Assembly Drawing A [PA.70]
Rev 0

Tekla Structures

Phase number & name	Qty
1 Phase 1	2

Prepared using Tekla Structures® (www.tekla.com)

Model :- New model 4

General Notes: All steelwork to comply with SANS 2001:CS1 & SANS 1921-3
All welds 6mm continuous fillet welds unless noted otherwise
All butt welds full penetration welds unless noted otherwise
Mark assembly at position shown for correct site orientation
All holes to be 22DIA for M20 bolts unless noted otherwise

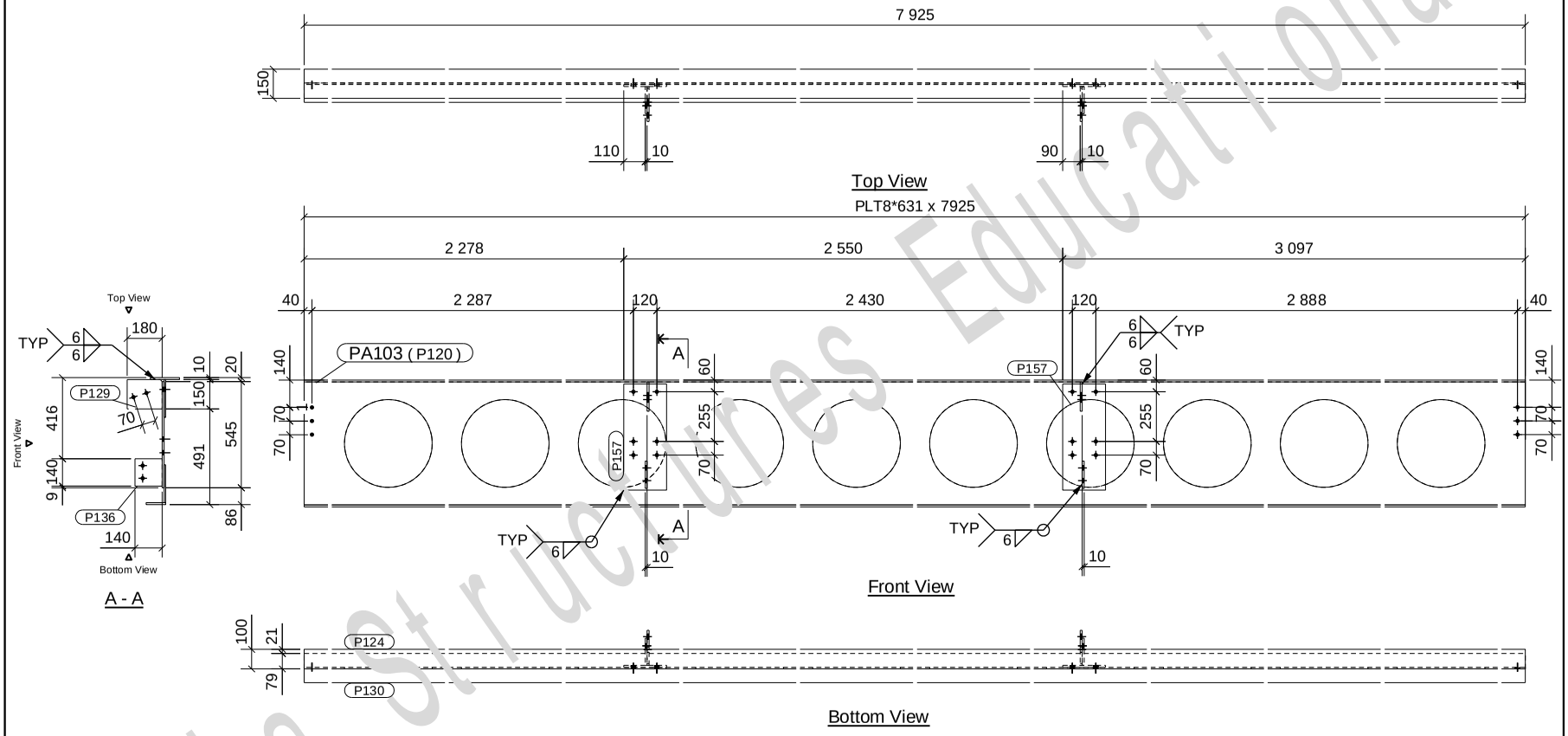

Material list for 1 Plate assembly marked PA103 - a total of 2 are required

Mark	No	Profile	Length	Grade	Paint area	Mass
P120	1	PLT8*631	7925	S355JR	7.1	314.0
P124	1	FL10*100	7925	S355JR	1.7	62.2
P129	2	FL10*150	180	S355JR	0.1	4.2
P130	1	FL10*150	7925	S355JR	2.5	93.3
P136	2	PLT10*140	140	S355JR	0.1	3.1
P157	2	PLT10*220	545	S355JR	0.5	18.8
Sub-total for 1 assembly					12.1	495.7
Total for 2 assemblies					24.2	991.4

2 'Plates' required marked PA103

Rev	Mark	Revision Description	Date

SAISC
Dry Floor Panel and Modular Access Floor Research
Power Street Germiston

Supplied by
Cadex SA (Tekla's SA Reseller)
Tel +27 11 463 1857/3641 Fax +27 11 463 9445
P O Box 411340
Craighall 2024, South Africa
info@CadexSA.com

POWERED BY TEKLA A TRIMBLE COMPANY

Drawn C Schoeman &
Scale 1:20
Issued
Revised
Project Number 1
Assembly Drawing A [PA.103]
Rev 0

Tekla Structures

Phase number & name	Qty
1 Phase 1	1

Prepared using Tekla Structures® (www.tekla.com)

Model :- New model 4

General Notes: All steelwork to comply with SANS 2001:CS1 & SANS 1921-3
All welds 6mm continuous fillet welds unless noted otherwise
All butt welds full penetration welds unless noted otherwise
Mark assembly at position shown for correct site orientation
All holes to be 22DIA for M20 bolts unless noted otherwise

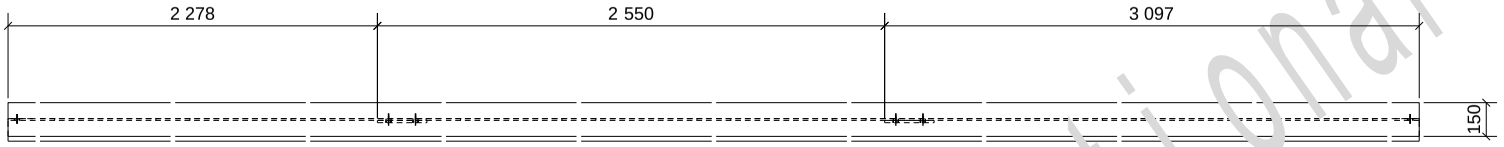

Top View

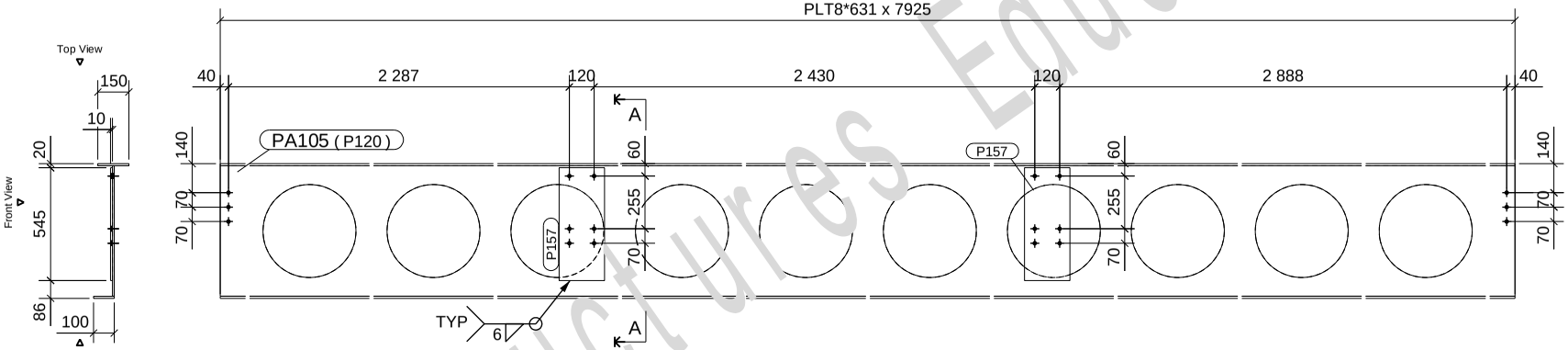

A - A

Front View

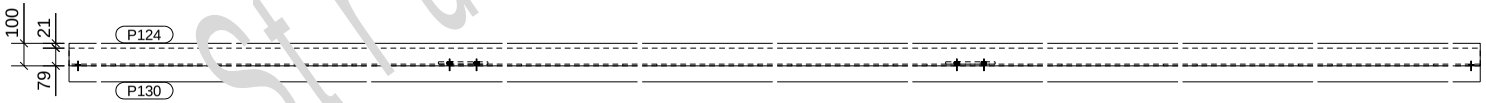

Bottom View

Material list for 1 Plate assembly marked PA105 - only 1 is required						
Mark	No	Profile	Length	Grade	Paint area	Mass
P120	1	PLT8*631	7925	S355JR	7.1	314.0
P124	1	FL10*100	7925	S355JR	1.7	62.2
P130	1	FL10*150	7925	S355JR	2.5	93.3
P157	2	PLT10*220	545	S355JR	0.5	18.8
Total for 1 assembly					11.9	488.4

1 'Plate' required marked PA105

Rev	Mark	Revision Description	Date

SAISC
Dry Floor Panel and Modular Access Floor Research
Power Street Germiston

Supplied by
Cadex SA (Tekla's SA Reseller)
Tel +27 11 463 1857/3641 Fax +27 11 463 9445
P O Box 411340
Craighall 2024, South Africa
info@CadexSA.com

POWERED BY TEKLA A TRIMBLE COMPANY

Drawn C Schoeman &
Scale 1:20
Issued
Revised
Project Number 1
Assembly Drawing A [PA.105]
Rev 0

Tekla Structures

Phase	Qty
Phase 1	3

Prepared using Tekla Structures® (www.tekla.com)

Model :- New model 4

General Notes: All steelwork to comply with SANS 2001:CS1 & SANS 1921-3
All profile notches to have 11mm radius unless noted otherwise

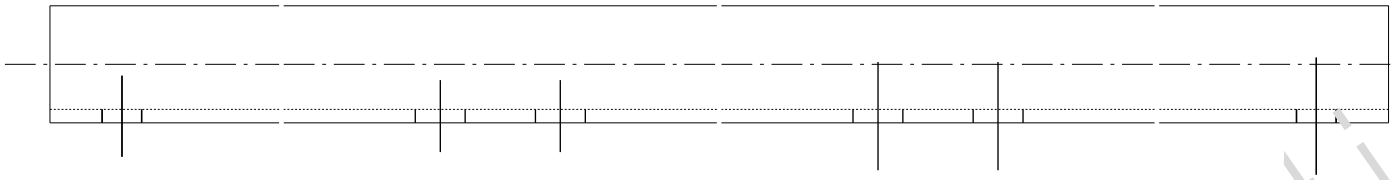

Bottom View

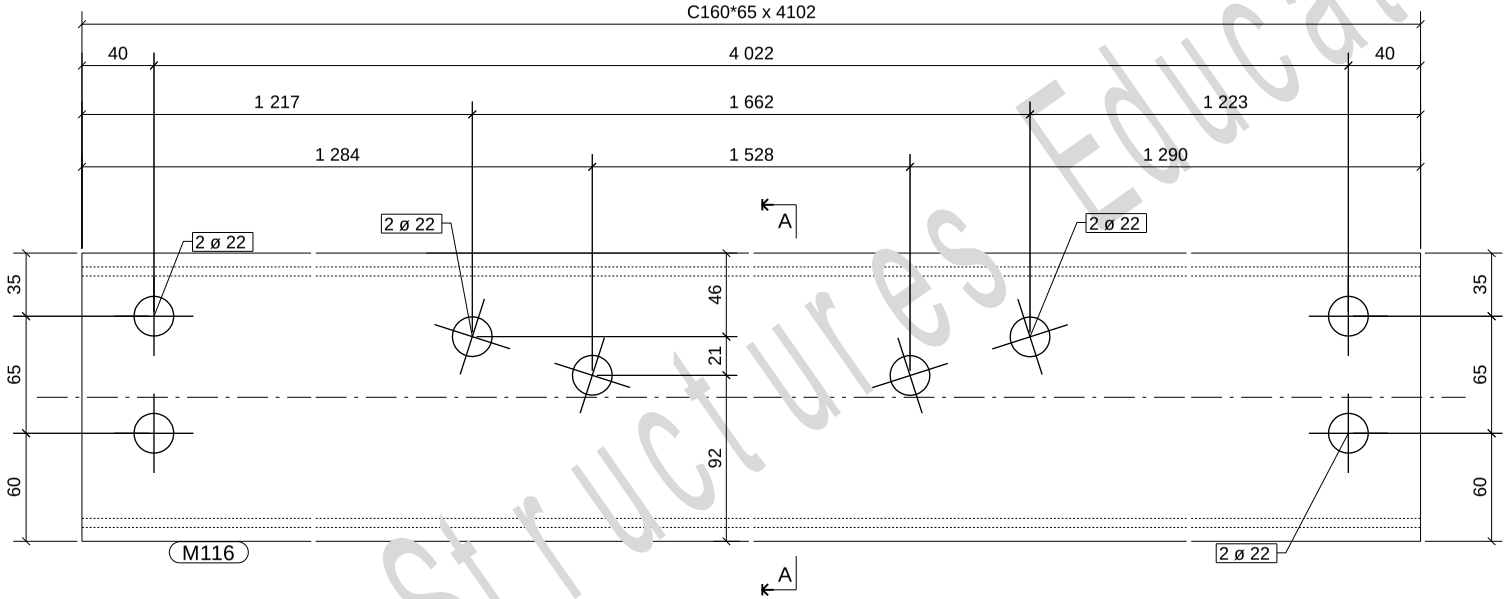

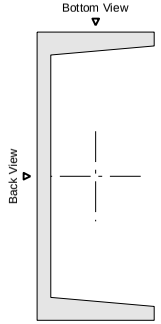

A - A

Back View

The part shown is required for the following assemblies:-
3 required for 3 'Purlin' assemblies marked A122

Material list for 3 parts named 'Purlin'

Mark	Profile	Grade	Length	Paint Area	Mass
M116	C160*65	S355JR	4102	1.1	78.3
		Total for 3 parts	12306	3.2	235.0

Tekla Structures

Rev	Mark	Revision Description	Date

SAISC
Dry Floor Panel and Modular Access Floor
Research
Power Street Germiston

Supplied by
Cadex SA (Tekla's SA Reseller)
Tel +27 11 463 1857/3641 Fax +27 11 463 9445
P O Box 411340
Craighall 2024, South Africa
info@CadexSA.com

POWERED BY TEKLA A TRIMBLE COMPANY

Drawn C Schoeman &
Scale 1:2,5
Issued
Revised
Project Number 1

Workshop Drawing W [M.116] Rev 0

Phase	Qty
Phase 1	12

Prepared using Tekla Structures® (www.tekla.com)

Model :- New model 4

General Notes: All steelwork to comply with SANS 2001:CS1 & SANS 1921-3
All profile notches to have 11mm radius unless noted otherwise

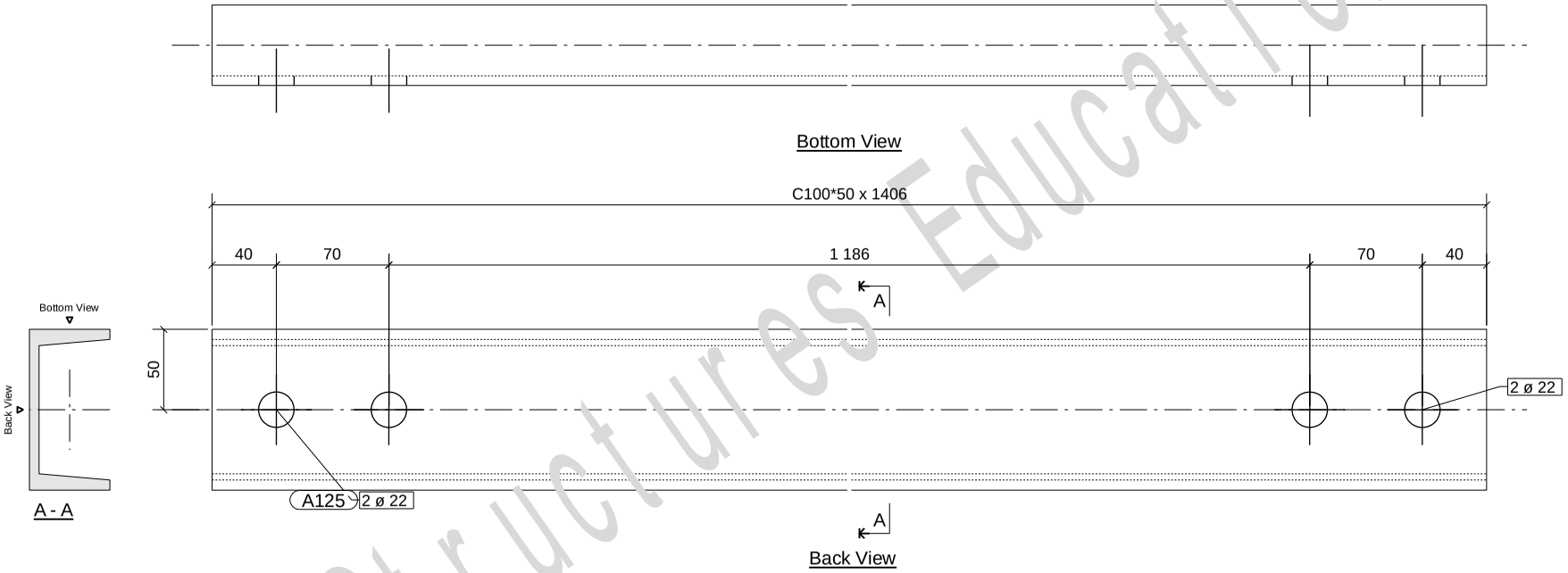

The part shown is required for the following assemblies:-
12 required for 12 'Purlin' assemblies marked A125

Material list for 12 parts named 'Purlin'

Mark	Profile	Grade	Length	Paint Area	Mass
A125	C100*50	S355JR	1406	0.3	15.0
		Total for 12 parts	16878	3.4	180.6

Tekla Structures

Rev	Mark	Revision Description	Date

SAISC
Dry Floor Panel and Modular Access Floor
Research
Power Street Germiston

Supplied by
Cadex SA (Tekla's SA Reseller)
Tel +27 11 463 1857/3641 Fax +27 11 463 9445
P O Box 411340
Craighall 2024, South Africa
info@CadexSA.com

POWERED BY TEKLA A TRIMBLE COMPANY

Drawn C Schoeman &
Scale 1:2,5
Issued
Revised
Project Number 1

Workshop Drawing W [A.125] Rev 0

Phase	Qty
Phase 1	4

Prepared using Tekla Structures® (www.tekla.com)

Model :- New model 4

General Notes: All steelwork to comply with SANS 2001:CS1 & SANS 1921-3
All profile notches to have 11mm radius unless noted otherwise

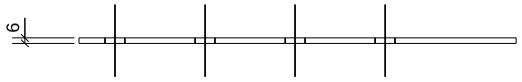

Bottom View

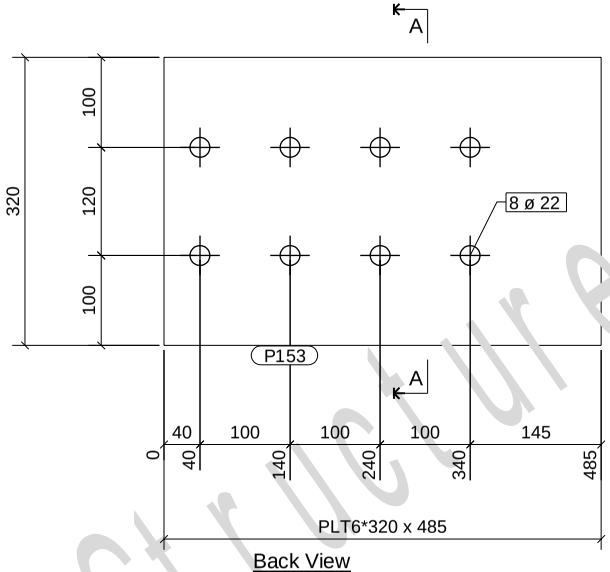

Back View

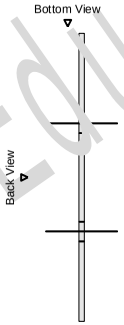

A - A

The part shown is required for the following assemblies:-
1 required for 1 'BEAM' assembly marked CB47
1 required for 1 'BEAM' assembly marked CB49
1 required for 1 'BEAM' assembly marked CB50
1 required for 1 'BEAM' assembly marked CB51

Material list for 4 parts named 'Plate'

Mark	Profile	Grade	Length	Paint Area	Mass
P153	PLT6*320	S355JR	485	0.3	7.3
		Total for 4 parts	1942	1.3	29.3

Tekla Structures

Rev	Mark	Revision Description	Date

SAISC
Dry Floor Panel and Modular Access Floor
Research
Power Street Germiston

Supplied by
Cadex SA (Tekla's SA Reseller)
Tel +27 11 463 1857/3641 Fax +27 11 463 9445
P O Box 411340
Craighall 2024, South Africa
info@CadexSA.com

POWERED BY TEKLA A TRIMBLE COMPANY

Drawn C Schoeman &
Scale 1:5
Issued
Revised
Project Number 1

Workshop Drawing W [P.153] Rev 0